PAST AND PRESENT DEEPWATER CONTOUR-CURRENT BEDFORMS AT THE BASE OF THE SIGSBEE ESCARPMENT, NORTHERN GULF OF MEXICO

A Dissertation

by

DANIEL A. BEAN

Submitted to the Office of Graduate Studies of
Texas A&M University
in partial fulfillment of the requirements for the degree of

DOCTOR OF PHILOSOPHY

August 2005

Major Subject: Oceanography

PAST AND PRESENT DEEPWATER CONTOUR-CURRENT BEDFORMS AT THE BASE OF THE SIGSBEE ESCARPMENT, NORTHERN GULF OF MEXICO

A Dissertation

by

DANIEL A. BEAN

Submitted to the Office of Graduate Studies of
Texas A&M University
in partial fulfillment of the requirements for the degree of

DOCTOR OF PHILOSOPHY

Approved by:

Co-Chairs of Committee,	William R. Bryant
	Niall C. Slowey
Committee Members,	Wilford D. Gardner
	Thomas W. C. Hilde
	Erik D. Scott
Head of Department,	Wilford D. Gardner

August 2005

Major Subject: Oceanography

ABSTRACT

Past and Present Deepwater Contour-Current Bedforms at the Base of the Sigsbee Escarpment, Northern Gulf of Mexico. (August 2005)

Daniel A. Bean, B.S., Fitchburg State College;

M.S., Texas A&M University

Co-Chairs of Advisory Committee: Dr. William R. Bryant
Dr. Niall C. Slowey

Using a high-resolution deep-towed seismic system, we have discovered a series of contour-current bedforms at the base of the Sigsbee Escarpment in the Bryant Canyon region of the northern Gulf of Mexico. We identify a continuum of bedforms that include furrows, meandering furrows, flutes and fully eroded seafloor. These contour-current bedforms are linked to current velocities ranging from 20 to upwards of 60 cm/s based on nearby current meter measurements and similar flume generated bedforms (Allen, 1969). We identify erosion and non-deposition of up to 25 meters of surface sediment at the base of Sigsbee Escarpment.

Using 3-D and high-resolution seismic data, sediment samples, and submersible observations from the Green Knoll area, we further define contour-current bedforms along the Sigsbee Escarpment. The study area is divided into eleven zones based on bedform morphology, distribution, and formation processes. We identify a contour-current bedform continuum similar to that of the Bryant Canyon region, while the data reveals additional features that result from the interaction between topography and contour-currents. Three regional seismic marker horizons are identified, and we

establish an age of ~19 kyr on the deepest horizon. The seismic horizons are correlated with very subtle changes in sediment properties, which in turn define the maximum depth of erosion for each of the individual bedforms.

Finally, we show for the first time that furrowed horizons can be acoustically imaged in three dimensions below seafloor. Analysis of imagery of several horizons obtained from 3-D seismic data from the Green Knoll region establishes the existence of multiple paleo-furrow events. The contour current pattern preserved by the paleo-furrows is similar to the presently active seafloor furrows. And, based on the morphology and development that we establish for the active seafloor furrows, we show that paleo-furrows are likely formed by currents that are in the same range as those measured today (20-60 cm/s), that erode into sediments with similar physical properties to the fine-grained hemipelagic sediments of the present-day seafloor. We further suggest the possibility that furrows are formed during inter-glacial highstands and buried during glacial lowstands.

DEDICATION

To Debora.

Our life begins now.

ACKNOWLEDGEMENTS

I would like to thank my committee co-chairs, Dr. Bryant and Dr. Slowey. Also, I would like to thank my other committee members, Dr. Gardner, Dr. Hilde, and Dr. Scott. Each member has provided time, attention, insight, and motivation that made this work possible.

I am indebted to WesternGeco, whose kind donation of 3-D seismic data enhanced our understanding of the furrows beyond measure. I thank NSF for funding the research cruise that collected the Bryant Canyon seismic data. For additional financial support and the opportunity to extend our research to the Green Knoll area, I thank members of our Joint Industry Project: BHP, BP, MMS, OTRC, and TAMU. For donation of the 3-D seismic interpretation software I am grateful to Seismic Micro-Technology.

I am thankful for every student who has ever participated on a deep-tow cruise, without whose voluntary participation my research would not have been completed. Thank you to Sandy Drews for taking care of the many things that make life at Texas A&M possible. I would also like to thank all the people I have interrupted over the years to ask inane questions, who kindly took the time to help me sort out my confusion.

Special thanks go to my wife, Debora Berti, for sticking with me over the years. You have been my most valued co-worker and my closest friend. Thank you for your patience, your time, your thoughts and your efforts.

To all the friends I have found at Texas A&M, thank you.

TABLE OF CONTENTS

CHAPTER Page

LIST OF FIGURES

FIGURE Page

FIGURE Page

FIGURE Page

LIST OF TABLES

CHAPTER I

INTRODUCTION

The continental rises of the world's oceans are not always the quiescent and unchanging environments they are often thought to be. Recent data from the Gulf of Mexico establishes the presence of an immense field of erosional bedforms covering vast areas of the seafloor at the base of the continental slope (Bryant et al., 2003). The field is dominated by hundreds of parallel furrows—linear grooves as deep as 10 meters and as wide as 30 meters that extend for tens to hundreds of kilometers. In some cases the furrows grade into structures having the appearance of numerous braided streams meandering and crisscrossing over the seafloor. Other areas have no furrows at all, but are pockmarked by numerous U-shaped, erosional flutes up to 50 meters wide. In the most extreme case, lack of bedforms indicates significant erosion with 10 meters or more of recent surface sediments having been completely removed. In all cases, the erosional bedforms follow the regional contours and are clearly affected by local topography (Bean et al., 2002). The presence of this extensive, well-structured field of erosional bedforms requires the long-term presence of high-velocity bottom currents. Understanding the modern-day link between contour currents and the specific erosional bedforms they generate is critical in establishing analogues that can be used as geologic markers for specific environmental conditions.

Previous work on deepwater contour-current bedforms in the Atlantic and Pacific has focused on identification of furrowed regions as well as specific bedform structure

---

This dissertation follows the style of Marine Geology.

and formation mechanisms (see review by Flood, 1983). Studies off the east coast of North America established the connection between the presence of furrows and the existence of strong bottom water flows such as the Western Boundary Under Current (e.g. Flood, 1983; Flood, 1994; Heezen et al., 1966). Similarly, massive mudwaves from the Bahama Outer Ridge, Bermuda Rise, Argentine Basin, and other areas have been shown to form via significant bottom currents at the base of the slope and are often found in association with furrows (e.g. Embley et al., 1980; Flood, 1994; Hollister et al., 1974; Lonsdale and Spiess, 1977; Manley and Flood, 1993). The significance of this study lies in our ability to look in detail at the correspondence between a spectrum of bedforms and a range of both current velocities and sediment strength. The maximum velocity in previous studies that can be associated with furrowed regions is only 20 cm/s. In contrast, current velocities at the base of the Sigsbee Escarpment where furrows form are up to 95 cm/s (Hamilton and Lugo-Fernandez, 2001). This offers a heretofore unique opportunity to examine a range of furrows and other bedforms, which, based on current measurements and submersible dives, are active today.

The presence of these active features has very practical implications, particularly when considering the major development of the petroleum industry in the Gulf of Mexico. Any equipment located within the water column or structures placed on the seafloor will necessarily be affected by any significant currents in the region. Since the contour-current bedforms provide a geological record of sustained high-velocity currents, areas of higher risk of exposure to high-velocity currents can be identified through study of the regional geology. By connecting the geologic features to measured

currents, assessment of potential impact over time can also be made. The connection of seafloor features to those created in the lab can begin to provide engineering constraints for structures placed on the seafloor or in the water column. Further engineering constraints can be identified for seafloor emplacements that may be exposed to the erosive potential of these significant, high-velocity bottom currents.

In this study we use a three-tiered approach to develop a complete picture of the structure and morphology of furrows and other contour-current bedforms along the base of the Sigsbee Escarpment in the Gulf of Mexico. We consider both the individual bedforms and the field of bedforms as a whole. In Chapter II we show that contour-current bedforms do not necessarily exist in isolation; rather, they are part of a larger continuum of bedforms that result from the broad interaction between contour currents and topography, as well as the detailed interaction between a gradation in current velocities and variable sediment physical properties. We hypothesize that variations in the seafloor bedforms preserve a record of the variations in the velocity and structure of the overlying flow field. This study offers an unprecedented look at the existence, structure and development of a complete progression of contour-current bedforms, and establishes them as a sedimentary proxy for long-term current strength, continuity, and distribution.

Chapter II follows up on the Bryant Canyon area study with a study of contour-current bedforms at the base of the Sigsbee Escarpment in the Green Canyon region of the Gulf of Mexico. The availability of additional data for this region allows us to both broaden our understanding and develop the details regarding the morphology and

distribution of contour-current bedforms along the Sigsbee Escarpment. We begin with a 3-D seismic dataset that provides the framework for the study. Additionally, the already detailed 3-D seismic data is augmented by even higher resolution deep-towed seismic data; thereby allowing this study to focus both on the broad regional development of contour-current bedforms as well as the fine details of key bedforms and features. In addition the multiple seismic data sets, we also use data from two *DSV Alvin* dives and two jumbo piston cores (courtesy of TDI Brooks International) within the study area.

Chapter III addresses three main hypotheses. First, there is a broad-scale pattern to the development furrows and other contour-current bedforms. By determining how the spatial distribution of individual bedforms fits within the larger regional picture, a better understanding of the link between bedforms and overlying current structure can be reached. Second, local bathymetry and topography are the primary controllers of bottom-water flow structure during the present-day highstand of sea level. This bathymetric control on bottom currents should be geologically represented in both the small-scale and large-scale contour-current bedform morphology and distribution. And third, a corresponding distribution of sediment properties will track both the spatial distribution and morphology of the contour-current bedforms. Sediment properties identified via seismic attributes and actual samples can be used to help understand the regional pattern to contour-current bedform evolution and distribution. In addition, the sediment and seismic analysis should allow for placing time constraints on the formation of the contour-current bedforms.

Chapter IV completes the study by taking our understanding of the present-day development of seafloor furrows and extending it into the geologic past. Having established the existence of a field of furrows on the seafloor at the base of the Sigsbee Escarpment in both the Bryant Canyon and Green Knoll regions of the Gulf of Mexico, it naturally followed to look for similar structures in the sub-seafloor seismic data. Given that the pattern and development of contour-current bedforms on the seafloor reveals the structure of the long-term bottom currents, the goal of Chapter IV is to identify analogous patterns in the subsurface that would provide information on the presence, structure, and variability of paleo-currents in a region. This portion of the study focuses primarily on the various forms of furrows, since they are laterally continuous enough to recognize in the sub-surface.

In Chapter IV the first concept we address is whether or not furrows are even present and can be imaged in the subsurface. We determine whether the erosion of a massive field of furrows at the base of the Sigsbee Escarpment is a unique occurrence, or a phenomenon that has occurred in the past, and, whether or not this cyclic pattern of furrowing is seismically preserved after infilling and burial. The second concept we deal with is the paleo-current implications of the furrowed horizons. By comparing any furrowed horizons to their modern analogues, what can we conclude regarding the location, direction, duration, and intensity of the furrow-forming paleo-currents? As with the present-day seafloor furrows, paleo-furrows offer the possibility of providing the equivalent of a geological current meter for entire regions of an ocean basin.

CHAPTER II

CONTOUR-CURRENT BEDFORMS IN THE BRYANT CANYON FAN AREA OF THE GULF OF MEXICO, SIGSBEE ESCARPMENT

Synopsis

Using a deep-towed seismic system, a fully developed series of contour-current bedforms was found in the Bryant Canyon area of the Gulf of Mexico, Sigsbee Escarpment. The present seismic records show much greater definition and detail regarding the progressive development of bedforms as related to topography, currents, and sediment strength than previously recorded. The bedform and contour current evidence includes proto-furrow surface features, parallel furrows, meandering furrows, flutes, and complete surface sediment removal. These bedforms embody a continuum of features that can be directly tied to current velocities ranging from 20 cm/s to upwards of 60 cm/s based on nearby current meter measurements and similar flume generated bedforms (Allen, 1969).. The contour-current bedforms identified in this study are on a much larger scale, yet are proportionally consistent with the flume generated bedforms. The Sigsbee Escarpment creates an obstruction to bottom currents causing bathymetric intensification of currents and resulting in substantial erosion. Overall, the data show the stepwise removal of up to 25 meters of surface sediment in a swath 20 km wide at the base of the Sigsbee Escarpment.

Introduction

The continental rises of the world's oceans are not always the quiescent and unchanging environments they are often thought to be. Recent data from the Gulf of

Mexico establishes the presence of an immense field of erosional bedforms covering vast areas of the seafloor at the base of the continental slope (Bryant et al., 2003). The field is dominated by hundreds of parallel furrows—linear grooves as deep as 10 meters and as wide as 30 meters that extend for tens to hundreds of kilometers. In some cases the furrows grade into structures having the appearance of numerous braided streams meandering and crisscrossing over the seafloor. Other areas have no furrows at all, but are pockmarked by dozens of U-shaped, erosional flutes up to 50 meters wide. In the most extreme case, lack of bedforms indicates significant erosion with 10 meters or more of recent surface sediments having been completely removed. In all cases, the erosional bedforms follow the regional contours and are clearly affected by local topography (Bean et al., 2002). The presence of this extensive, well-structured field of erosional bedforms requires the long-term presence of high-velocity bottom currents. Understanding the link between active contour currents and the specific erosional bedforms they generate is critical for establishing geologic markers for specific environmental conditions.

Previous work on deepwater contour-current bedforms in the Atlantic and Pacific has focused on identification of furrowed regions as well as specific bedform structure and formation mechanisms (see review by Flood, 1983). Studies off the east coast of North America established the connection between the presence of furrows and the existence of strong bottom water flows such as the Western Boundary Under Current (e.g. Flood, 1983; Flood, 1994; Heezen et al., 1966). Similarly, massive mudwaves from the Bahama Outer Ridge, Bermuda Rise, Argentine Basin, and other areas have been

shown to form via significant bottom currents at the base of the slope and are often found in association with furrows (e.g. Embley et al., 1980; Flood, 1994; Hollister et al., 1974; Lonsdale and Spiess, 1977; Manley and Flood, 1993). The significance of this study lies in our ability to look in detail at the correspondence between a spectrum of bedforms and a range of both current velocities and sediment strength. The maximum velocity in previous studies that can be associated with furrowed regions is only 20 cm/s. In contrast, current velocities at the base of the Sigsbee Escarpment where furrows form are up to 95 cm/s (Hamilton and Lugo-Fernandez, 2001). This offers a heretofore unique opportunity to examine a range of furrows and other bedforms, which based on current measurements and submersible dives are active today.

We show that contour-current bedforms do not necessarily exist in isolation; rather, they are part of a larger continuum of bedforms that result from the broad interaction between contour currents and topography, as well as the detailed interaction between a gradation in current velocities and variable sediment physical properties. Our hypothesis is that variations in the seafloor bedforms preserve a record of the variations in the velocity and structure of the overlying flow field. This study offers an unprecedented look at the existence, structure and development of a complete progression of contour-current bedforms, and establishes them as a sedimentary proxy for long-term current strength, continuity, and distribution.

Geological and Oceanographic Setting

The northern Gulf of Mexico continental slope is an exceptionally broad region with some of the most variable topography to be found along any ocean margin. The

breadth and variable topography of the slope and rise results from the presence and movement of vast subsurface salt units (e.g., Bouma and Roberts, 1990; Bryant et al., 1990; Coleman et al., 1991). The subsurface movement of a massive allocthonous salt sheet has led to the uplift and creation of the Sigsbee Escarpment—a structure marking the southern limit of the salt sheet and having a relief of 800 meters or more, along with local slope angles in excess of 20° (Liu and Bryant, 2000). This significant topographic structure should result in bathymetric intensification of existing contour currents. Consequently, the core of such bottom currents would be strongest near the escarpment and weaken with distance from the escarpment. Geological evidence for this scenario is presented below.

Few details are presently known about deep currents in the Gulf of Mexico; however, it is known that the Loop Current, which is the primary surface current structure in the Gulf, has an indirect connection to the regional deep currents (Hamilton, 1990; Hamilton and Lugo-Fernandez, 2001). The Loop Current enters through the Yucatan Channel, meanders through the Gulf of Mexico, and exits through the Florida Straits to form the Gulf Stream. As the base of the Loop Current or one of the eddies that periodically spin off impinges on the slope, the potential for the generation of deep currents in the form of topographic Rossby waves exists (Hamilton, 1990; Hamilton and Lugo-Fernandez, 2001; Sturges et al., 1993). Nowlin et al. (2001) show modeled westward-flowing high-velocity bottom currents that closely track bathymetric contours along the Sigsbee Escarpment. Indeed, current meters at the base of the escarpment confirm the existence of recent current events in excess of 50 cm/s and lasting for

periods of weeks (Hamilton and Lugo-Fernandez, 2001). Such intense recurring flow events are assumed to be the primary means of controlling the evolution of deepwater contour-current bedforms in the Gulf of Mexico.

Results and Discussion

We recently surveyed a region of the Sigsbee Escarpment in the Bryant Canyon Fan area of the Gulf of Mexico using the TAMU deep-towed seismic system (Fig. 1). The system includes a 3.5 kHz subbottom profiler and 100 kHz sidescan sonar. The TAMU deep-tow system uses a positively buoyant fish body attached to a depressor anchor chain to maintain a near constant altitude of 30 m above seafloor. The survey includes six perpendicular crossings of the escarpment, one crossing of the proximal Bryant Canyon Fan and main channel axis, and one crossing of the distal Bryant Canyon Fan running parallel to the escarpment. To determine fish position we assumed the fish followed the ship track except during turns, and calculated the layback based on triangulation of cable out and fish depth. Uncertainties in fish position do not affect any geologic interpretations. Post-processing of the data also included smoothing of depth data from the pressure transducer, bottom-tracking, and depth correction of the seismic data for the variable depth and altitude of the fish.

Inferences about relative current velocity in the region are based on three independent lines of reasoning: 1) Given that the flux of sediment to the seafloor is uniform across the region (Lee et al., 1996), changes in bed thickness are due to either differential deposition or erosion. 2) The relationship between bedform morphology and velocity is comparable to that documented in a lab study by Allen (1969). 3) Erosion

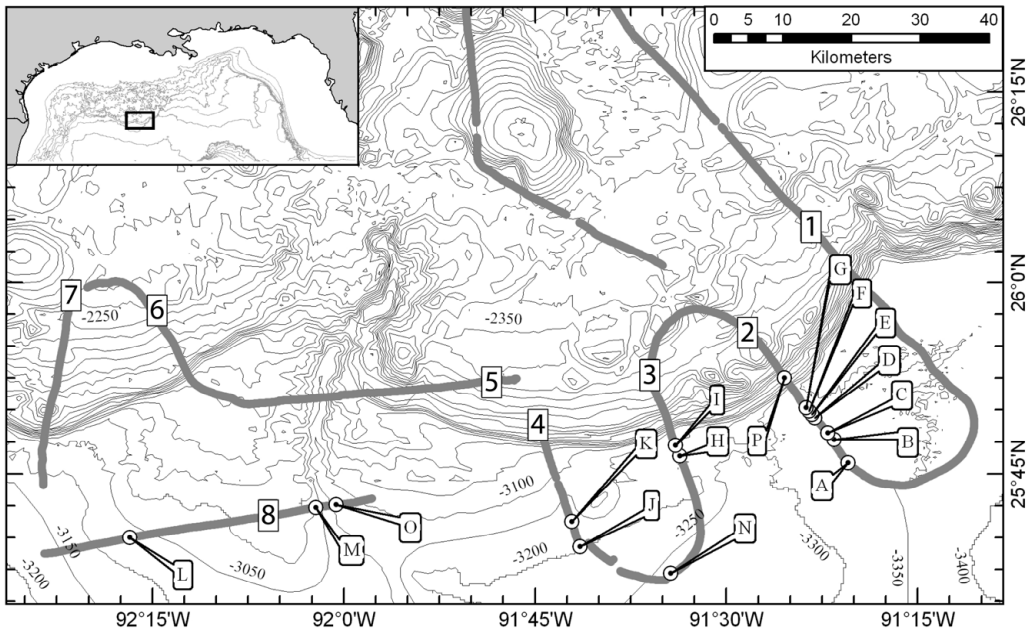

Fig. 1. Bryant Canyon Bathymetry and Survey Map.
Numbers indicate the survey line segment. Letters indicate the location of the seismic data in Fig. 2. Contours are in 50 m intervals. The inset map shows the Bryant Canyon survey area location (black square).

resistance increases with maximum burial depth due to consolidation of fine-grained sediments. These ideas establish three unique points of reference for defining the link between bottom current velocities and resulting geological signatures. The following results and discussion will deal first with the morphological progression of furrows with distance from the Sigsbee Escarpment, followed by a selection of a few key isolated bedforms that deviate from the aforementioned morphological progression.

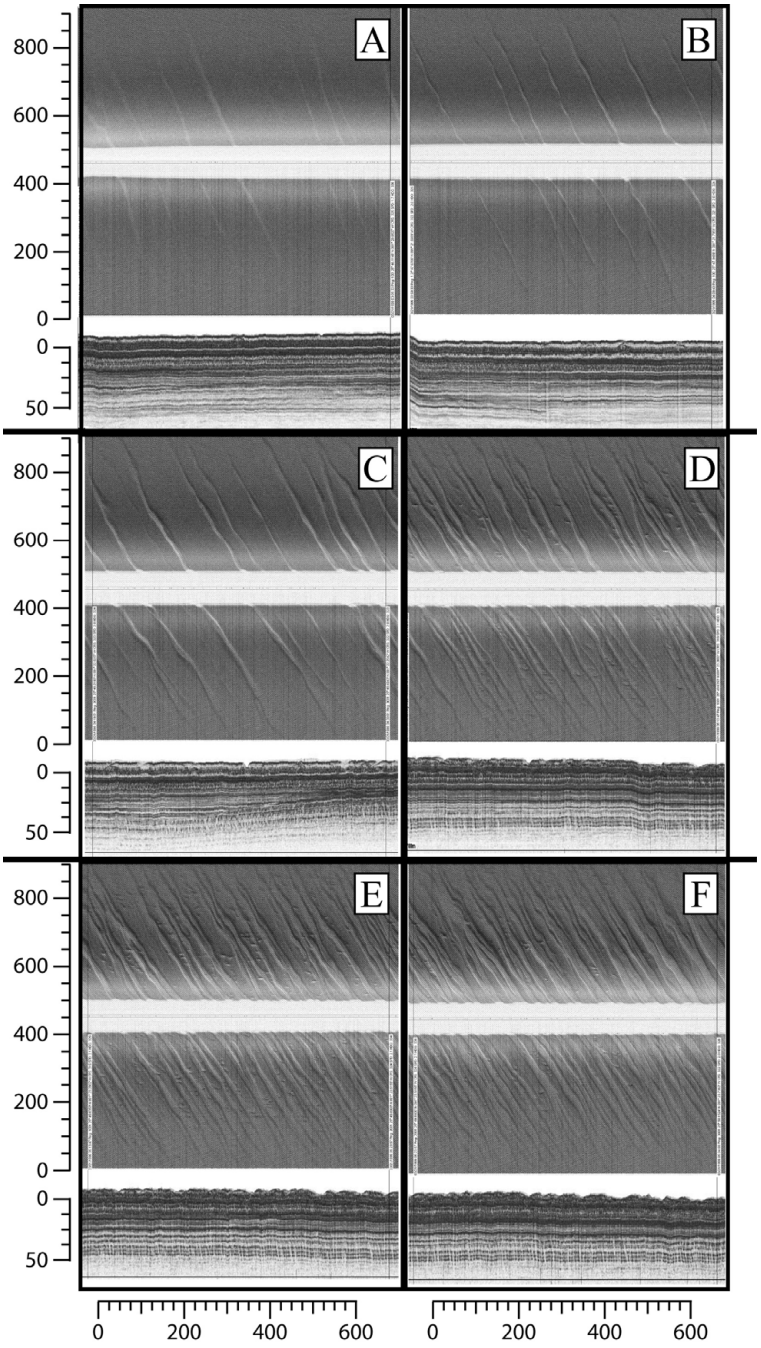

Fig. 2. Deep-Tow Records of Contour-Current Bedform Types.
Shown here are sidescan and subbottom records of the various contour-current bedform types. The location of each lettered record is identified in Fig. 1. All depth and range scales are in meters. A-F: Development of furrows from low flow to high flow conditions. G: Complete removal of the top 5 m of sediment. H-I: Development of flutes with and without furrows. J-K: Pre-furrow development. L: Extreme case of erosional parallel furrows with 10 m of sediment removal. M: Meandering furrows. N: Tuning-fork junctions indicate bi-directional flow. O: Cut off of furrows due to surface sediment removal. P: Characteristic furrows on the Sigsbee Escarpment showing lineations from outcropping layers.

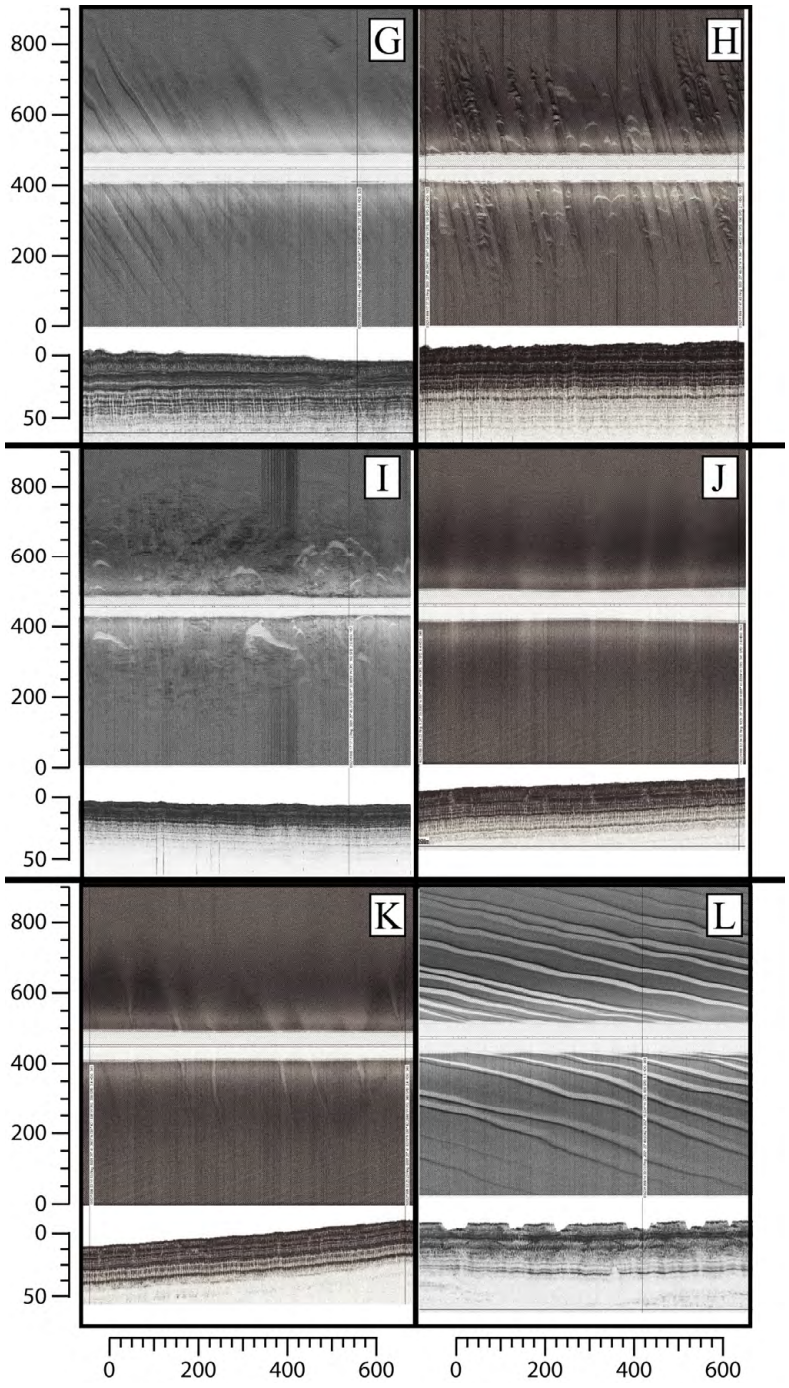

Fig. 2. Continued.

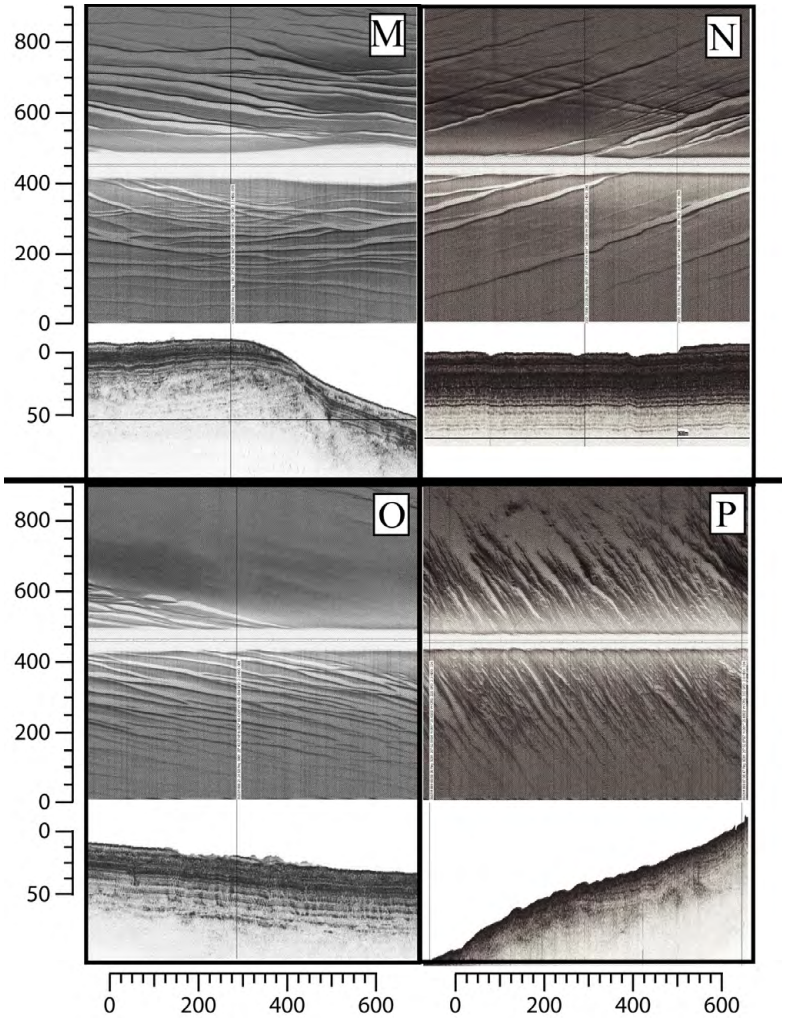

Fig. 2. Continued.

Lines 2 and 3 (Fig. 1) show the most well defined progression of contour current features in the study area. This is where the Sigsbee Escarpment pushes farthest out onto the rise and may locally intensify the bottom currents that follow the escarpment. The first seafloor evidence of contour currents is seen approximately 15 km seaward of the escarpment, as narrow (5-10 m), widely spaced (75-200 m), parallel lineations (Fig. 2-A, B). Under these apparent low current velocity conditions—20 to 30 cm/s based on Allen (1969)—the only evidence of erosion in the subbottom record is small, shallow

hyperbolics. Approaching 7 km from the escarpment, the parallel lineations become more distinct, wider (5-15 m), and closer spaced (25-150 m) (Fig. 2-C, D). The change in bedform character is most likely due to an increase in current strength that is evident in the subbottom record as erosional furrows, 4-5 m deep.

An additional aspect of furrows is that tuning-fork junctions develop, which have been shown to point in the downstream direction of flow as adjacent furrows merge into a single furrow (Allen, 1969; Dyer, 1970). Over most of the survey, visible junctions indicate that the predominant direction of flow in the region is from east to west, and is in close agreement with measured and modeled currents (Hamilton and Lugo-Fernandez, 2001; Nowlin et al., 2001). A further change in bedform character occurs between 7 and 3 km from the escarpment as furrow spacing decreases to less than 25 m (Fig. 2-E, F). It is also crucial to note that there is no significant increase in depth of erosion between 10 and 3 km from the escarpment. Rather, the furrows simply become wider (5-50 m) as the furrow walls continue to erode until adjacent furrows actually merge. Erosion appears to stop at a high amplitude reflector that is continuous throughout the survey area, indicating higher strength, less erodible sediment (Fig. 3).

Within 3 km of the Sigsbee Escarpment the bottom currents apparently approach their highest velocity. The bedforms continue to widen and merge, as the top 5-10 m of soft, easily erodible sediment is slowly removed, resulting in features that are no longer truly furrows since there are only narrow bands (< 25 m) of residual, uneroded material. Eventually, only a flat, featureless, seafloor remains, caused by the complete removal of

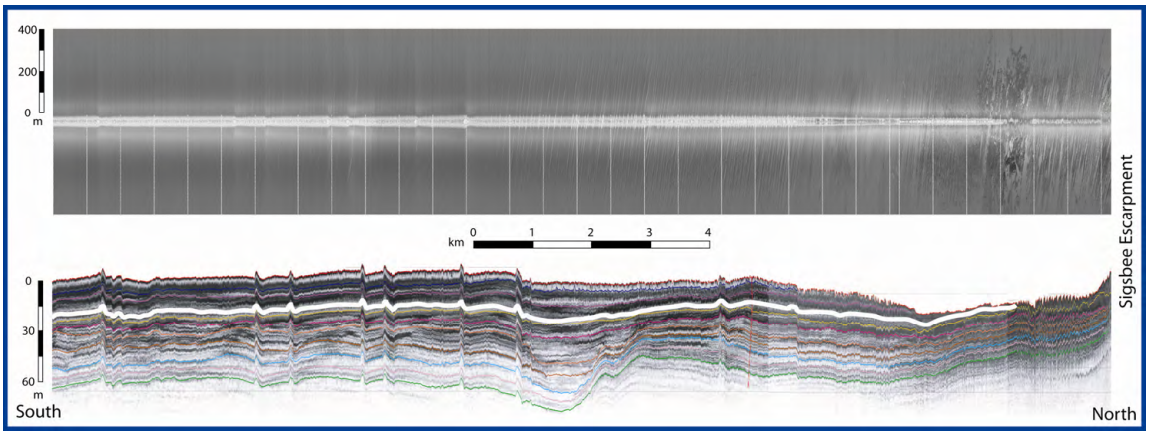

Fig. 3. Contour-Current Bedform Transect.
Here is shown Line 2 (see Fig. 1) approaching the Sigsbee Escarpment. The upper panel shows the 100 kHz sidescan sonar imagery and the lower panel shows the 3.5 kHz subbottom profile. The maximum erosional horizon (white line) indicates up to 25 meters of sediment removal or non-deposition at the truncation and exposure closest to the escarpment.

the softer surface sediments and exposure of the erosion-resistant deeper sediments (Fig. 2-G). Within the closest 1 km of the escarpment, currents reach such extreme velocities—60 to 85 cm/s based on Allen (1969)—that U-shaped erosional flutes become the predominant bedform (Fig. 1-H,I). Not only do the flutes form in the softer interfurrow sediments, but the currents near the escarpment are strong enough to erode flutes in the stronger underlying sediments that marked the maximum depth of erosion for the furrows—further supporting the concept of increasing current strength nearer the topographic control of the escarpment. Similar to tuning-fork junctions, the flute morphology also confirms the dominant long-term current direction, albeit under maximum current velocity conditions, as their apexes point upstream (Allen, 1969). In all cases of the survey, the flutes point to the east, indicating a westward flowing current.

Along with the well-ordered morphological progression of bedforms seen in relation to proximity of the escarpment, there are also isolated areas where bedforms

develop from more localized interaction between currents, topography, and sediments. The first feature appears to occur under a low velocity region, as defined by the previous bedforms, and may actually be a proto-furrow bedform (Fig. 2-J). On the sidescan record, the features appear as broad (25-100 m), parallel, linear, poorly defined, low amplitude regions. These proto-furrows have no subbottom erosional definition, and the center of each broad lineation is associated with a weaker, structureless return in the subbottom. We suggest the proto-furrow bedform results from the initial concentration of coarser grained material by helical cells, reflecting the processes that will eventually lead to furrow erosion and development. This is confirmed in Fig. 2-K as the broad proto-furrow bands narrow down into well-defined furrows. The proto-furrow bedforms appear to have developed in a low current velocity region created by the cutback of the Sigsbee Escarpment into the Bryant Canyon (*i.e.*, out of the focused flow along the escarpment).

Meandering furrows occur under lab conditions as a midway phase between parallel furrows and flute formation at velocities of 35 to 45 cm/s (Allen, 1969). While this bedform is not seen clearly in lines 2 and 3, it is found associated with a slight elevation of the seafloor along the levee of the Bryant Canyon channel (Fig. 2-M). There are two likely influences affecting the flow in this region. The first is the topographic obstruction of the channel levee. Flow over this obstruction can lead to an increased velocity as the flow is focused over the top of the levee (Hunt and Snyder, 1980). The velocity may increase just enough to move the flow into the higher velocity regime of the meandering furrows. Additionally, if we consider transition from straight

to meandering and braided streams as a possible analogue of these furrow bedforms, the type of sediment load carried within the channels themselves as well as slope changes can lead to a change in bedform morphology. A straight channel will transition to meandering and then braided geometries as the sediment transport moves from suspended, to mixed, to bed load transport, or as slope and velocity are increased (Schumm et al., 2000). As primarily a turbidity flow conduit, the Bryant Canyon channel axis probably contains more sands and silts than the surrounding seafloor—particularly given the exposure of deeper horizons on the channel wall (Fig. 2). The availability of larger grain sizes could initiate mixed or bed load transport mechanism that results in a morphology change similar to that of meandering and braided streams. While the slope change of the channel wall would simultaneously increase the probability of forming meandering or braided morphologies.

Sediment strength is also an important consideration in the contour-current bedform development. Fig. 2-L shows extremely well developed furrows that erode up to 10 m of the surface sediments and are deeper than most other furrows of the study area. The furrows are deeper because the high-amplitude layer that marks the typical maximum depth of erosion for the region is buried under a thicker surface sediment layer, while the currents were strong enough and operated over a long enough period to reach the maximum depth. It is assumed that the high amplitude layer is a high-strength, erosion-resistant horizon. A second example clearly shows a sharp cutoff between a furrowed region and a featureless seafloor that is associated with complete removal of the soft, upper 5 m of sediments (Fig. 2-O). Again, the maximum depth of erosion for

the existing currents occurs as soon as the higher-strength, high-amplitude horizon is exposed.

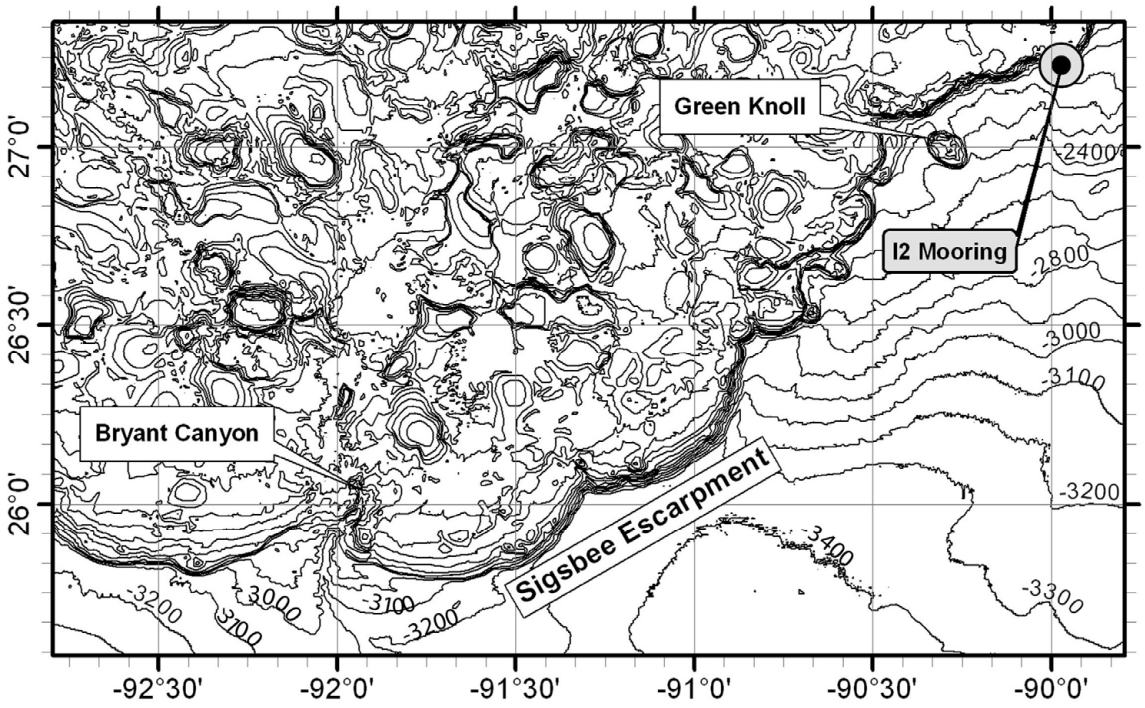

Fig. 4. Location of MMS Current Meter Mooring I2.
The MMS current meter mooring was located east of Green Knoll, at the base of the Sigsbee Escarpment. The mooring recorded high-velocity currents between September and December of 1999.

The morphology of the contour-current bedforms indicates the dominant current direction in the region as well as its variability. As mentioned previously, tuning-fork junctions pointing downstream and flutes pointing upstream imply a strong East to West flow for the region; however, sidescan records from the flanks of the Bryant Canyon Fan show evidence of tuning-fork junctions occurring in opposite directions along with cross-cutting relationships between different furrow groups (Fig. 2-N). This occurrence indicates that significant changes in current direction occur and last over time periods

long enough to develop contour-current bedforms. Indeed, current measurements made at the base of the escarpment (Fig. 4 & Fig. 5) display bi-directional flow of similar magnitude and lasting weeks in each direction (Hamilton, 1990; Hamilton and Lugo-Fernandez, 2001). Sedimentary evidence for eastward flow may be less in the study region simply due to lack of coverage by the discrete seismic lines across the Sigsbee Escarpment.

The final distinct contour-current bedform seen in the region is found on the flanks of the Sigsbee Escarpment. Furrows are actually eroded into the exposed older layers of the escarpment (Fig. 2-P). However, the character of the sidescan record is much different than that of the furrows on the rise. The furrows of the escarpment have many smaller lineations within them that may be a result of eroding into the layered sediments of the escarpment and tracking the bedding planes of those exposures. The ability to erode the older, presumably high-strength exposures of the escarpment implies potentially higher velocity currents than in the flute regions at the base of the escarpment as well as a means of shaping the escarpment itself.

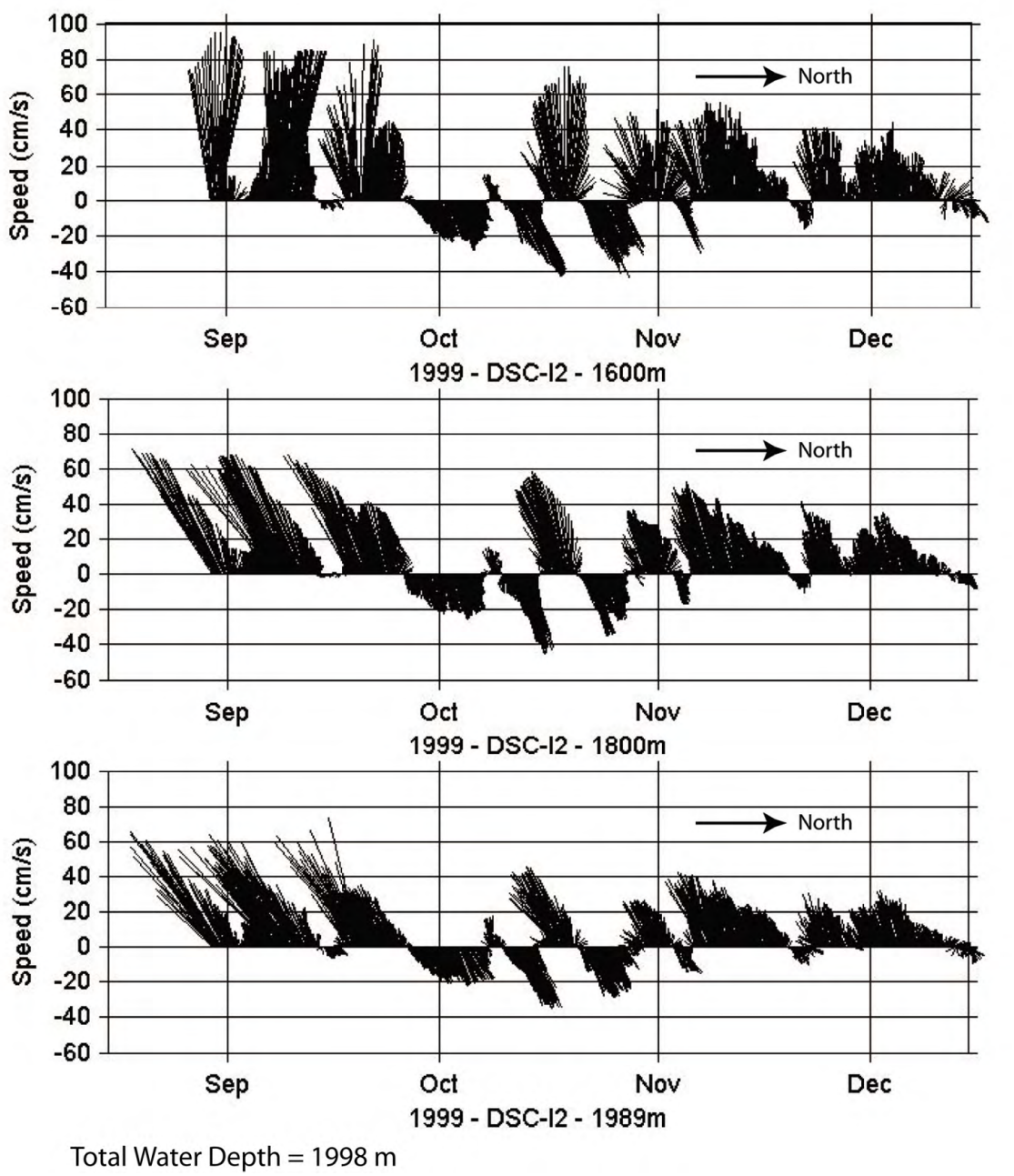

Fig. 5. MMS I2 Current Meter Record.
The I2 Current meter was located at the base of the Sigsbee Escarpment near the Mississippi Canyon. The data show week-long bi-directional flow events, dominated by more intense westward flow. Data is from Nowlin et al. (2001), see also (Hamilton and Lugo-Fernandez, 2001).

Conclusions

A range of contour-current bedform morphologies exists and has been described using deep-towed subbottom and sonar data. One of the most interesting aspects of the contour-current bedforms found in the Bryant Canyon is their near perfect replication of bedforms created in the lab by Allen (1969). Not only are the various bedforms well represented, but a smooth transition from one bedform to the next is seen in a near seamless continuum on a scale four orders of magnitude larger than that of the lab study. Despite the scale difference, initial indications are that the current velocities related to each bedform regime are similar to those measured in the flume studies by Allen (1969), with the parallel furrows developing under current velocities between 20 and 30 cm/s, meandering furrows at 35-45 cm/s, and flutes at 60-85 cm/s. Published data from an MMS current meter in the eastern Gulf of Mexico at the base of the Sigsbee Escarpment records week long periods of currents approaching 100 cm/s (Hamilton and Lugo-Fernandez, 2001). These long-term, high-velocity currents are strong enough to erode the furrows and flutes we see in the soft Holocene and Late Pleistocene sediments of the region. The presence of high-velocity currents and existing bedforms indicate that the erosional process is a recent and ongoing event. Furthermore, the link between bedform and overlying current velocity provides a sedimentary proxy that provides a continuous, long-term record that is not possible with the point current measurements made today. This correlation suggests it is possible to predict the maximum likely velocities, adding confidence to accurately assessing safety factors when placing structures and equipment

on the seafloor. And, it provides information for both refining and verifying the accuracy of current oceanographic circulation models.

The data from this study also illustrate the mechanism by which entire sections of the geological record can be wiped out over extensive areas in the deep sea. Accordingly, the presence of furrows or flutes in the sedimentary record would indicate decreased sedimentation and/or significant sediment transport in conjunction with strong bottom currents at the time of formation of such an identified horizon. The most visible contour-current bedform, furrows, have been identified along the margins of many other ocean basins (Flood, 1983). It is therefore likely that active contour-current bedforms are presently one of the most significant seafloor features of the world's deep ocean basin margins. They are an indicator of long-term, high-velocity currents that can remove massive amounts of sediment and provide a mechanism for shaping the margins of the world's oceans (e.g., Heezen et al., 1966). In the future, the ability to associate identified contour-current bedforms to co-located velocity measurements will be an important step in understanding deepwater circulation, both past and present. Likewise, sediment samples will be necessary to understand the erosional limits of the contour currents associated with each contour-current bedform.

CHAPTER III

3-D AND HIGH-RESOLUTION SEISMIC ANALYSIS OF FURROWS AND RELATED CONTOUR-CURRENT BEDFORMS IN THE GREEN KNOLL AREA OF THE GULF OF MEXICO, SIGSBEE ESCARPMENT

Synopsis

This study expands on recent work in the Bryant Canyon mega-furrows area of the Gulf of Mexico (see Chapter II). Here we analyze data from the Green Knoll area of the Gulf of Mexico that define contour-current bedforms along the Sigsbee Escarpment. The data include four complete 3-D seismic surveys, a high-resolution deep-tow seismic survey, two jumbo piston cores, and *DSV Alvin* observations. The study area has been divided into zones based on bedform morphology, distribution, and formation processes and includes: deflection and splay pattern, rectilinear furrows, transverse bedforms, gradational furrow spacing, meandering furrows, flutes, mudwaves, recirculation scour, upslope furrows, topographically isolated furrows, and obstacle scour. Using the 3-D seismic data as a framework, we show that the large-scale pattern of contour-current bedforms on the seafloor is a record of the interaction between the contour currents and the topography. Higher velocity contour current bedforms are found closer to the topographic highs of the Sigsbee Escarpment and Green Knoll. The overall range of velocity in the region is estimated based on bedform morphology and available current meter data to range between 20 and 140 cm/s. Subtle changes in sediment physical properties and currents result in dramatically different bedform morphologies. Three regional marker horizons are identified that define the maximum depth of erosion for

each of the individual bedforms. We determine the maximum age for onset of furrowing in the region to be 10 ka and calculate a maximum erosion rate of 1 cm/yr for furrows. These contour-current bedforms are part of a continuum that defines the presence and velocity structure of geologically long-term currents at the base of the Sigsbee Escarpment in the northern Gulf of Mexico.

Introduction

Recent work in the Bryant Canyon area of the Gulf of Mexico has identified the presence of seafloor mega-furrows and other associated contour-current bedforms at the base of the Sigsbee Escarpment (see Chapter II). These bedforms are important for several reasons: 1) The bedforms serve as long-term records of contour current location, direction and relative velocity. 2) The bedforms are consistent with current meter measurements that indicate ongoing weeklong events of high-velocity currents in excess of 50 cm/s. 3) A complete continuum of contour-current bedforms exists that validates the work of Allen (1969) on a scale that is four orders of magnitude larger than in the lab. 4) The bedforms are geologic evidence for the mobilization and transport of a massive amount of sediment in the deep ocean.

The presence of these active features has very practical implications, particularly when considering the major development of the petroleum industry in the Gulf of Mexico. Equipment located within the water column or structures placed on the seafloor will necessarily be affected by any significant currents in the region. Since the contour-current bedforms provide a geologic record of sustained high-velocity currents, areas of higher risk of exposure to high-velocity currents can be identified. By associating the

geologic features with measured currents, assessments of potential impact over time can also be made. The comparison of actual seafloor features to those created in the lab can provide engineering constraints for structures placed on the seafloor or in the water column that may be exposed to the erosive potential of these significant, high-velocity bottom currents.

Given these important scientific and practical implications, it is essential to study the mega-furrows and associated contour-current bedforms in an area that has a more direct connection to ongoing petroleum exploration and production operations than the original Bryant Canyon study area (see Chapter II). The deepwater Green Knoll region offered an ideal opportunity for further study due to increasing industry interest, as is evident from the number of wells being placed along the Sigsbee Escarpment in the region (Fig. 6). Consequently, this study focuses on the Green Knoll area of the Gulf of Mexico at the base of the Sigsbee Escarpment. Industry collected 3-D seismic data, provided by WesternGeco, allowed the initial detection of furrows in the Green Knoll region (Bean, 2002; Bryant et al., 2001). Recent work on the Atlantis and Mad Dog prospects has provided additional data and incentives to study the furrows of the region (Niedoroda et al., 2003; Scott et al., 2001).

As with the initial study of Gulf of Mexico furrows in the Bryant Canyon area (see Chapter II) this study focuses on the morphology and distribution of seafloor furrows along the Sigsbee Escarpment; however, the present study offers some additional advantages over the Bryant Canyon study. The primary advantage is the

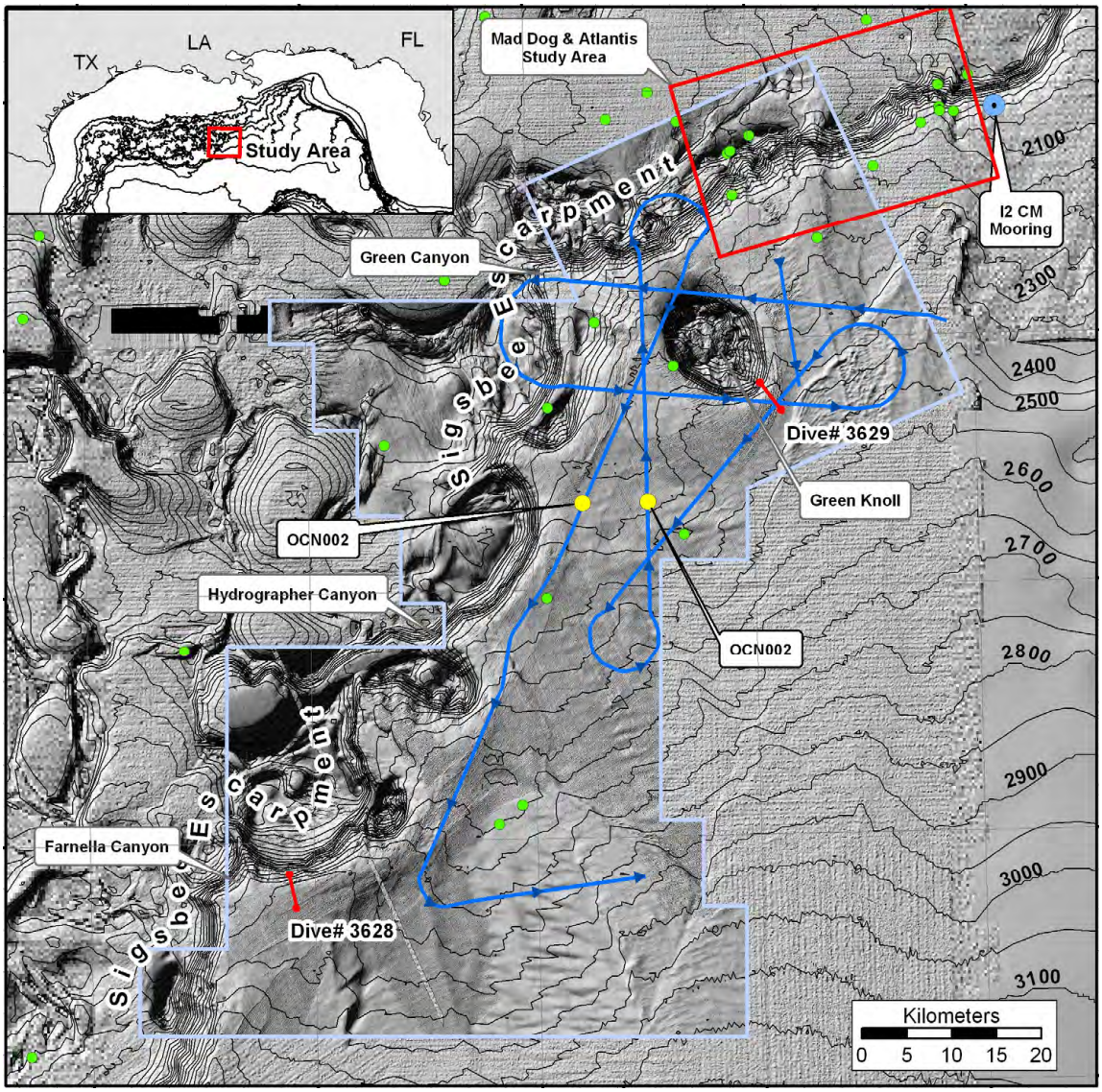

Fig. 6. Study Area Location and Bathymetry.
The main study area map contour lines were generated from Seabeam bathymetry at a 50 m interval. The high resolution (15 m grid) shaded relief (light blue outline) was generated from the 3-D seismic seafloor horizon pick and can be compared against the lower resolution of the background shaded relief generated from Seabeam data (50 m grid). Well locations (green circles) of the region are based on MMS 2003 data and indicate the progressive offshore movement of petroleum exploration and production. Also, the location of recent industry related slump study around the Mad Dog and Atlantis prospects is identified (red outline). Additional data locations shown are the 2000 *DSV Alvin* dives (red lines) at Farnella Canyon and Green Knoll, the 2004 deep-tow cruise track (blue line), and the 2004 jumbo piston core locations (yellow dots). The inset shows an overview of the northern Gulf of Mexico coastline with bathymetry at 400 m contour intervals and the coverage of the main map (red outline). **(Note: Exact position information is not provided on any images containing 3-D seismic data due to the proprietary nature of the datasets.)**

availability of a 3-D seismic dataset (provided courtesy of WesternGeco) covering over 230 lease blocks and comprised of 4 major surveys. The seafloor extraction (discussed below) from this 3-D seismic dataset provided the framework for designing a Texas A&M University (TAMU) Deep-Tow high-resolution seismic survey over the same area (Fig. 6), allowing us to maximize coverage of key features for the greatest scientific benefit. Thus, the already detailed 3-D seismic data is augmented by even higher resolution deep-towed seismic data, enabling this study to focus both on the broad regional development of contour-current bedforms and the fine details of key bedforms and features. In addition, we also have data from two *DSV Alvin* dives and two jumbo piston cores (courtesy of TDI Brooks International) within the study area (Fig. 6), to provide information on sediment properties, ongoing seafloor processes, and true bedform geometry.

This study addresses three main hypotheses. First, there is a broad-scale pattern to the development furrows and other contour-current bedforms. By determining how the spatial distribution of individual bedforms fits within the larger regional picture, a better understanding of the link between bedforms and overlying current structure can be reached. Second, local topography is the primary controller of bottom-water flow structure during the present-day highstand of sea level. This bathymetric control on bottom currents should be geologically represented in both the small-scale and large-scale contour-current bedform morphology and distribution. And third, the distribution of sediment properties will track both the spatial distribution and morphology of the contour-current bedforms. Sediment properties, identified via seismic attributes and

actual samples, can be used to help understand the regional pattern of contour-current bedform evolution and distribution. In addition, the sediment and seismic analysis should allow time constraints to be established for the formation of the contour-current bedforms.

Geological and Oceanographic Setting

The northern Gulf of Mexico continental slope is an exceptionally broad region with some of the most variable topography to be found along any ocean margin. The breadth and variable topography of the slope and rise results from the presence and movement of vast subsurface salt units (e.g., Bouma and Roberts, 1990; Bryant et al., 1990; Coleman et al., 1991). The subsurface movement of a massive allocthonous salt sheet has led to the uplift and creation of the Sigsbee Escarpment—a structure marking the southern limit of the salt sheet and having a relief of 800 meters or more, along with local slope angles in excess of 20° (Liu and Bryant, 2000). Additionally, seaward of the Sigsbee Escarpment an isolated, massive, salt-cored diapir forms the structure of Green Knoll (Fig. 7). The salt diapir is disconnected in both structure and origin from the salt sheet that forms the leading edge of the Sigsbee Escarpment (Weimer and Buffler, 1992). These significant topographic structures should result in bathymetric intensification of existing contour currents both along the escarpment and around the knoll.

Few details are presently known about deep currents in the Gulf of Mexico; however, it is known that the Loop Current, which is the primary surface current

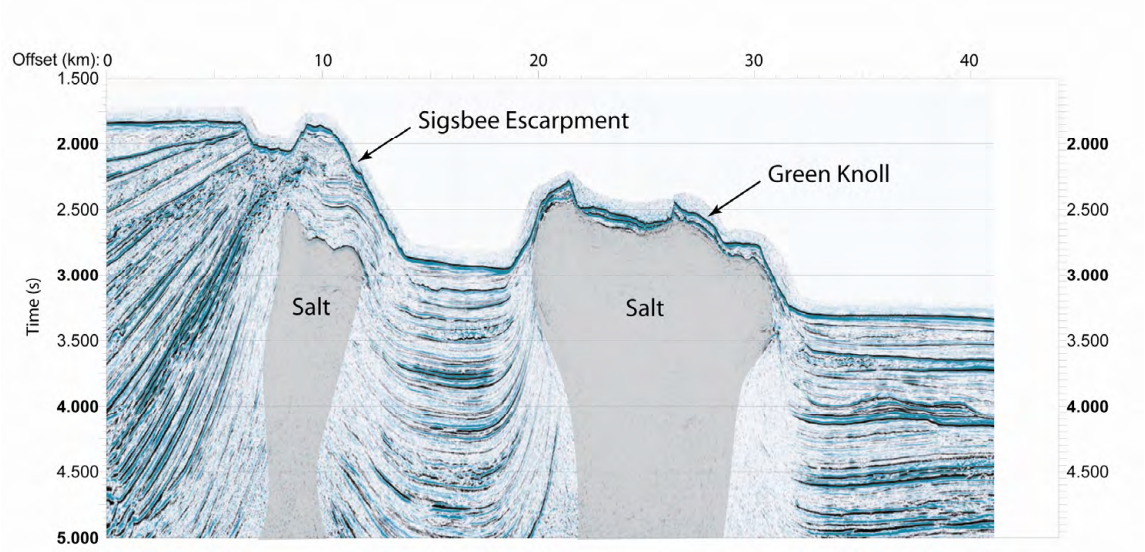

Fig. 7. 3-D Seismic Profile across the Sigsbee Escarpment and Green Knoll.

structure in the Gulf, has an indirect connection to the regional deep currents (Hamilton, 1990; Hamilton and Lugo-Fernandez, 2001). The Loop Current is a result of the Yucatan Current meandering through the Gulf of Mexico and exiting through the Florida Straits to form the Gulf Stream. As the base of the Loop Current or one of the eddies that periodically spin off impinges on the slope, the potential for the generation of deep currents in the form of topographic Rossby waves exists (Hamilton, 1990; Hamilton and Lugo-Fernandez, 2001; Sturges et al., 1993). Nowlin et al. (2001) show modeled westward-flowing high-velocity bottom currents that closely track bathymetric contours along the Sigsbee Escarpment. Indeed, current meters at the base of the escarpment record data (Fig. 5) confirming the existence of bi-modal current events in excess of 50 cm/s and lasting for periods of weeks (Hamilton and Lugo-Fernandez, 2001). Such

intense recurring flow events are assumed to be the primary mechanism controlling the evolution of deepwater contour-current bedforms in the Gulf of Mexico.

Methods

This study uses two seismic datasets. The first dataset is a 3-D seismic volume that was collected and provided by WesternGeco. The seismic dataset is comprised of 4 complete surveys in the Green Knoll and Farnella Canyon regions (Fig. 6). The surveys cover nearly 5000 km^2 of the seafloor along the Sigsbee Escarpment. Line spacing is 20 m and trace spacing is 12.5 m. The sample rate for the data is 4 ms and the volume includes the first 5 seconds of time/amplitude data. The seismic data have had the following primary processing methods applied: deconvolution, phase correction, dip move-out stacking, modified residual migration, and residual amplitude compensation. The processed data was loaded into Kingdom Suite (a 3-D seismic interpretation program provided to TAMU, Department of Oceanography courtesy of Seismic Micro-Technology). Following data loading, the amplitudes were balanced across the surveys using standard RMS method to enable valid relative amplitude mapping and comparison across surveys. The primary horizon that will be discussed in this study is the seafloor horizon, which was picked as the first peak amplitude and gridded at a 15 m. The grid interval was chosen as close as practical to the in-line and cross-line grid spacing to retain nearly the full resolution of the raw data.

The second seismic dataset was recently collected using the TAMU deep-tow system as part of a Joint Industry Project (JIP) to study furrows in the Green Knoll region of the Gulf of Mexico. The TAMU deep-tow system used for this survey is a

modified Benthos SIS3000 system with a Chirp subbottom profiler (2-7 kHz) and Chirp sidescan (90-110 kHz). The TAMU deep-tow system uses a positively buoyant fish body in conjunction with a depressor anchor chain to maintain a near constant altitude of 30 m above seafloor. The survey covered a distance of ~370 km at the base of the Sigsbee Escarpment (Fig. 6), and was designed to cross a number of key features identified from the available 3-D seismic data that will be discussed below. To determine fish position we assumed the fish followed the ship track except during turns, and calculated the layback based on triangulation of cable out and fish depth. Uncertainties in fish position do not affect any geologic interpretations, and fish position can be fine-tuned by overlaying the sonar data on the 3-D seismic seafloor horizon. Post-processing of the seismic data included bottom-tracking, depth correction to account for the variable depth and altitude of the fish, and amplitude balancing to allow for relative amplitude comparisons. For all subsequent deep-tow imagery, the polarity for both subbottom and sidescan data are represented as darker returns being equivalent to higher amplitudes.

In addition to the two seismic datasets, this study looks at two dives made by the *DSV Alvin* in conjunction with the ongoing furrows study (Fig. 6). The first dive was made on the southeast edge of Green Knoll—an isolated bathymetric high created by a salt diapir and rising over 600 meters above the sea floor (Fig. 7). The *DSV Alvin* traveled 4.5 km along the sea floor and up the flank of Green Knoll. We chose this location because, based on the 3-D seismic data, the furrows on the south side of Green Knoll are some of the largest furrows identified along the Sigsbee Escarpment so far.

On the second dive, the *DSV Alvin* covered another 4.5 km across the contour current region at the base of the Sigsbee Escarpment at the eastern edge of Farnella Canyon. This site was chosen to try to capture data from some of the additional high-velocity contour-current bedforms associated with furrowed regions. Both dives collected video, pictures, and cores and provided an excellent opportunity to witness the true nature of these contour-current bedforms *in situ*.

The final data considered in this study come from two jumbo piston cores provided by TDI Brooks International (Fig. 6). The cores were taken west of Green Knoll—one in a non-furrowed region (OCN001) and one in the middle of the main furrow field (OCN002). Core OCN001 was taken to determine more about the nature of the anomalous non-furrowed zone that appears to be in the lee of the westward flowing contour currents (see Chapter II) moving around Green Knoll. Core OCN002 was positioned to look at the standard sediment characteristics associated with dominant furrow type of the region.

Core analysis began with non-destructive testing using a GeoTek Multi-Sensor Core Logger (MSCL). This equipment measures density across a whole-round core using gamma ray attention of a 5mm collimated beam. The theory, methods, and calculations involved in determining density, water content, and porosity from gamma-ray attenuation are well documented (e.g., Boyce, 1973; Boyce, 1976; Evans, 1965; Evans and Cotterell, 1970; Harms and Choquette, 1965). Additionally, P-wave velocity is measured across the same location by measuring acoustic travel times across the measured path length of the core diameter. For a discussion of theory and calculations

see Schultheiss and Mcphail (1989), and Weber et al. (1997). Using the density and velocity, reflection coefficient values were calculated (Yilmaz, 2001) for comparison with the high-resolution seismic data. Following logging with the MSCL, the cores were split lengthwise, photographed, and described. Finally, undrained shear strength measurements were taken every 5 cm using a Wykeham Farrance WF23500 laboratory vane following ASTM standard methods (ASTM-D4648, 1994). Collecting these data from the cores allows cross-correlation of sedimentology, physical properties, acoustic properties and high-resolution seismic data.

Results and Discussion

Overview

The 3-D seismic dataset is the most extensive available for this study and also provides enough detail to identify the key seafloor features; therefore, it will provide the framework for examining all other datasets and will be used to understand the regional development of the various contour-current bedforms. Using the 3-D seismic data, the seafloor in the Green Knoll region can be divided up into several zones based on bedform morphology (Fig. 8):

- Deflection and splay pattern
- Rectilinear furrows
- Transverse bedforms
- Gradational furrow spacing
- Meandering furrows
- Flutes
- Mudwaves
- Recirculation scour
- Upslope furrows
- Topographically isolated furrows
- Obstacle scour

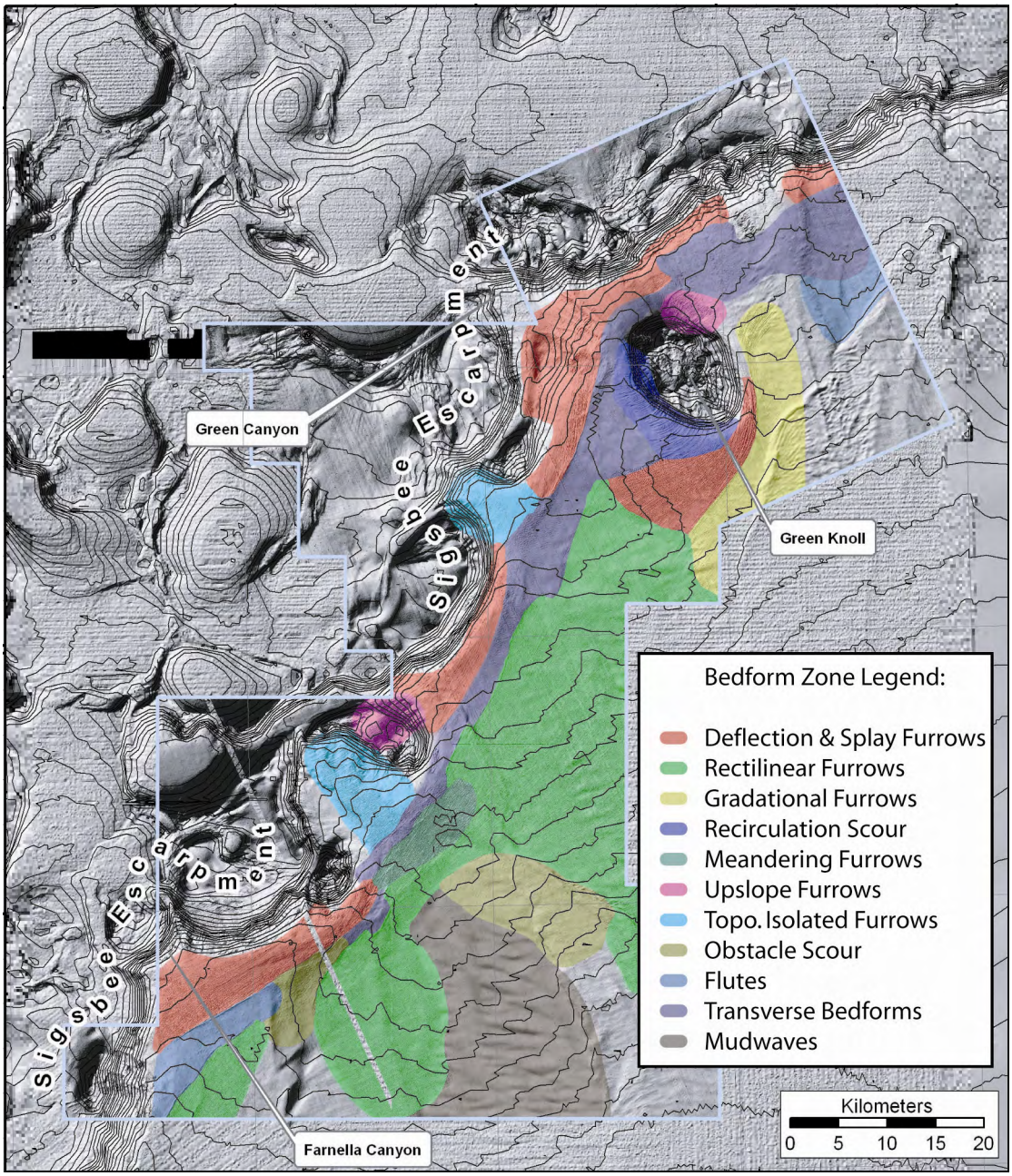

Fig. 8. Green Knoll Contour-Current Bedform Zones.
Overlain on the shaded bathymetry map of the Green Knoll region are the primary bedform zones identified based on general bedform morphology and distribution patterns from the 3-D seismic seafloor bathymetry. The lower resolution background image is generated from Seabeam data. Only the 3-D seismic data provides the resolution necessary to identify a majority of the bedform types.

In the results and discussion that follow, all data will be addressed from the perspective of these zones. To provide an overview of the zones, the basic morphological characteristics of the dominant zonal bedforms are summarized in Table 1 and Table 2. Each zone will be characterized using example bathymetry and profiles from the 3-D seismic data as located in Fig. 9, and cross-correlated when possible with the nearest high-resolution seismic data as identified by seismic line segment number in Fig. 10. Additionally, data from the jumbo piston cores and *DSV Alvin* dives (Fig. 6) will be used to refine and ground truth the interpretation of the two seismic datasets.

Table 1. Contour-Current Bedform Morphology 3-D / High-Resolution Comparison.
The bracketed values ([ ]) indicate measurements approximated by applying a 1/5 factor to the 3-D seismic data except for the largest spacings above 50 m.

		3-D Seismic Based Measurements			Deep-Tow Based Measurements		
Profile	Zone / Feature	Width (m)	Spacing (m)	Width:Spacing Ratio	Width (m)	Spacing (m)	Width:Spacing Ratio
A	Furrow Refraction	50-200	50-200	1:1	10-40	10-200	1:1 - 1:20
B	Furrow Splay	50-100	50-100	1:1	10-20	15-100	1:1 - 1:10
C	Furrow Refraction	50-200	50-200	1:1	[10-40]	[10-200]	[1:1 - 1:20]
D	Furrow Splay	50-100	50-100	1:1	[10-20]	[10-100]	[1:1 - 1:10]
E	Rectilinear Furrows	50-75	50-75	1:1	[10-15]	[10-75]	[1:1 - 1:8]
F	Rectilinear Furrows	50-75	50-75	1:1	[10-15]	[10-75]	[1:1 - 1:8]
G	Rectilinear Furrows	50-100	50-100	1:1	[10-20]	[10-100]	[1:1 - 1:10]
H	Rectilinear Furrows	50-100	50-100	1:1	10-25	10-120	1:2 - 1:12
I	Gradational Furrows	50-75	100-800	1:2 - 1:16	10-15	10-800	1:1 - 1:30
J	Gradational Furrows	50-75	50-100	1:1 - 1:2	[10-15]	[10-100]	[1:1 - 1:10]
K	Gradational Furrows	50-100	50-100	1:1	[10-20]	[10-100]	[1:1 -1:5]
L	Gradational Furrows	50-75	50-300	1:1 - 1:6	[10-15]	[10-300]	[1:1 - 1:30]
M	Recirculation Scour	50-250	50-250	1:1	10-50	10-250	1:1-1:5
N	Meandering Furrows	75-125	75-125	1:1	10-25	10-100	1:1 - 1:4
O	Upslope Furrows	50-125	50-125	1:1	[10-25]	[10-125]	[1:1 - 1:13]
P	Upslope Furrows	75-125	75-125	1:1	[15-25]	[15-125]	[1:1 - 1:8]
Q	Upslope Furrows	50-150	50-150	1:1	10-30	10-150	1:1 - 1:15
R	Topo. Isolated Furrows	50-125	50-125	1:1	[10-25]	[10-125]	[1:1 - 1:13]
S	Topo. Isolated Furrows	50-150	50-150	1:1	[10-50]	[10-150]	[1:1 - 1:15]
T	Obstacle Scour	100-200	100-200	1:2	[20-40]	[20-200]	[1:1 - 1:10]
U	Obstacle Scour	50-100	50-250	1:1 - 1:5	[10-20]	[10-250]	[1:1 - 1:25]
V	Flutes	50-250	50-500	1:1 - 1:10	[10-250]	[10-500]	[1:1 - 1:50]
W	Transverse Bedforms	100-200	100-200	1:1	100-200	100-200	1:1
X	Transverse Bedforms	75-100	75-100	1:1	75-100	75-100	1:1
Y	Mudwaves	1000-2500	1000-2500	1:1	[1000-2500]	[1000-2500]	[1:1]
Z	Mudwaves	1000-2500	1000-2500	1:1	[1000-2500]	[1000-2500]	[1:1]

Table 2. Contour-Current Bedform Morphology and Orientation.
The dominant flow direction is the general compass direction toward which the current is flowing as determined from the bedform indications. Estimated flow velocities are based both on where the bedforms fall within the erosional current marks described by Allen (1969) and estimated velocities for neighboring bedforms.

Profile	Zone / Feature	Relief (m)	Cross Section	Orientation (degrees)	Dominant Flow Direction	Estimated Flow Velocity (cm/s)
A	Furrow Refraction	1-10	Assymetric	(-10)-20	SW	20-45
B	Furrow Splay	1-3	Symetric	40-70	SW	20-30
C	Furrow Refraction	<1	Symetric	0-30	SW	>140
D	Furrow Splay	1-2	Symetric	30-55	SW	>140
E	Rectilinear Furrows	1-4	Symetric	40-55	NE / SW	20-30
F	Rectilinear Furrows	1-4	Symetric	45-55	NE / SW	20-30
G	Rectilinear Furrows	1-4	Symetric	30-40	NE / SW	20-30
H	Rectilinear Furrows	1-4	Symetric	35-45	NE / SW	20-30
I	Gradational Furrows	<1	Symetric	20-50	SW	<20
J	Gradational Furrows	<1	Symetric	5-40	SW	<20
K	Gradational Furrows	1-4	Symetric	10-40	SW	<20
L	Gradational Furrows	<1	Symetric	30-40	NE	<20
M	Recirculation Scour	1-4, 5-20	Variable	60-80	NE	>85
N	Meandering Furrows	2-4	Symetric	30-40	NE / SW	30-45
O	Upslope Furrows	<2	Symetric	50-80	SW	>85
P	Upslope Furrows	2-10	Symetric	50-80	SW	>85
Q	Upslope Furrows	1-4	Symetric	40-50	SW	20-45
R	Topo. Isolated Furrows	1-4	Symetric	60-65	SW	20-45
S	Topo. Isolated Furrows	<1	Symetric	25-40	SW	20-45
T	Obstacle Scour	<2	Variable	40-50	NE / SW	20-30
U	Obstacle Scour	<2	Variable	50-60	NE / SW	60-140
V	Flutes	<2	Variable	40-50	SW	60-85
W	Transverse Bedforms	<2	Assymetric	140-170	NE	85-140
X	Transverse Bedforms	<1	Assymetric	130-150	NE / SW	85-140
Y	Mudwaves	5-20	Assymetric	80-90	NE / SW	15-30
Z	Mudwaves	2-15	Assymetric	90-100	NE / SW	15-30

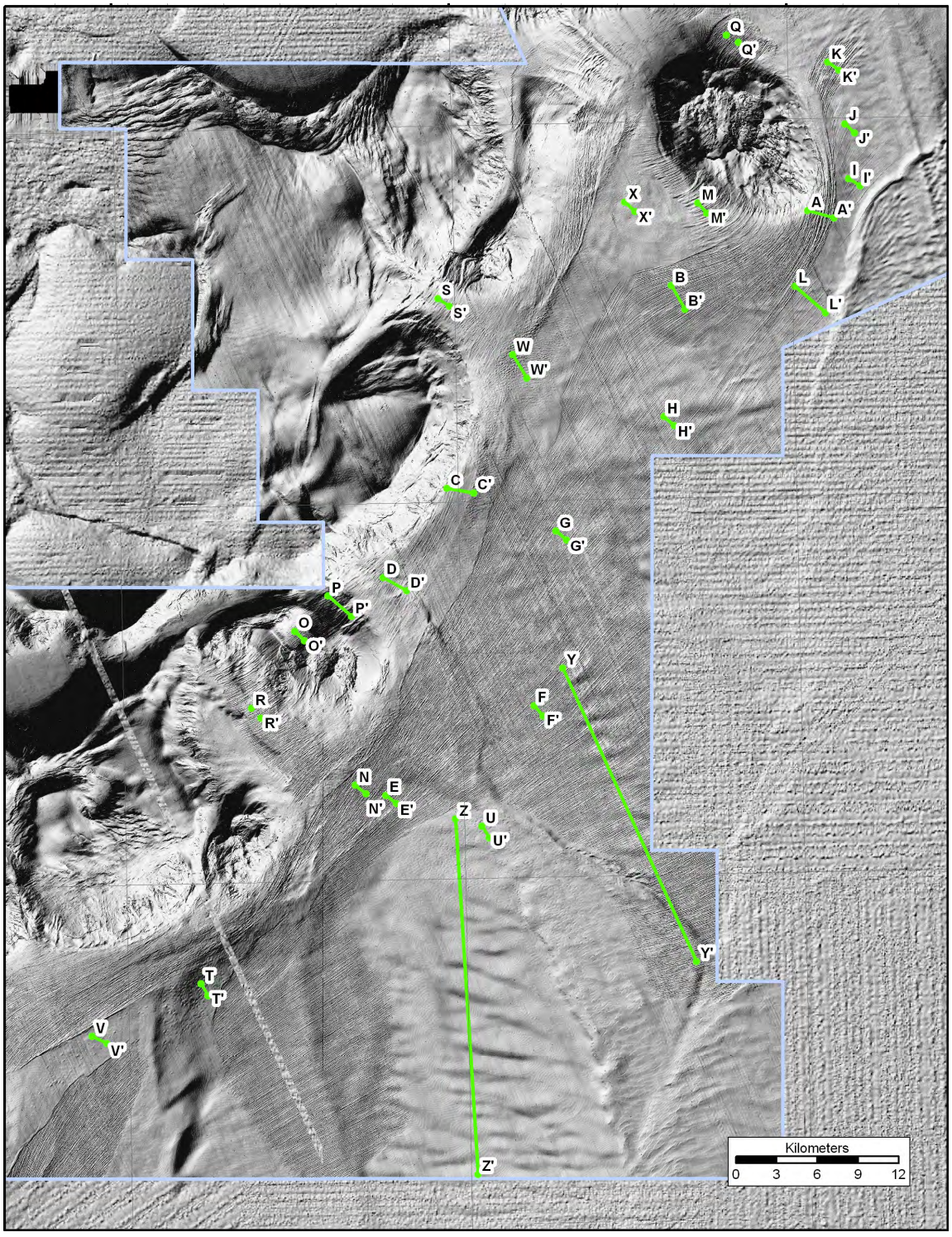

Fig. 9. 3-D Seismic Profile Locations.
Shaded bathymetry of the Green Knoll study area is shown with location and letter designations of 3-D seismic bathymetry profiles (green lines) that will be used to characterize the various bedform zones.

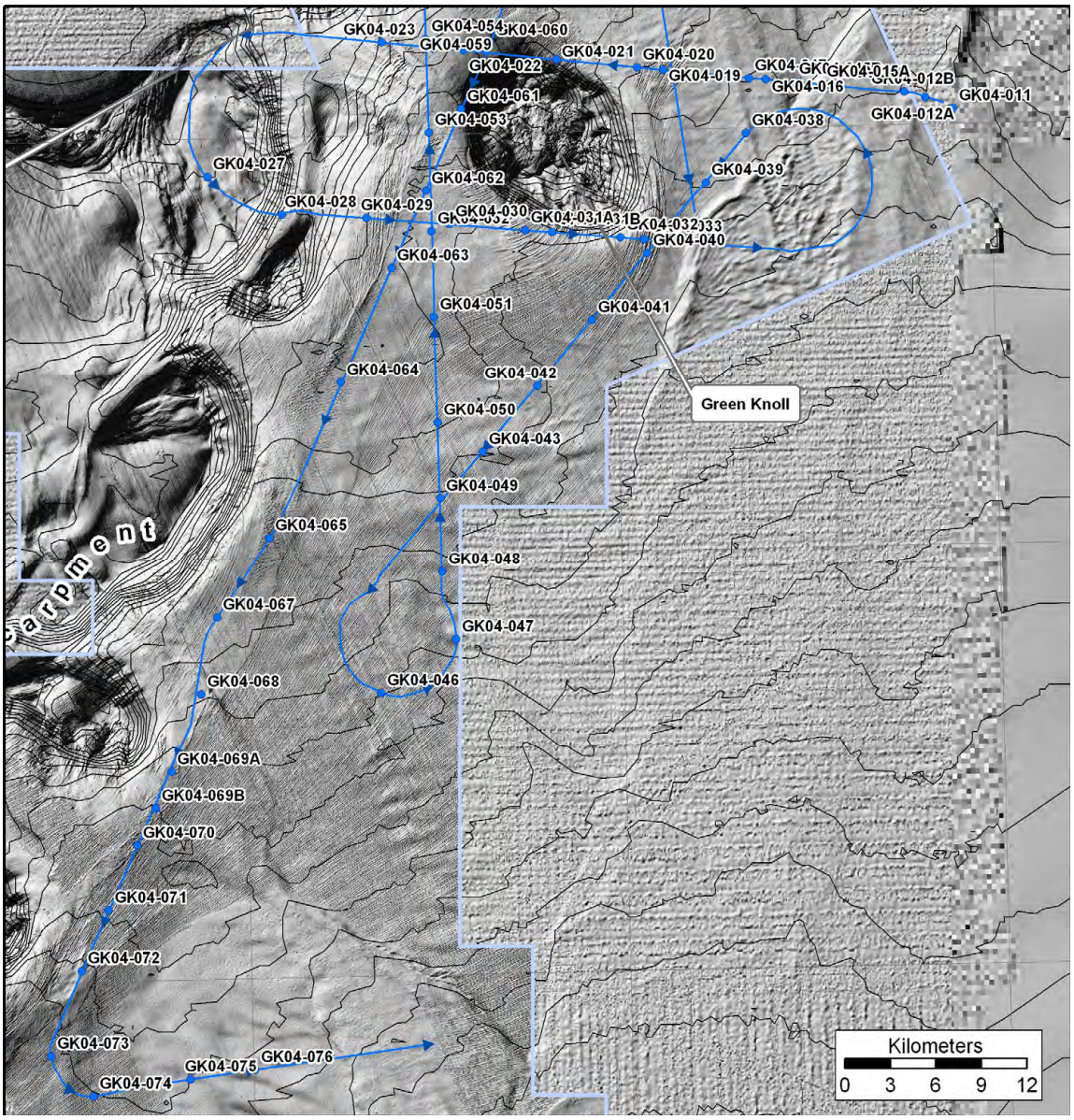

Fig. 10. Deep-Tow Profile Location Map.
The blue line indicates the cruise track and data location of the GK04 deep-tow seismic cruise with blue arrows indicating the direction of travel. The labeled blue dots indicate the location of the start of each seismic data segment or profile. The last three digits of each profile label will be used to identify the profile in subsequent figures and the text.

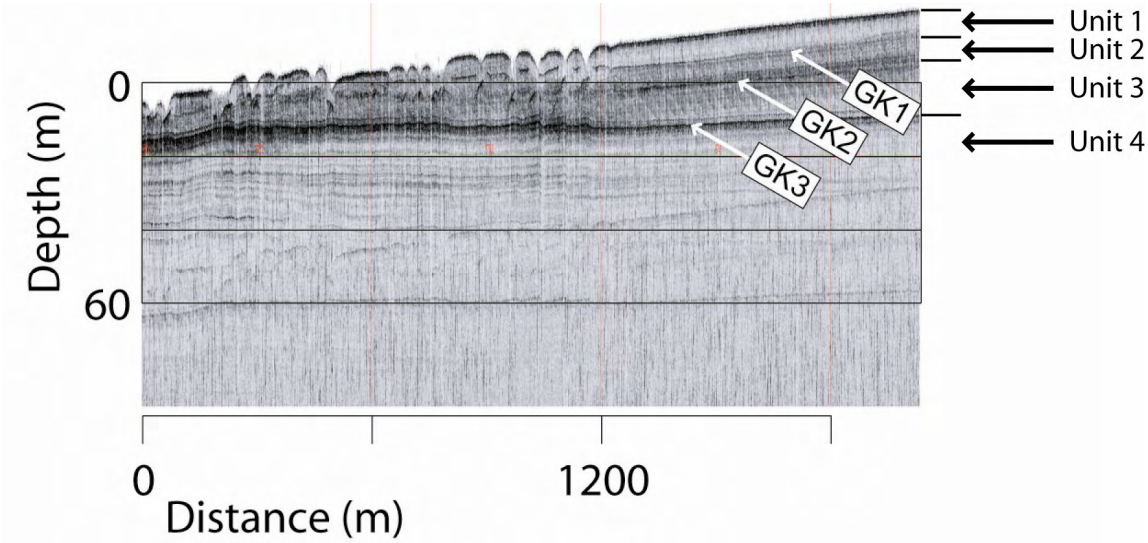

Fig. 11. Example Deep-Tow Subbottom Profile.
A typical deep-tow subbottom profile is shown with the primary marker beds (GK1, GK2, and GK3) along with their associated depositional units (Unit 1 – Unit 4).

As a means of reference for the deep-tow subbottom data, three primary seismic reflectors can be identified along with their associated sedimentary layers throughout the study area (Fig. 11). Although not always present, the marker beds (GK1, GK2, and GK3) will be identified when possible in the deep-tow subbottom records. Horizons GK1 and GK2 tend to be variable in character, making them more difficult to identify in some seismic segments. Horizon GK1 is a low amplitude reflector that marks the base of a thin reflector-free zone (Unit 1) and often outcrops at the walls of furrows. Horizon GK2 is a medium amplitude reflector that often appears as a doublet and frequently marks the base of furrow erosion. Unit 2 is typically reflector free, or contains few very low-amplitude returns. The most persistent of the reflectors across the study area is horizon GK3. The GK3 reflector can be identified as a triplet having a strong central high-amplitude return that is bounded on the top and bottom by two thinner high-

amplitude returns. Unit 3 (above GK3) typically has a fair number of low-amplitude reflectors, while Unit 4 (below GK3) is usually parallel bedded with numerous medium-amplitude reflectors. These unique characteristics allow GK3 to be most easily identified throughout the records.

Regarding the seismic data, it is important to note that there is a distinct difference in the morphology of bedforms as characterized by the 3-D seismic data and the high-resolution deep-tow data. The high-resolution data inherently collects data that is better able to resolve the details of the seafloor and subbottom, but lacks overall coverage. Given a center frequency of 4.5 kHz on the chirp subbottom transducer and a water velocity of 1500 m/s, one wavelength is equivalent to 0.33 m. Also, given that typical resolution for a given frequency is $^1/_4$ to $^1/_8$ of the wavelength (Sheriff, 1977), the vertical resolution of this high-resolution seismic data is theoretically better than 0.1 m. Additionally, the lateral resolution, based on a towfish speed of 2.5 knots is 0.68 m. In contrast, the best lateral resolution possible for the 3-D seismic data is 12.5 m by 20 m, and the horizons used by this study are gridded at 15 m. Vertically, the theoretical resolution of the 3-D seismic data is more difficult to determine because of the use of multiple channels, multiple geometries, and extensive data processing. Consequently, the best practical way to assess the 3-D seismic vertical resolution is by comparison to the high-resolution seismic data (Fig. 12). Evaluation of co-located high-resolution and 3-D seismic data shows that the 3-D data accurately represents the general relief of the group of features and the large-scale spacing; however, the 3-D data misrepresents the

details of individual bedforms both laterally and vertically. Thus, the resolution of the 3-D seismic data inherently smoothes all surfaces, both vertically and horizontally.

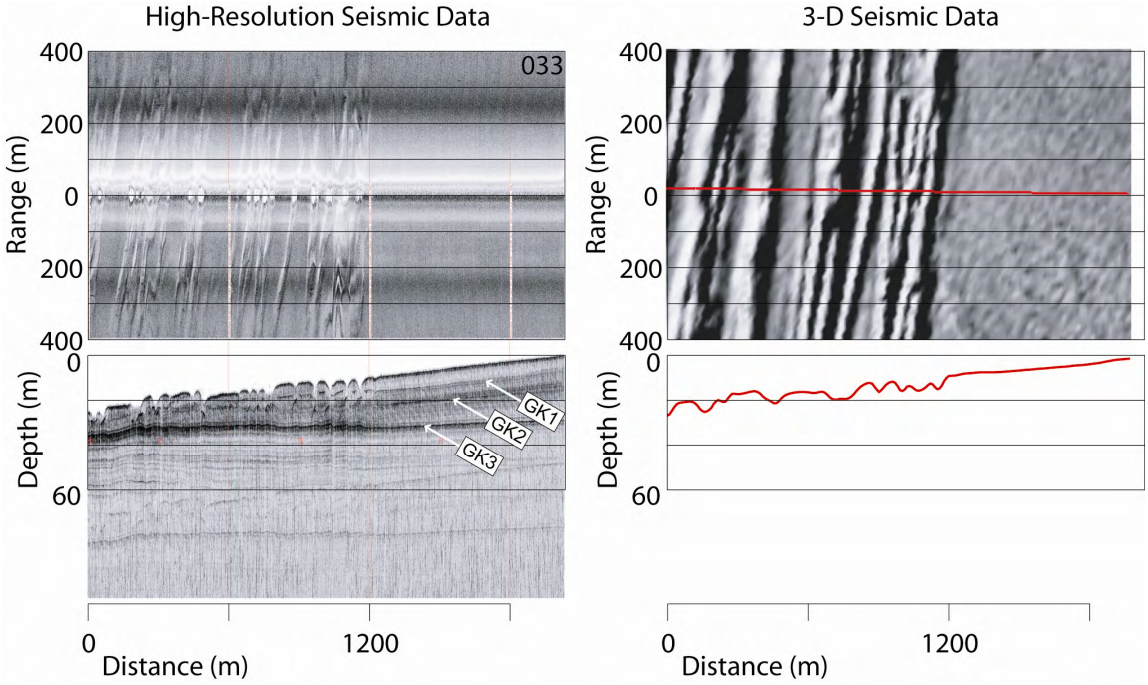

Fig. 12. Deep-Tow vs. 3-D Seismic Resolution Comparison.
The left panel shows deep-tow seismic profile 033 with sidescan on top and subbottom on bottom. The right panel shows the co-located 3-D seismic data with shaded bathymetry on top and the corresponding bathymetric profile (red line) on bottom. The 3-D seismic data picks up the overall relief and large-scale spacing, but misrepresents the detailed relief and small-scale spacing of individual features.

Despite being a surface towed system subject to spherical spreading and comprised of a lower frequency air gun pulse than the deep-tow pulse, and processed with only a 4 ms sample rate, the fact remains that the 3-D seismic data does image these very small contour-current bedforms (Fig. 12). Two key factors play into this ability to resolve such small features: 1) the acoustic response of a feature much smaller than any given grid cell can dominate the acoustic return for that cell, and 2) features with lateral

continuity across multiple grid cells increase the chances of creating an interpretable seismic signature. A specific example of these concepts could be seen when the surface-towed $[TAMU]^2$ sidescan sonar system resolved 4 inch layout cables in 1000 m of water because the acoustic contrast of the cable dominated single grid cells and the cable was laterally continuous allowing it to be interpreted (Hilde et al., 1991). So, we have shown that both the 3-D seismic data and high-resolution data can resolve the contour-current bedforms; however, the ability to resolve details is much better for the deep-tow data than the 3-D seismic data, while the coverage of the deep-tow data is much more limited as compared to the 3-D seismic data. This is the essence of why these two datasets are both complimentary and necessary to provide a complete picture of the contour-current bedforms.

The seismic resolution difference becomes critical as we consider the detailed morphology of the contour-current bedforms. An example of the resolution difference can be seen by comparing two images of the main furrow field as recorded by the 3-D seismic data and the deep-tow data (Fig. 13). If we considered only the 3-D seismic data, the furrow field has the appearance of a smoothly undulating surface with relatively evenly spaced furrows of equal dimension forming a sine-like cross-sectional profile; however, the high-resolution deep-tow data reveals something quite different in the details. Rather than being evenly spaced 50-100 m wide furrows, the furrows are actually only 10-20 m wide with a highly variable 10 – 120 m spacing; giving rise to a width-to-spacing ratio as high as 1:12. The vertical resolution of the 3-D data is sufficient to define the existence of these very low relief features, but underestimates the

relief by 1-2 m. Furthermore, the horizontal resolution causes the furrows to appear much broader and more regular than in reality. This critical limitation of resolution must always be kept in mind when considering the 3-D data.

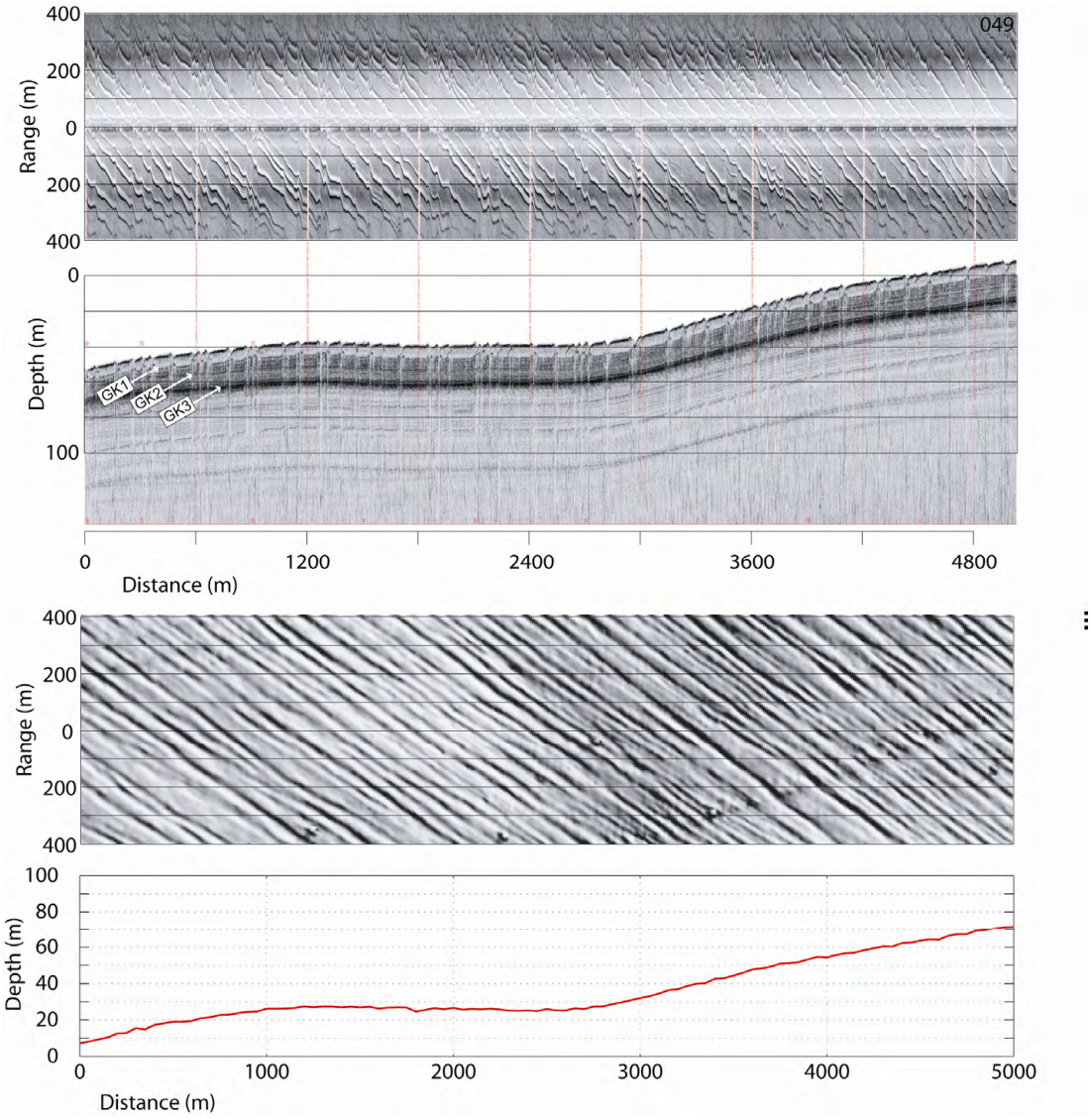

Fig. 13. Main Furrow Field Deep-Tow vs. 3-D Seismic Resolution Comparison.
The upper panel shows deep-tow seismic profile 049 with sidescan on top and subbottom on bottom. The right panel shows the co-located 3-D seismic data with shaded bathymetry on top and the corresponding bathymetric profile (red line) on bottom. The 3-D seismic data slightly underestimates the furrow relief, smoothes the furrow profiles, and misrepresents the details of furrow spacing and the furrow field.

Based on multiple comparisons, the dimensional relationships between the different seismic datasets appear to hold. Furrows that are 10 m apart or less are easily resolved by the high-resolution deep-tow data, but the 3-D data tends to merge these furrows into a single feature. Conversely, furrows that are >50 m apart are resolved by both the high-resolution and 3-D seismic data. Consequently, the deep-tow based measurements in Table 1 that are between brackets are based on an empirical relationship where actual feature dimensions can be estimated as $^1/_5$ the bedform dimensions determined via 3-D seismic data. And, bedform spacings above 50 m determined from the 3-D seismic data are considered valid. As such, this paper will use the width and spacing measurements based on deep-tow data for all morphological descriptions.

The 3-D data not only provides a detailed bathymetry of the region, but the relative amplitude of the seafloor return can also be mapped (Fig. 14). A broad look at the relative amplitude values for the region reveals that the areas closest to the highest slopes also have the highest amplitude return. The higher amplitudes are interpreted to be caused by either a change in sediment type, or an exposure of deeper, previously compacted layers. Since the dominant sediment source on the continental slope and rise is hemipelagic sedimentation, it is expected that the major cause for relative amplitude changes across the region is sediment exposures. This is certainly likely along the flanks of the Sigsbee Escarpment and Green Knoll as the salt uplifts have exposed previously buried sedimentary layers (Fig. 7); however, this does not explain the higher amplitude

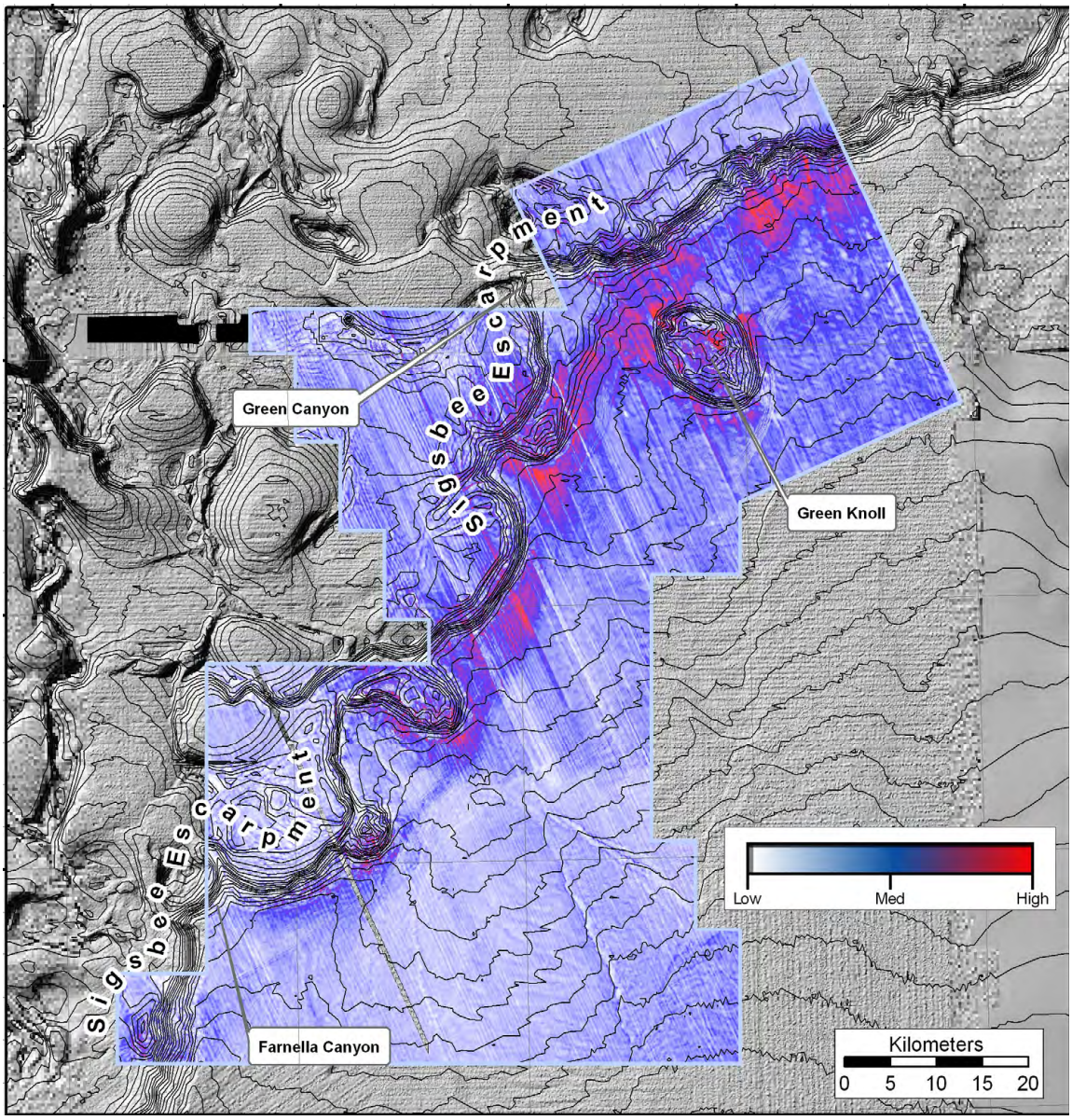

Fig. 14. 3-D Seismic Seafloor Amplitude.
Above is shown a map of the relative amplitude of the 3-D seismic seafloor horizon picked from the peak amplitude of the first return. In general the areas closest to the steepest slopes have the highest amplitude, as would be expected from slumps, outcropping layers, and eroded surfaces.

at the base of the escarpment and knoll. The high amplitude reflections at the base of the escarpment have two possible interpretations (Lee and George, 2004): 1) slumps and debris flows from the flanks of the Sigsbee escarpment, and 2) erosional exposure of

older sediments. The erosional exposure of older sediments naturally would support the idea of erosional contour currents flowing around the topographic relief of the seafloor.

Deflection and Splay—Green Knoll

The deflection and splay pattern that occurs around Green Knoll is one of the most prominent features of the shaded bathymetry of the study area (Fig. 15). The pattern of furrowing clearly preserves the deflective nature of bottom currents around the significant topography of Green Knoll. Currents moving from northeast to southwest are intensified as they encounter the relief of the knoll. This leads to a highly compressed region of flow around the southern side of the knoll. After accelerating around the knoll, the flow separates from the knoll topography and the furrows preserve a record of the splaying pattern as the currents spread laterally across the continental rise and away from Green Knoll. An excellent summary of flow past three-dimensional obstacles is given by Baines (1995). Some of the key features of flow past an obstacle are: 1) compression of streamlines around the obstacle, 2) flow intensification and deflection around the obstacle, 3) flow separation coming over the top of the obstacle, 4) recirculation vortices in the lee of the obstacle, 5) generation of helical vortices in the lee of the obstacle, and 6) turbulence and vortex shedding downstream of the obstacle. Each of these features is preserved via the bedforms surrounding Green Knoll. The deflection and splay zone is one example and additional examples will be presented as the remaining bedform zones are discussed.

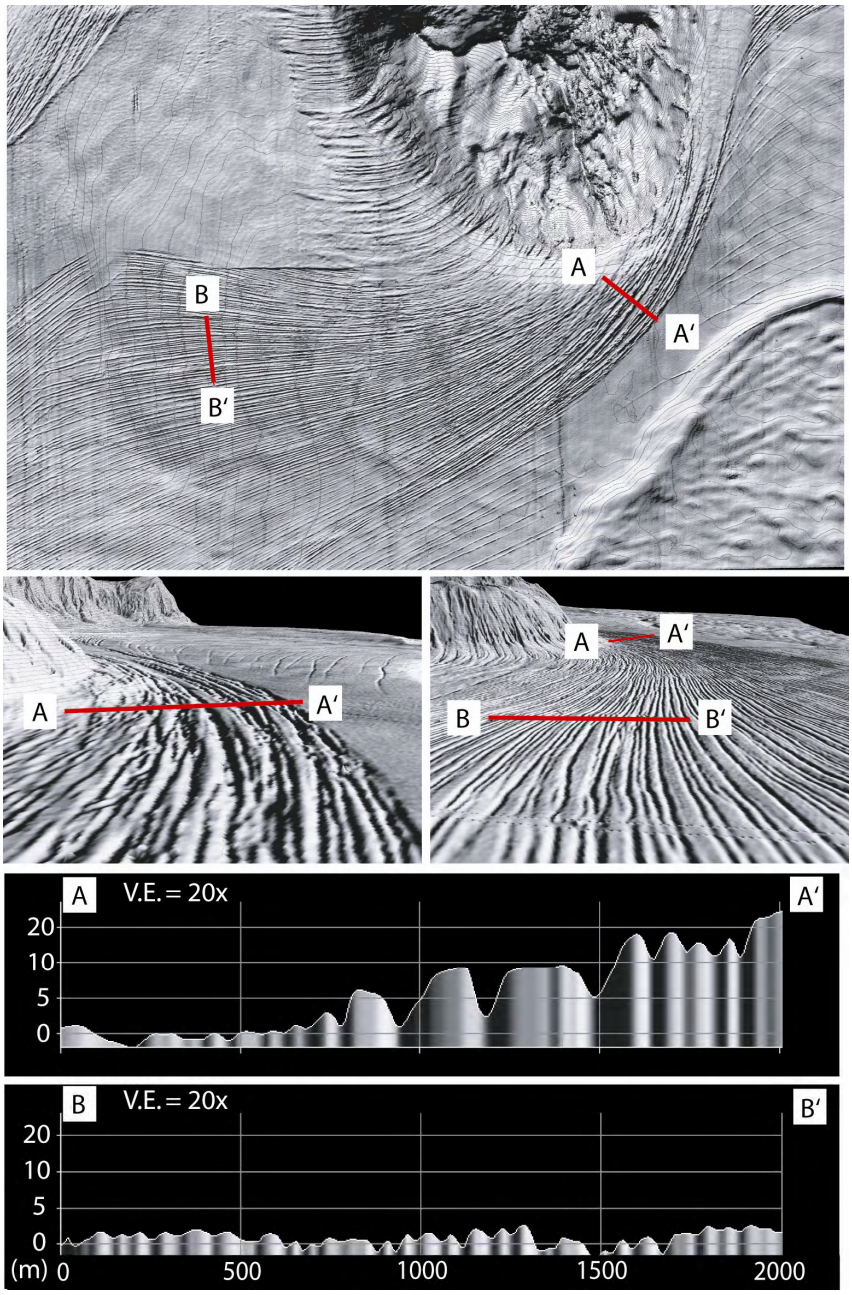

Fig. 15. 3-D Seismic Bathymetry and Profiles A&B of the Green Knoll Deflection and Splay Zone. Moving from top to bottom, the first panel shows a plan view of the shaded 3-D seismic bathymetry of the deflection and splay bedforms adjacent to Green Knoll with profiles A and B indicated (North is up). Contour lines are at 10m intervals. The next two panels show a perspective view of the bathymetry and profiles. The bottom two panels show the cross-sectional shaded bathymetry profiles for lines A and B. The vertical exaggerations on both bathymetry profiles are 20x. All subsequent 3-D seismic bathymetry and profile imagery will follow this format with changes in scale and vertical exaggeration indicated on the images. The most extensive erosion of furrows in the entire study area is seen on the outer edges of the deflection zone indicated by A-A′. The splay zone (B-B′) shows much less relief and more linear furrows.

The data reveal several key characteristics of the Green Knoll deflection and splay zone (Fig. 15). The deflection zone on the southern side of Green Knoll is characterized by furrows having the largest relief of the entire study area (1-8 m). Line A-A′ shows the furrow width, spacing and relief to be somewhat variable in the zone of highest deflection. The furrow profiles appear slightly asymmetric with the steeper walls on the north side of a given furrow. Plus, the deflecting furrows sweep through a directional change of 30° and up to an additional 50° if the splay zone is also considered. Interestingly, this area with such large deep and wide furrows simply stops at 2 km distance from the knoll; the seafloor becomes flat, featureless and uneroded. Additionally, the bathymetry exhibits a moat at the base of Green Knoll that coincides with the extent of the erosion and splay region (Fig. 15).

The deep-tow seismic data (Fig. 16 and Fig. 17) confirms the furrow widths to be 10-40 m, furrow spacing to vary widely between 10 and 200 m, and the resulting width:spacing ratio to be between 1:1 and 1:20. The sidescan data clearly shows the furrow pattern around the knoll and the extremely abrupt change between furrowed and non-furrowed regions of the seafloor. The high-resolution sidescan further confirms the flat, featureless character to the seafloor outside the furrowed deflection zone. It is important to note that the sidescan data is able to pick up subtle furrow stringers that are less than 10 m wide and less than 2 m deep and run between the major furrows of the region. These are interpreted as relatively young furrows that develop from subtle shifts in the currents as they move around the knoll.

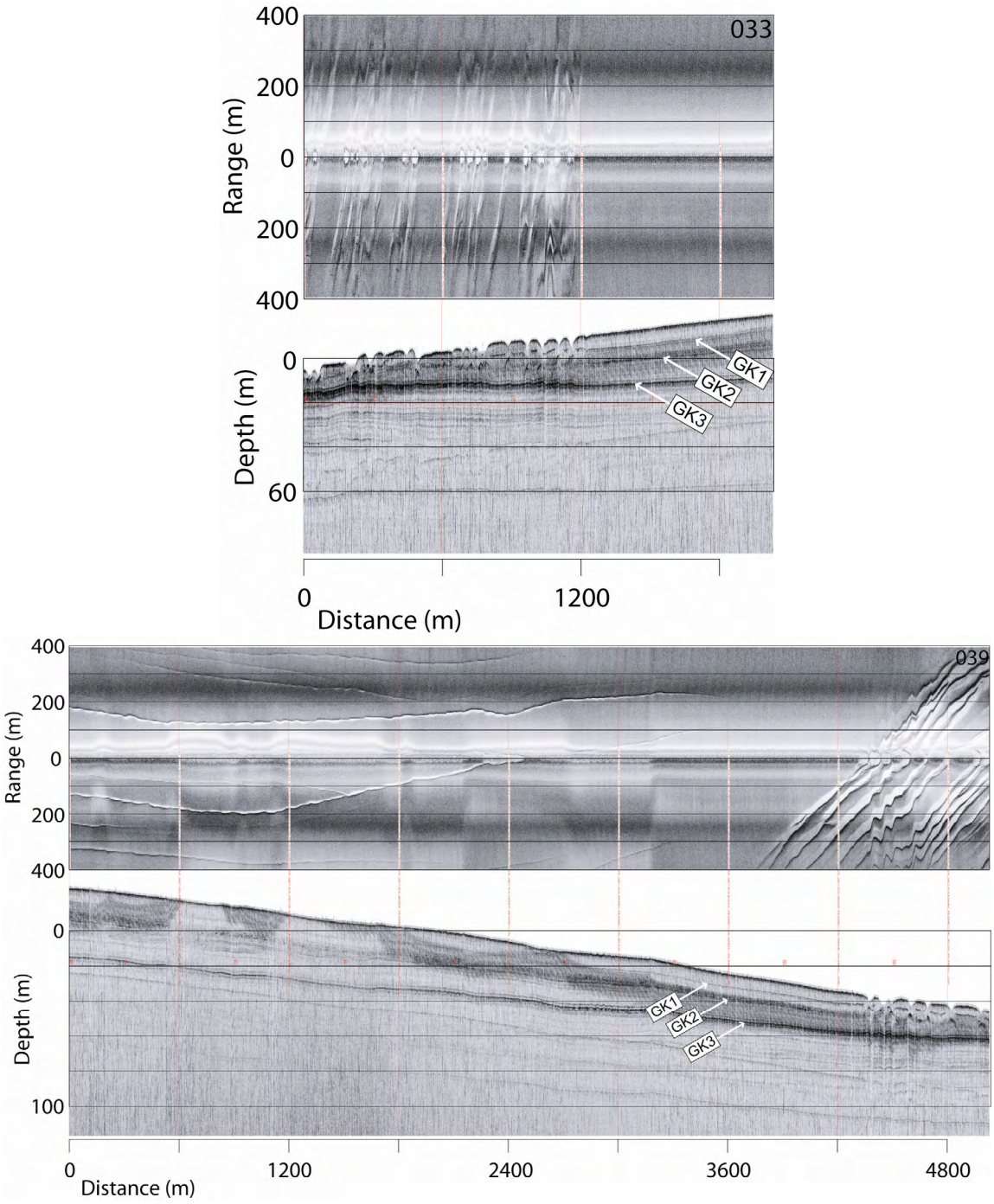

Fig. 16. Deep-Tow Profiles 033 and 039 across the Green Knoll Deflection Zone.
For each profile shown, the upper record is sidescan with the polarity set to: high amplitude = black and low amplitude = white. The lower record is subbottom profile with marker beds identified. The profile number is indicated on the upper right hand corner of each image. The location of the profile can be found on Fig. 10. All subsequent deep-tow imagery will follow this same scheme. The beds can be seen to thin toward Green Knoll and the furrows erode down to horizon GK2.

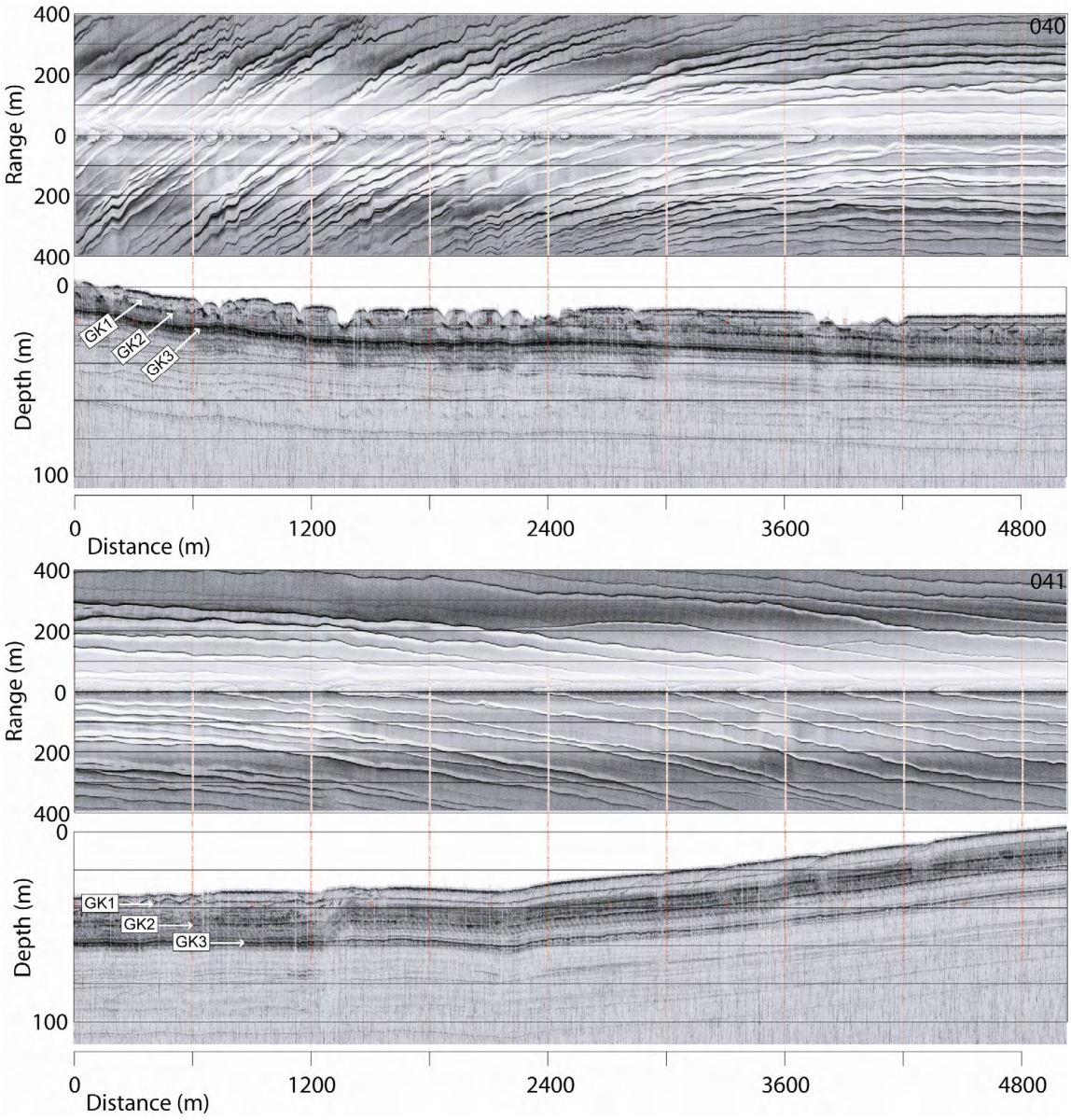

Fig. 17. Deep-Tow Profiles 040 and 041 across the Green Knoll Deflection and Splay Zone.
The deflective nature of the furrows and the increasing furrow separation of the splay can be seen on the sidescan profiles. Erosion in the deflection zone is down to horizon GK2 while erosion in the splay zone is only down to horizon GK1. Note that some of the subbottom signature is actually picking up the undulatory side echoes of furrows near the sidescan nadir.

The subbottom data from the deflection and splay zone contains all three marker beds that have been identified for the survey area. Horizon GK1 outcrops on the furrow walls and GK2 marks the maximum depth of furrow erosion in this zone. The moat around Green Knoll results from a thinning of Units 1-3. Unit 1 thins from 4 m down to 3 m. Unit 2 pinches out completely from 3 m. And, Unit 3 thins from 7 m to 3 m. The thinning of beds around Green Knoll onto a flat-lying horizon, suggests preferential deposition under decreasing currents as the distance from the higher velocity core of the currents flowing around Green Knoll increases. The fact that the furrows exist in these thinned beds results from three possible options: 1) the furrows were syn-depositional with the thinning sequence, 2) the furrows eroded into a previously existing thinned sequence, or 3) a combination of both. The profiles of the furrows most closely match the Type 1C furrow of Flood (1983) with steep erosional walls and common central ridges in the furrow floors. This type of furrow is typically found in regions where erosion equals or exceeds deposition.

Significantly, the deflection zone appears to be the only area where furrows have anything resembling an asymmetric profile. The apparent asymmetry may stem from two possibilities: more intensive erosion due to increased bathymetric intensification of the current closer to the knoll and a thickening of the surface beds away from the knoll that leads to the appearance of asymmetry.

The Green Knoll furrow deflection zone is also one of the sites of the *DSV Alvin* dives (#3629, Fig. 6). This allowed us the opportunity to truly ground truth some of the seismic data and develop more of the details of furrow formation and maintenance in the

region. Several key features were identified (Fig. 18). The non-furrowed region to the south of the deflection zone was further confirmed, so that at 3 levels of resolution (3-D seismic, high-resolution seismic, and visual) the non-furrowed region appears as an undisturbed, flat, featureless, hemipelagic sedimentation. Many of the furrows contained a central ridge down the axis of the furrow and the existence of heavily eroded, residual walls between furrows suggests that the origin of the central ridge may be the merging of two furrows and eventual removal of the adjoining wall. Additionally, the furrow walls were confirmed to be quite steep and approached 90° in places. The only way to maintain such a high angle in the soft muds of the region is have situation of constant scour and erosion. Current indicators were also common within the furrows themselves: crescent shaped arrangement of sand-sized particles, obstacle scours, biogenic extensions bending in the current, and foram sand ripples.

Of particular interest are the foram sand lag deposits common in the axis of the furrow and high concentrations of pteropod shells both in the furrow axis and along the furrow walls (Fig. 18). The presence of a central lag deposit supports the furrow formation mechanism suggested by Flood (1983), where coarser material is concentrated in the convergent region between helical flow cells. This concentration of larger grain sizes performs two functions: it tends to lock in the helical flow pattern (Embley et al., 1980; McLean, 1981; McLelland et al., 1999; Pantin et al., 1981), and it provides a mechanism for enhanced erosion in the convergent region (Allen, 1969; Flood, 1983; McLelland et al., 1999). Considering the amount of sand that could be concentrated

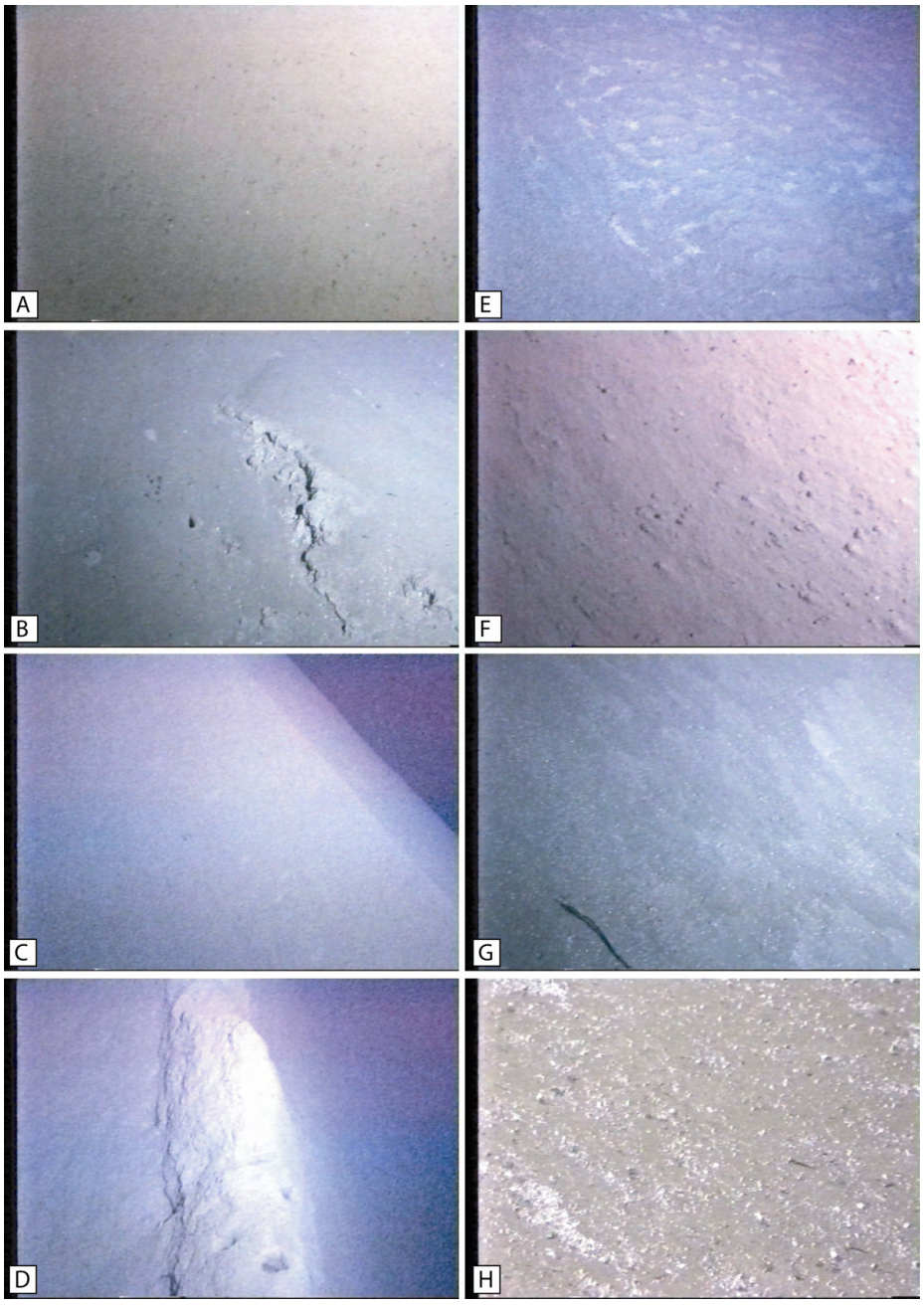

Fig. 18. Green Knoll Alvin Dive Imagery.
Images from *DSV Alvin* dive #3629. (A) Featureless region outside the furrow deflection zone. (B) Typical central ridge at the axis of a furrow. (C) Steep walls between adjacent furrows. (D) Highly eroded wall between furrows—possible origin of furrow central ridge identified in B. (E) Foram sand ripples within a furrow containing high concentrations of pteropod shells. (F) Obstruction scour current indicators on a furrow wall. (G) Current indications on a furrow floor. (H) Large numbers of pteropod shells found on furrow walls and floors contribute significantly to erosion.

during the erosion of an 8 m furrow, it is not surprising that the central axes of the furrows form lag deposits. The lag deposits often formed fields of ripples that were up to 5 cm high and several meters wide covering the axis of the furrows. Furthermore, the depth of these furrows and the presence of ripples in the foram sand lag deposits suggests that a flow regime different from the helical cell formation mechanism may exist within the furrows themselves.

The pteropod shells were highly significant, both as current indicators and as part of the erosion process. Along the furrow walls, the pteropod shells were arranged in linear bands at a 45° angle down the slope of the wall with the base of the band being in the downstream direction of the current. This is a classic example of the balance between gravity and current, where gravity would tend to move the pteropod shells straight down the face of the wall and the current would tend to move the pteropod shells straight along the face of the wall—the net result being a band of pteropod shells at a 45° angle down-slope and down-current. Again this suggests the possibility of a different flow regime within the furrows than above the furrows. Close examination of the foram sands and particularly the pteropod shells revealed their importance in the erosion process. The large size-to-mass ratio made them particularly susceptible to saltation by the strong currents that were flowing within the furrows. The impact of the shells and tests during the saltation process was observed to knock loose significant sized aggregates (>1cm in many cases) from the furrow walls. In a study of saltation effects, this ballistic momentum transfer was found to contribute up to 3.5% to the total transported load (Amos et al., 1998). The saltation effects appear to permit the

breakdown and entrainment of clay aggregates at lower flow velocities than may be predicted for a simply cohesive clay system with no sand sized particles. Thus, when considering the erosion rates of furrows, it will be important to take into consideration the increased erosion rates resulting from intensive saltation by lag deposits of larger grain-sized particles within the furrows and particularly along the walls of the furrows.

Deflection and Splay—Sigsbee Escarpment

The topographic effects of Green Knoll that result in furrowing may be different than those of the Sigsbee Escarpment since the knoll is an isolated obstruction that sits further from the high-velocity core of the contour current that is presumed to track the more continuous and extensive contours of the Sigsbee Escarpment. There are several deflection and splay zones along the escarpment as individual sections of the escarpment appear to protrude into the main current flow (Fig. 8). In all cases the deflection and splay pattern indicates a northeast to southwest current flow direction along the escarpment. Also, the 3-D seismic data reveals a high amplitude pattern at the base of the escarpment that coincides with each of the deflection and splay patterns. The higher amplitude in the Sigsbee Escarpment zones as compared to the analogous Green Knoll zone, suggests the exposure of more consolidated, older sediments in the Sigsbee zones—a sign of more intensive erosion near the escarpment than near the knoll. This would be consistent with the assumption that the high-velocity core of the contour current parallels the bathymetry of the Sigsbee Escarpment and velocities decrease with distance from that core.

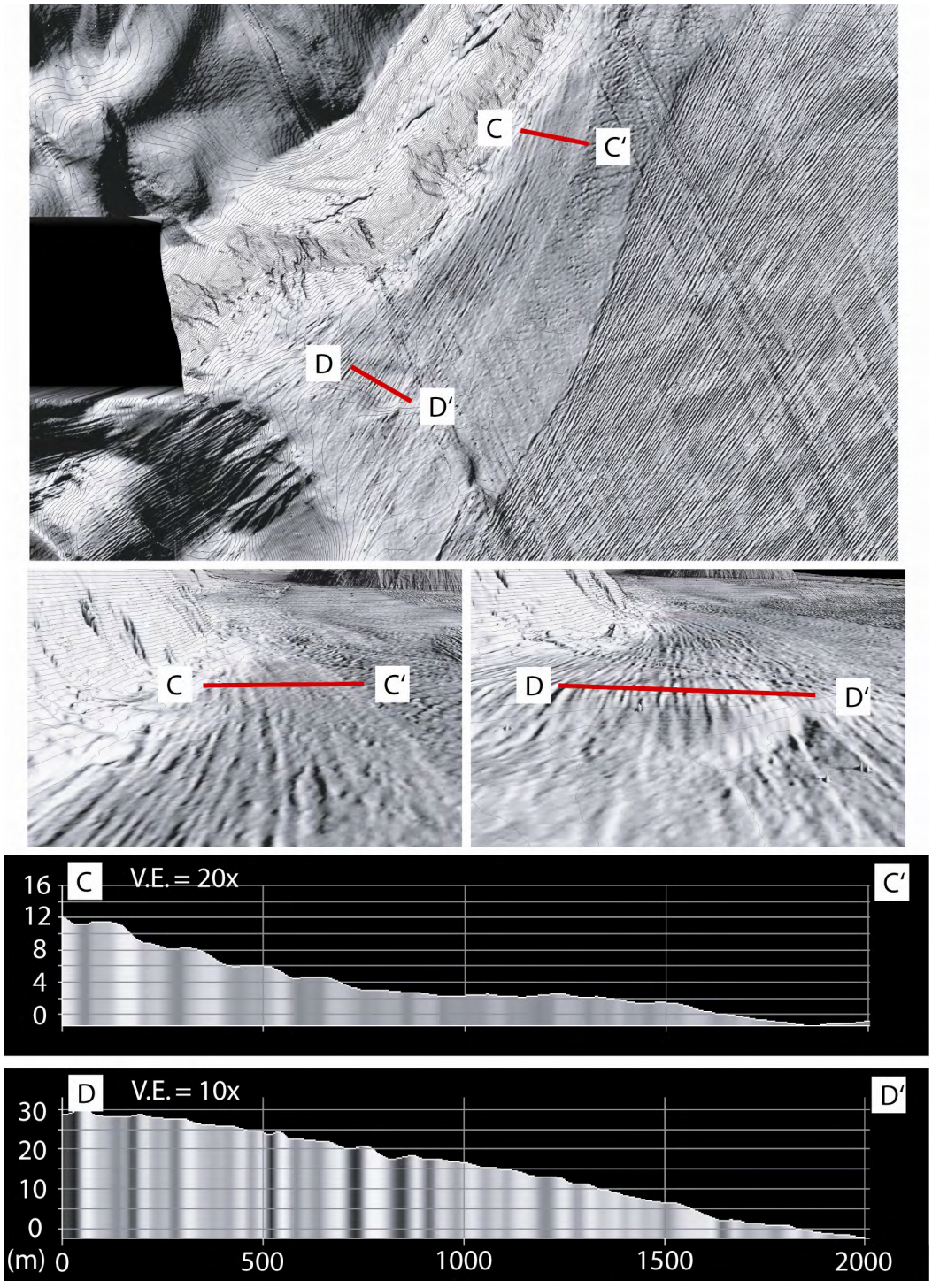

Fig. 19. 3-D Seismic Bathymetry and Profiles of the Sigsbee Escarpment Deflection and Splay Zone. Note the vertical exaggerations as indicated. Comparing these profiles with the Green Knoll deflection and splay zone (Fig. 15) shows much less relief due to removal of upper soft sediments and exposure of highly consolidated deeper sediments.

On the 3-D seismic seafloor bathymetry, the furrows of the Sigsbee deflection and splay zones are relatively easy to pick out due to the shading (Fig. 19); however, the relief of these furrows is less than 2 m in the splay and less than 1 m in the deflection area. Consequently, the furrows of the deflection are poorly defined and increase in definition through the splay zone. As with the Green Knoll region, the Sigsbee deflection zone is tightly compressed around the escarpment and the furrows pass through a 30° change orientation; however, the splay zone adds only an additional 25° change in orientation, which is less than the Green Knoll splay. This subtle difference in orientation range is most likely due to the deflection limit forced by the continuous presence of the escarpment, whereas the Green Knoll splay opens onto a flat seafloor with no constricting topography. Also similar to the Green Knoll zone, the deflection zone has a sharply defined boundary with the adjacent seafloor. However, the adjacent seafloor in this case is not flat and featureless, but is a transverse bedform zone that will be discussed below.

Deep-tow records GK04-029 (Fig. 20) crosses a similar Sigsbee deflection and splay zone to the northeast of that depicted in Fig. 19. The furrow characteristics are also similar with widths of 10-40 m, spacings ranging from 10-200 m, and relief of less than 2 meters. The abrupt transition between furrows and transverse bedforms also exists. The most striking information comes from the subbottom data. Horizon GK1 does not exist in this region and horizon GK2 eventually pinches out onto GK3. Furthermore, the furrows only appear to erode into Unit 3. The transverse bedform zone is defined by the exposure of Unit 2 and the deflection and splay zone is defined by the exposure of Unit

3. As the furrows move up the base of the Sigsbee Escarpment, Unit 3 pinches out completely, leaving Horizon GK3 exposed. Significantly, the currents appear to be unable to erode furrows into the GK3 horizon, as the limit of visible furrowing coincides with the complete removal of all sediments above GK3 (Fig. 21).

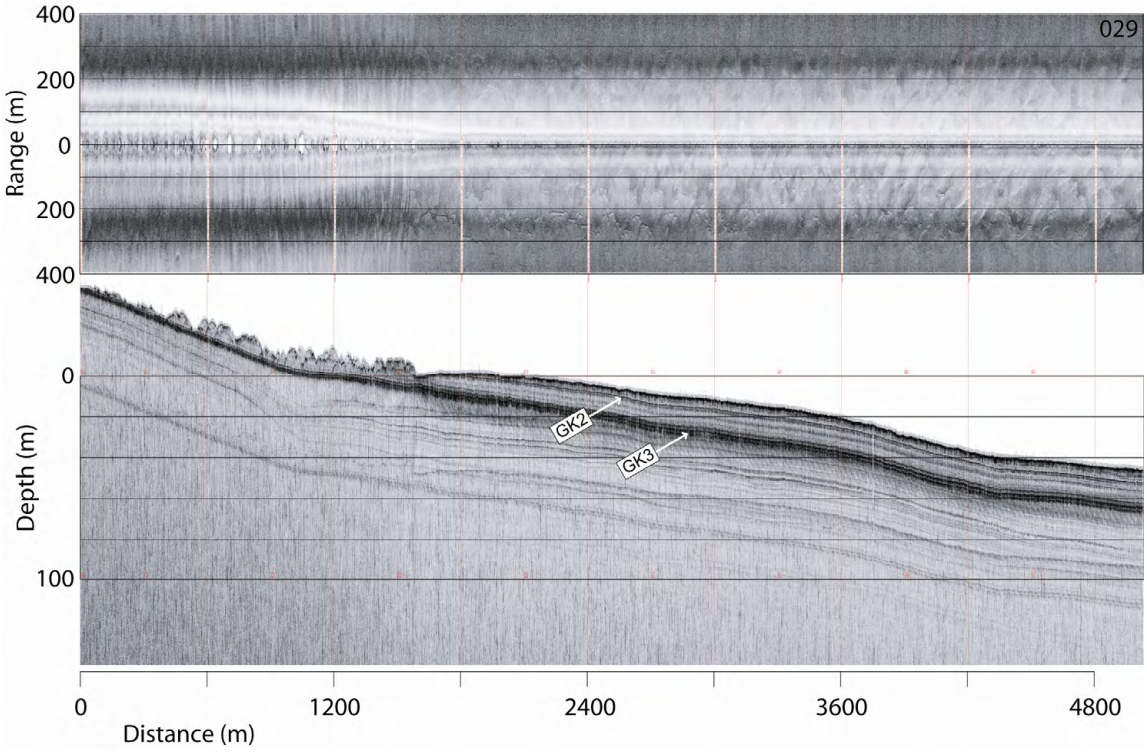

Fig. 20. Deep-Tow Profile 029 of the Sigsbee Deflection and Splay Zone.
The furrows are only eroded into Units 1 and 2. Horizon GK3 marks the maximum depth of furrow erosion. The subbottom furrow geometry appears to be distorted by side echoes. The deflection and splay zone shows a distinct boundary against the transverse bedform zone and the transverse features are seen to erode into Unit 2.

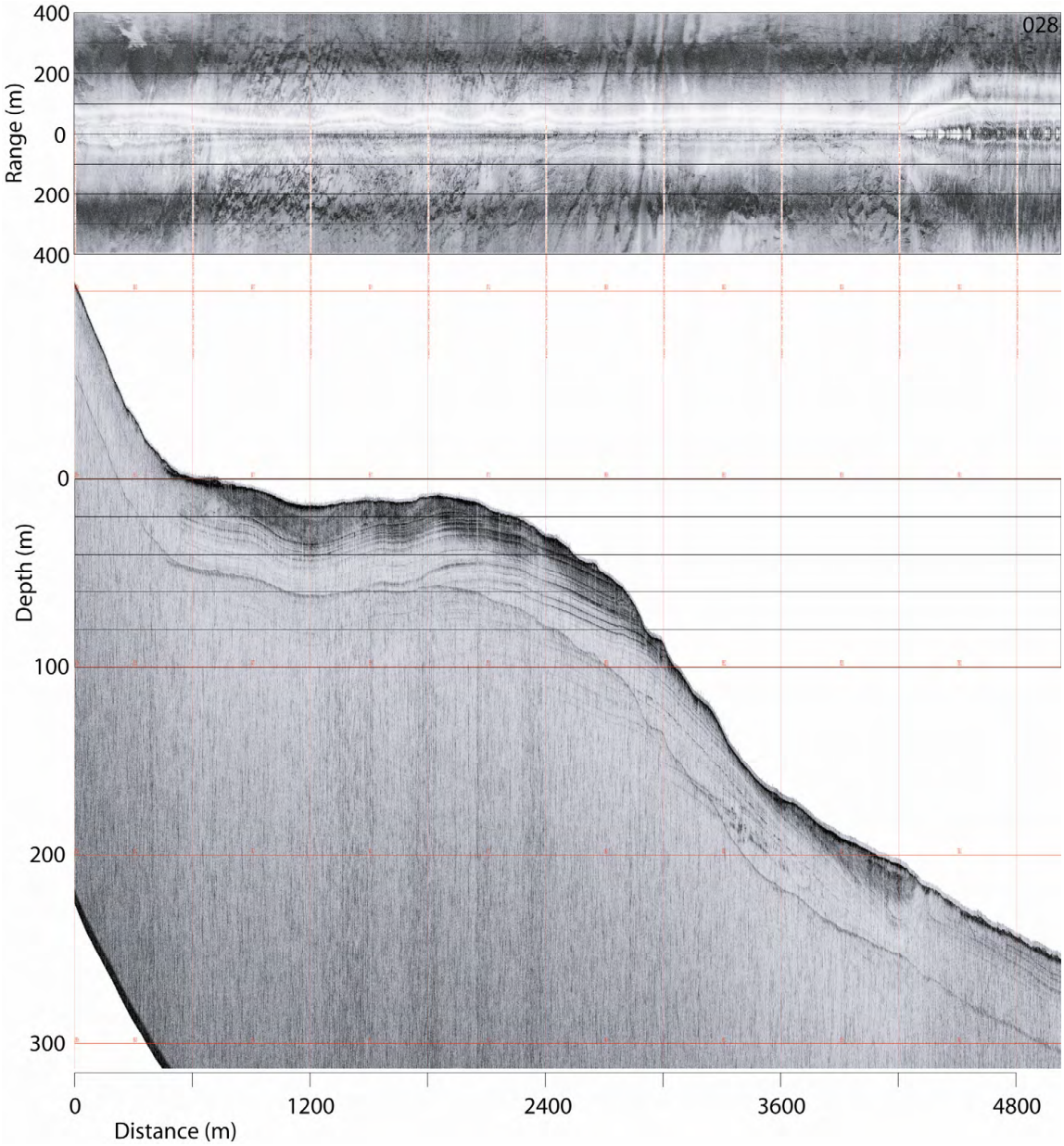

Fig. 21. Deep-Tow Profile 028 of Sigsbee Deflection and Splay Zone.
The far right of the image shows the last of the furrows just barely eroded into the remains of Horizon GK3. No contour currents are eroded into the exposed layering of the Sigsbee Escarpment, except the sidescan shows an indication of possible flutes or transverse bedforms eroded into the ponded sediment of the scarp bank.

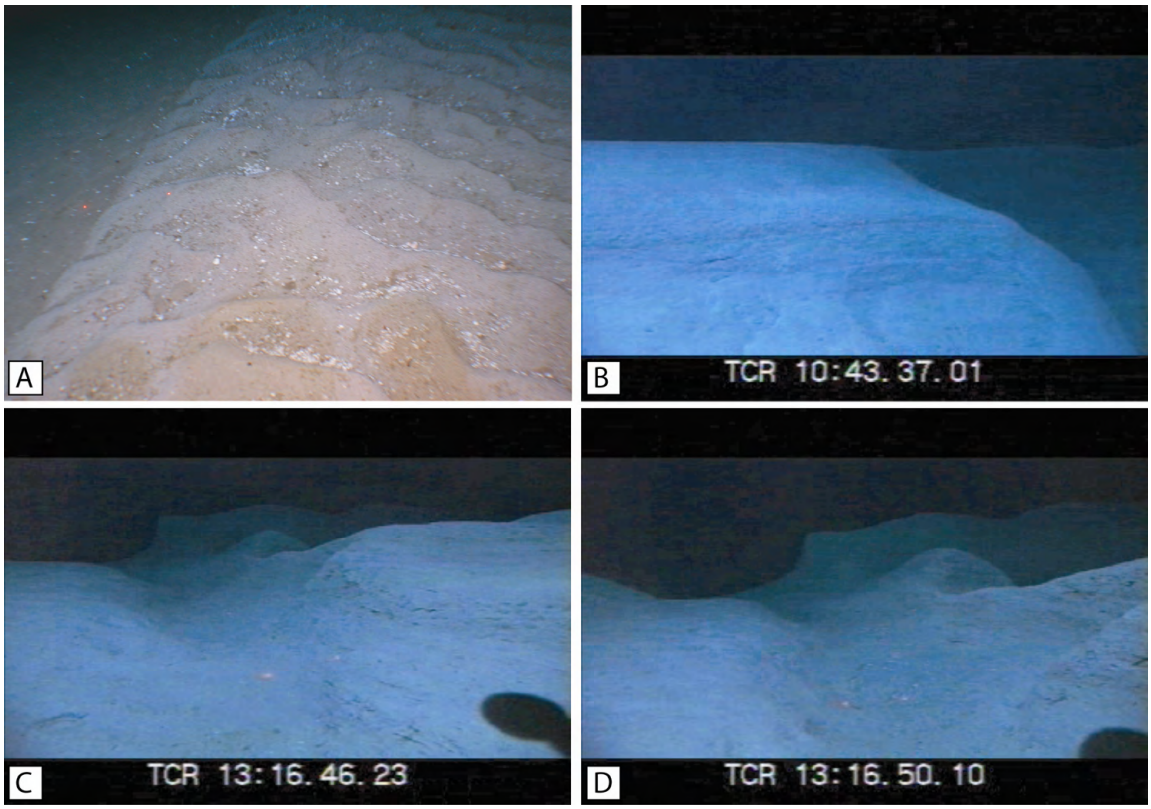

Fig. 22. Farnella Canyon *DSV Alvin* Dive# 3629 Imagery.
A) Foram sand ripples with concentrations of pteropod shells in the troughs. B) Curved vertical erosion scarps of flute formation showing exposed bedding planes and highly consolidated sediments. C) Nearly vertical wall along a more linear furrow-like bedform. D) Remnants of eroded furrow walls showing more of the highly scoured seafloor and sub-linear trends.

A second *DSV Alvin* dive was located in the deflection and splay zone at the southwestern edge of the study are in Farnella Canyon. The imagery from the dive reveals several characteristics of the deflection and splay zone (Fig. 22). Similar to the Green Knoll zone, foram sand and pteropod lag deposits were common in the axes of the furrows of this region; however, the degree of erosion in this area was much higher. Given that the furrows of the Sigsbee deflection and splay zones appear to erode into Unit 3 and expose horizon GK3, the *Alvin* imagery confirms this scenario. Many of the

furrow walls were vertical cuts into the seafloor with obvious exposed older bedding planes. All recent sediment appeared to be scoured away as there was no soft, hemipelagic sedimentation either in or between furrows. This is consistent with the higher amplitude return of the 3-D seismic data for the Sigsbee deflection and splay zones. Many of the observed features were the expected low-walled (<2 m) linear furrows, but there were also many deep (1-4 m) flute marks scoured into the seafloor. Apparently the 3-D seismic could not resolve the individual flute marks from within the more coherent structuring of the field of linear furrows. Also of interest, was that while Green Knoll had an obvious strong (>1 knot) current moving material through the furrows, there was no apparent current in the Farnella Canyon furrows. This implies that the currents are much more spatially and temporally variable than might be expected.

Rectilinear Furrows

The Green Knoll area seafloor is dominated by the main rectilinear furrow field. This zone extends for over 60 km along the Sigsbee Escarpment and is over 25 km wide (Fig. 8). Even assuming the widest furrow spacing of the region (100 m), there would be over 250 rectilinear furrows side-by-side across the zone. This is the most complete picture of a furrow field ever imaged. Based on the flume studies of Allen (1969), the current velocities in this main furrow field area should be 20-30 cm/s. This certainly falls within the range of measured and modeled currents for the region. Interestingly, these currents must consistently fall within the 20-30 cm/s velocity window over long periods of time to create and maintain such a large, uniform, and coherent zone of rectilinear furrows. The currents are known to alternate between a dominant northeast to

southwest flow and southwest to northeast flow (Fig. 5), both tracking the orientation of the Sigsbee Escarpment.

Four profiles along the rectilinear furrow zone are shown (Fig. 23) to help characterize the bedforms of this region. The picture that emerges from the 3-D seismic data is a uniform field of furrows with only very subtle changes throughout. As can be seen from Table 1 and Table 2, the southwestern end of the field has slightly narrower furrows by 5m, slightly closer spacing by 25 m, the same relief (1-4 m), and a minor increase in orientation by 10°-15°. All the furrows of this region appear to have a relatively symmetric profile. Based on this information, the rectilinear furrow zone would fall into the Type 1A classification (Flood, 1983), which implies a region where sedimentation exceeds erosion. This is an interesting contrast to the reverse case of the deflection and splay zones. The small change in furrow orientation corresponds to the change in orientation of the Sigsbee Escarpment, confirming the contour following nature of the furrow-forming currents.

Looking in closer detail at the deep-tow data, several the furrow characteristics can be clarified. From Fig. 24 the consistent nature of furrow width and spacing and relief is apparent; however the spacing is not quite as regular as expected from the 3-D seismic data. All three marker horizons are found throughout the region, with the main furrow field being eroded only into Unit 1. In areas such as this, where the overall furrow pattern reveals no obvious directionality, the current direction can be determined from the presence of tuning-fork junctions. Generally, when furrows join into a tuning-fork

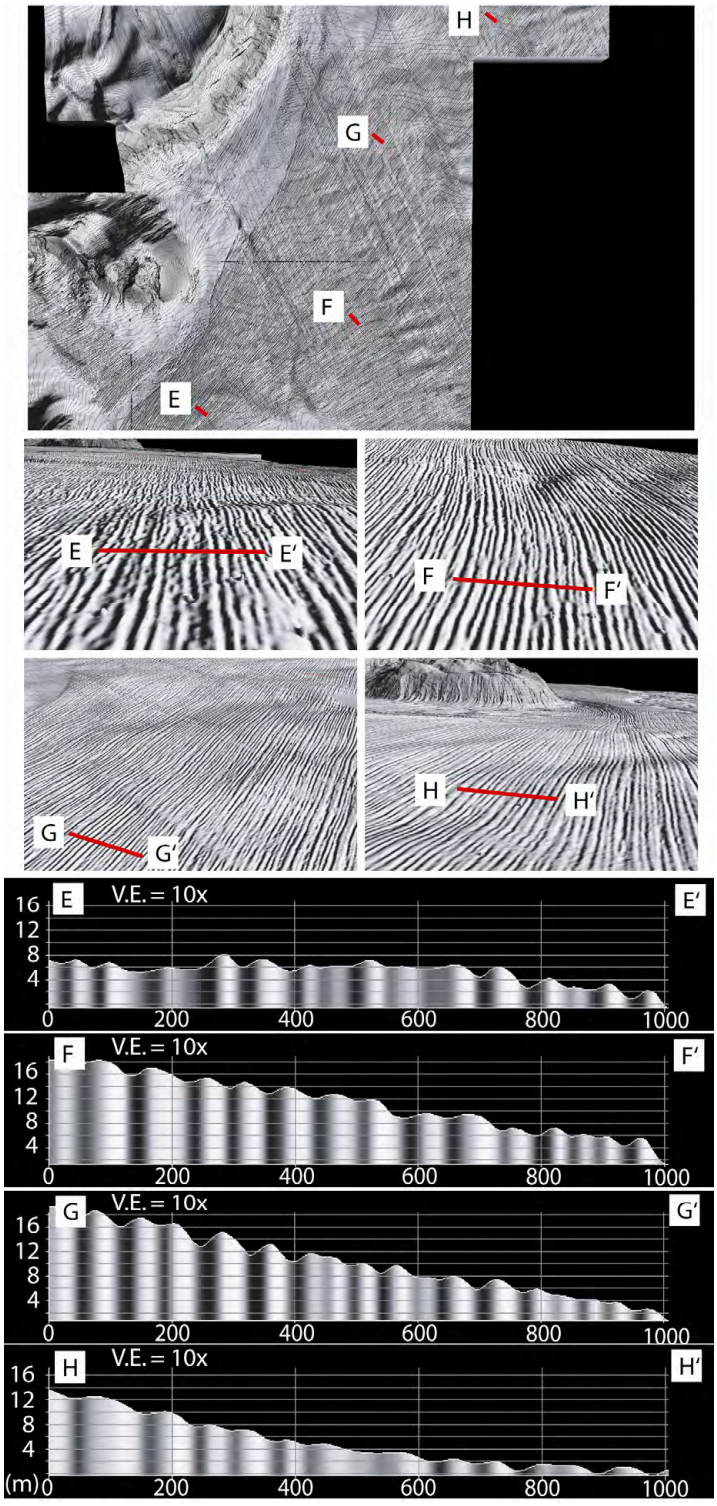

Fig. 23. 3-D Seismic Bathymetry and Profiles E-H from the Rectilinear Furrow Zone.
Four separate profiles within the rectilinear furrow zone. Almost no change in geometries is visible. A slight decrease in furrow relief is apparent in profile H-H′.

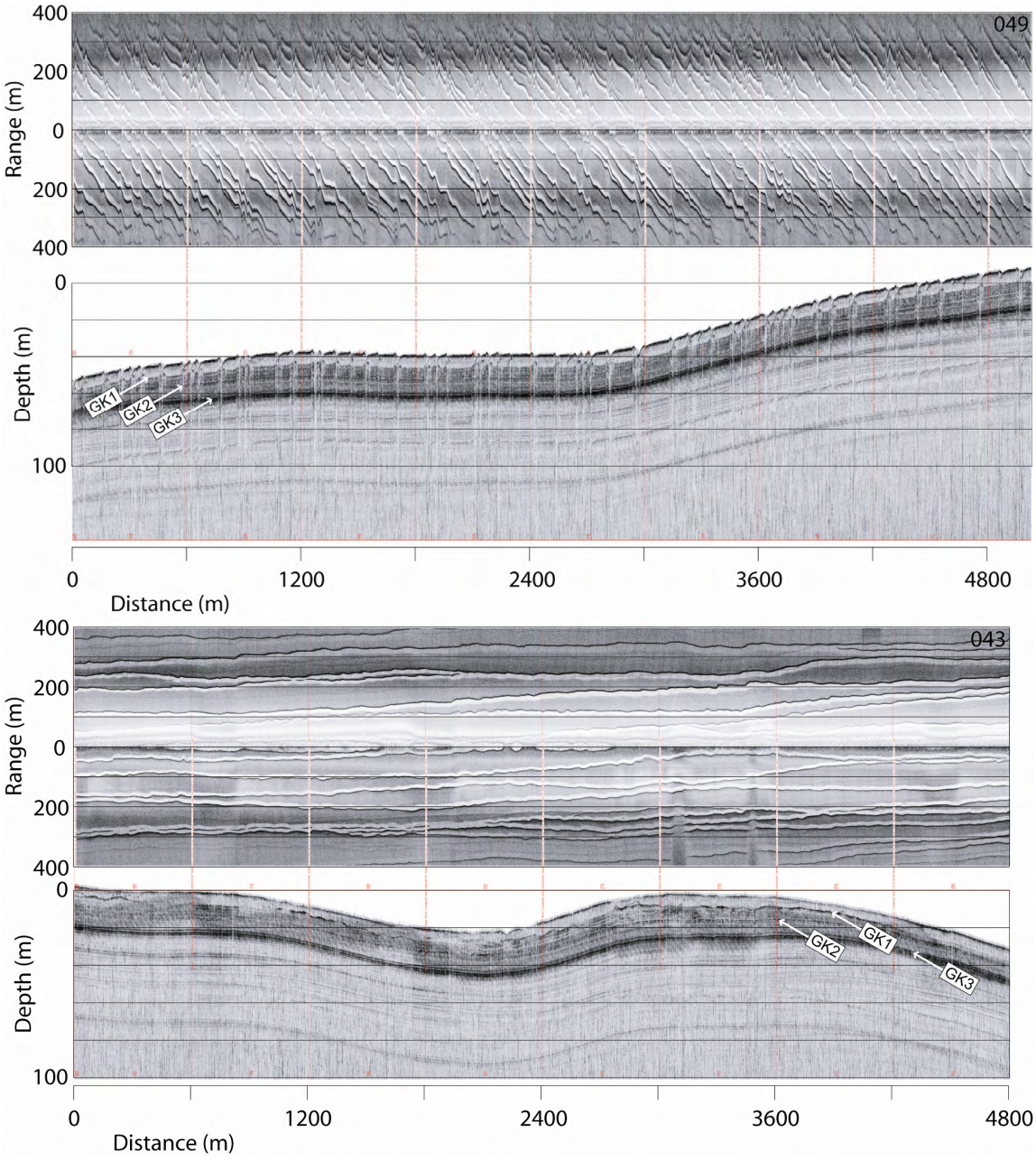

Fig. 24. Deep-Tow Profiles 049 and 043 across the Rectilinear Furrow Zone.
The perpendicular crossing of the furrows shows how abundant the furrows of this region are. Comparison of these profiles with the 3-D seismic data (Fig. 23) shows how much narrower they are than the 3-D data would indicate. All three marker horizons are present and the furrows are only eroded into Unit 1. Profile 043 shows some side echoes in the subbottom that confuse the return from horizon GK1. Tuning fork junctions can be seen on the profile 043 sidescan and indicate the presence of bidirectional flow.

junction they will join in the downstream direction of flow (Dyer, 1970), providing an excellent geologic indicator of current direction. As can be seen from Fig. 24, the tuning-fork junctions actually occur in both directions, supporting the idea of bi-directional currents flowing along the Sigsbee Escarpment. It is also important to note that the furrows appear to be unaffected by the gentle, rolling topography of the continental rise. Profiles 043 and 049 (Fig. 24) are both crossing a series of 10-20 m mudwaves (discussed below) but there is no apparent change in furrow morphology across the waves themselves. Thus, the presumed helical cells that form the furrows appear to be capable of bottom-following behavior across gradual changes in topography.

Arguably, the most interesting feature within the rectilinear furrow zone is a junction zone of furrows having two markedly different orientations (Fig. 25). This junction occurs between furrows associated with the Green Knoll splay zone and those of the main rectilinear furrow zone. Along with the 3-D seismic data, the deep-tow records over the furrow junction location reveal additional details of this region (Fig. 26). Furrow spacing at the junction is approximately double that of the outer rectilinear furrows. There is a gradational merging of the opposing furrow orientations moving away from the escarpment until there is no distinction in orientation. And, a slight deflection of the splay furrows along the junction is associated with apex of ridge created by the edge of the erosional moat around Green Knoll. All three marker horizons exist beneath the junction furrows. The most extreme difference in orientation occurs at the location where furrows fade out on the sidescan due to decreased furrow

relief, and Unit 1 pinches out on the subbottom. The question that arises is: How is it possible to generate a sudden shift of 45° in furrow orientation? Beginning with what we know, the deflection and splay zone furrows record strongly dominant flow from northeast to southwest, since a converging furrow pattern adjacent to Green Knoll could not be created if flow were from the southwest. And, the outer rectilinear furrows have been shown to have bi-directional tuning-fork junctions indicating bi-directional flow. We propose that the remaining flow associated with the inner rectilinear furrows is unidirectional and from southwest to northeast (Fig. 25).

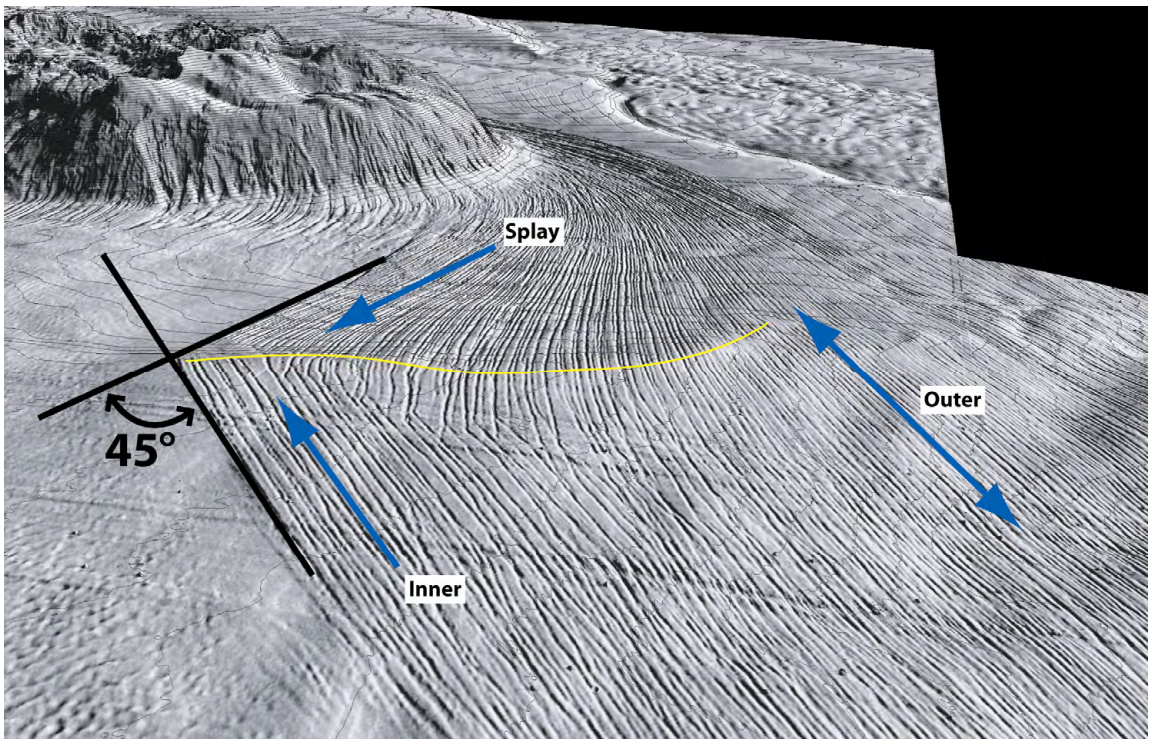

Fig. 25. Rectilinear Furrow and Furrow Splay Junction.
Perspective view of the junction between furrows oriented with the Green Knoll splay zone and those oriented with the rectilinear furrow zone. The yellow line identifies a slight bathymetric high associated with the axis of the rim of the erosional moat surrounding Green Knoll. The blue arrows indicate the proposed primary flow direction associated with the unidirectional splay zone, the bidirectional outer furrow zone, and the unidirectional inner furrow zone.

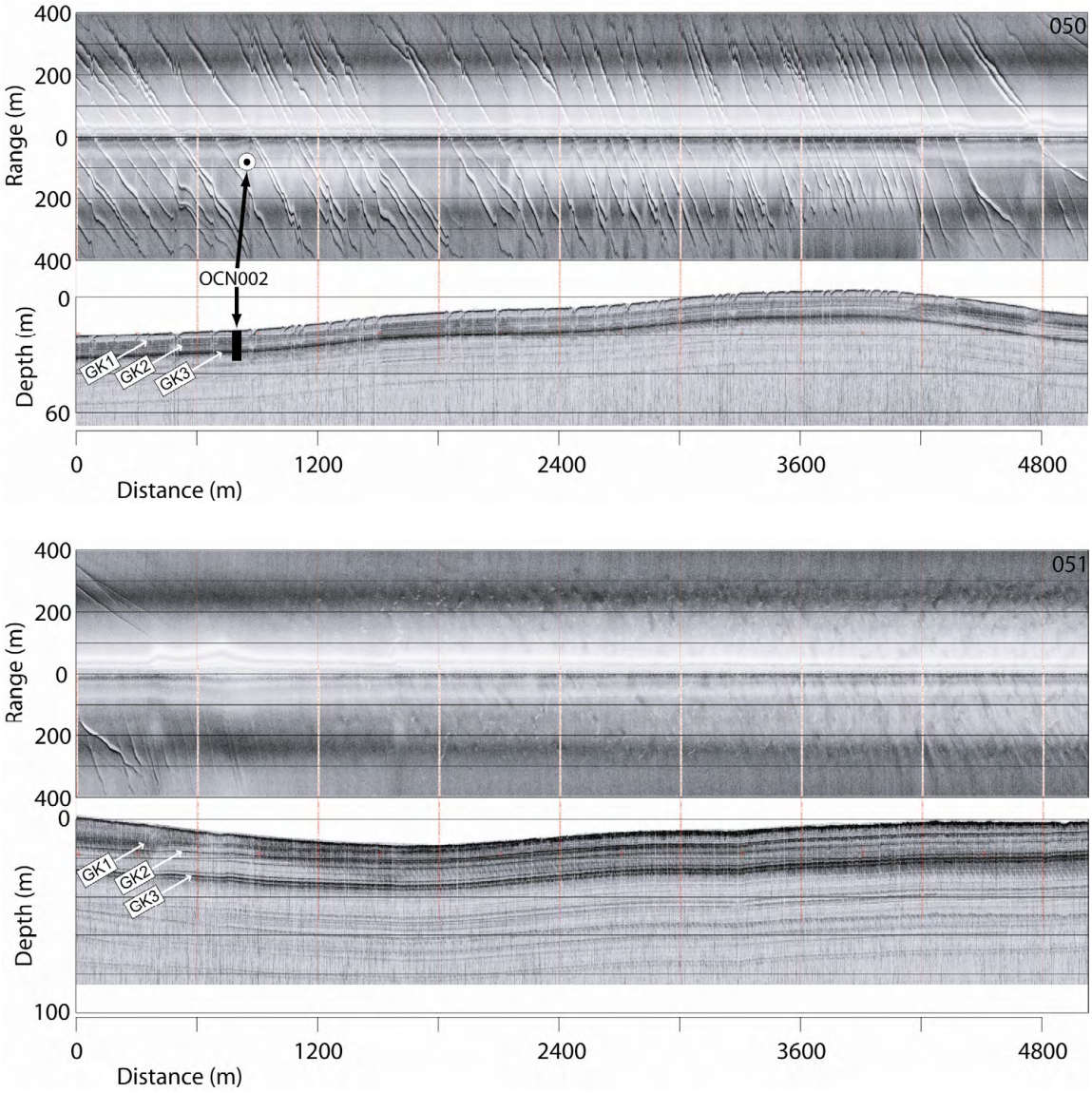

Fig. 26. Deep-Tow Profiles 050 and 051 across the Furrow Junction Zone.
The approximate location of core OCN002 is shown on the sidescan and subbottom of profile 050. Compared against the subbottom data OCN002 is seen to penetrate all three marker horizons. The merging and cross-cutting furrows of the junction are seen at the end of 050 and the beginning of 051. The furrow spacing is seen to be greater than in Fig. 24 indicating the possible creation of bedforms only from one direction of flow. The furrows dissipate on 051as Unit 1 pinches out onto horizon 1 and the record continues into the transverse bedform zone.

There are several reasons for the above proposed flow pattern. First, it is important to remember that the furrows are only a geologic record of the dominant flow direction when helical cells are coherent enough in the long term to produce furrows. Flow that is turbulent or does not develop consistent helical flow cells, should not generate furrows. Second, it is not possible to generate an instantaneous direction change in unconstrained fluid flow. Third, the inner furrows do not align with other furrows coming around the north side of Green Knoll, nor do they align with furrows created on the lee side of Green Knoll that result from flow over the knoll in a southwesterly direction; but, the inner furrows do align with the adjacent Sigsbee Escarpment from the southwest. Fourth, furrow spacing in the junction region is double that of the outer furrows. Given that the outer furrows are bi-directional, it is likely that the subtle differences in helical cell formation from two different directions result in two slightly offset and intermingled furrow sets. Indeed, the slightly irregular spacing evident on the deep-tow sidescan records may result from this bi-directional scenario. Finally, the orientation dichotomy gradationally decreases moving into the outer furrow region as the escarpment and knoll topography have less of an influence on the current flow field. For these reasons, we suggest that even though the bottom currents in the region are bi-directional, the local flow can result in unidirectional bedform morphology. Specifically, where helical cells originating from the southwest intersect with unaligned furrows of the splay zone, the roughness of the furrow crossing appears to break down the helical cells preventing continuation of the inner furrows. Likewise, where helical cells originating from the

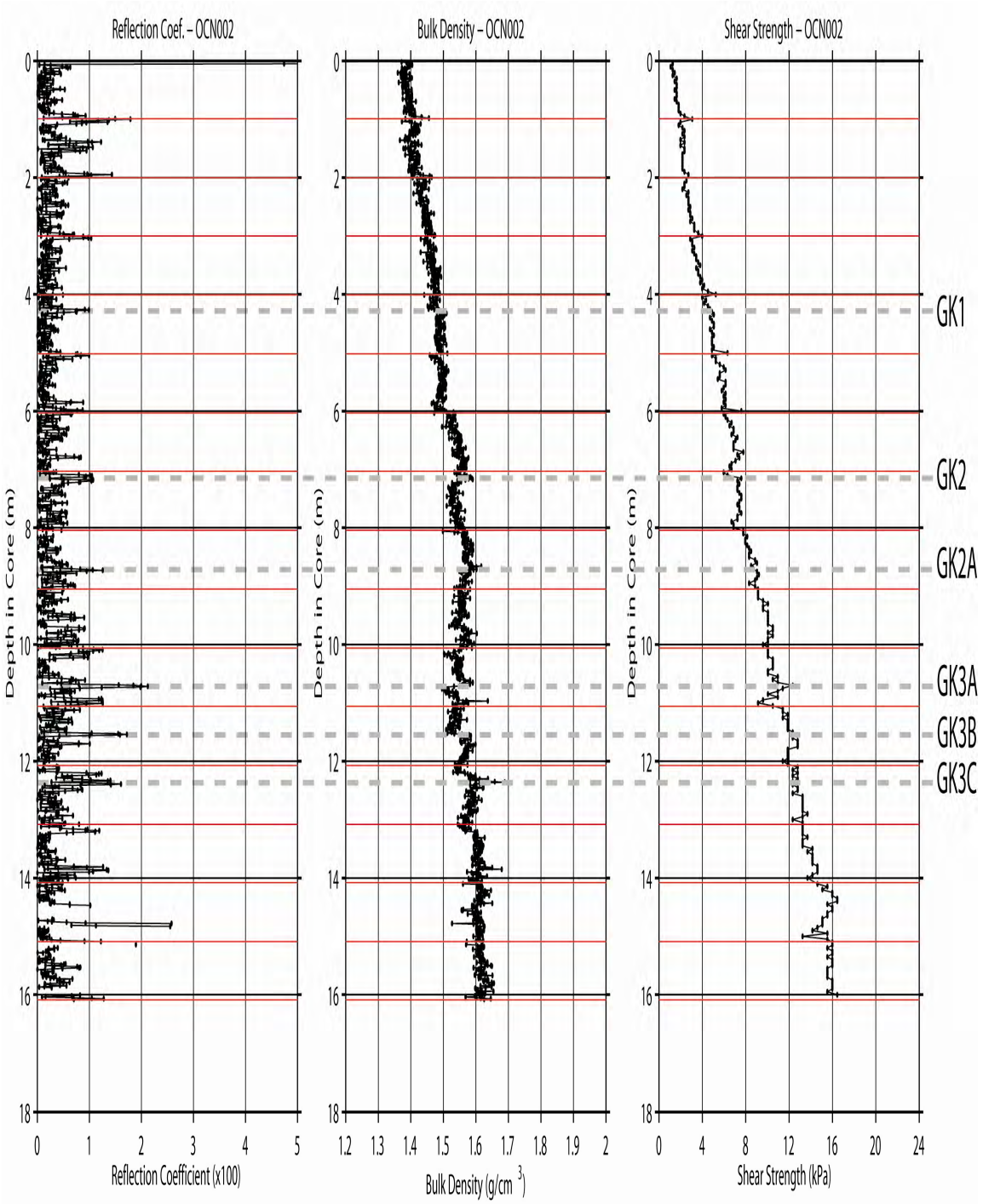

Fig. 27. Core OCN002 Reflection Coefficient, Bulk Density, and Shear Strength.
The reflection coefficient was calculated over a running 5 cm interval based on the 5cm resolution of the high-resolution seismic data. The reflection coefficient is also an absolute value to account for the envelope detection of the returned seismic signal. Seismic horizons GK1, GK2, and GK3 are identified. Horizon GK2A is an internal reflector to Unit 3. The triplet GK3 is divided into its components as GK3A, GK3B, and GK3C. Red lines indicate core section breaks.

northeast in the splay zone intersect with unaligned furrows of the inner furrow zone, the helical cells again are broken down by the seafloor roughness of the unaligned furrows thereby preventing continuation of splay zone furrows. Finally, the alignment of the furrows in the outer furrow zone allows bidirectional continuation of furrows as the helical cells do not appear to be interrupted by any misalignment of furrows.

One final dataset available for the rectilinear furrow region is a jumbo piston core (OCN002) taken from the main furrow field (Fig. 6). The location of the core relative to the high-resolution seismic data can be seen in Fig. 26, which identifies the core location in the relatively featureless area between furrows. Using the high-resolution subbottom data to define the depth of the primary reflectors, horizons GK1, GK2 and GK3 can be located in the jumbo piston core based on peaks in the reflection coefficient (Fig. 27). Furthermore, the individual peaks of the GK3 triplet can be identified along with an internal reflector to Unit 3 (horizon GK2A). Although the seismic peaks correspond to abrupt changes in bulk density the down core trend is a simple linear increase in density and shear strength. The linear increase implies relatively continuous sedimentation with no significant erosional surfaces. Because of the uniform nature of the sediments, subtle changes in density, velocity, and shear strength result in acoustically significant seismic horizons.

Using the data from Fig. 27, the horizons can be identified on the core lithology (Fig. 28 and Fig. 29). The acoustically transparent Unit 1 is a very soft, high water content, hemipelagic silty clay with no visible layering. The lack of bioturbation and internal

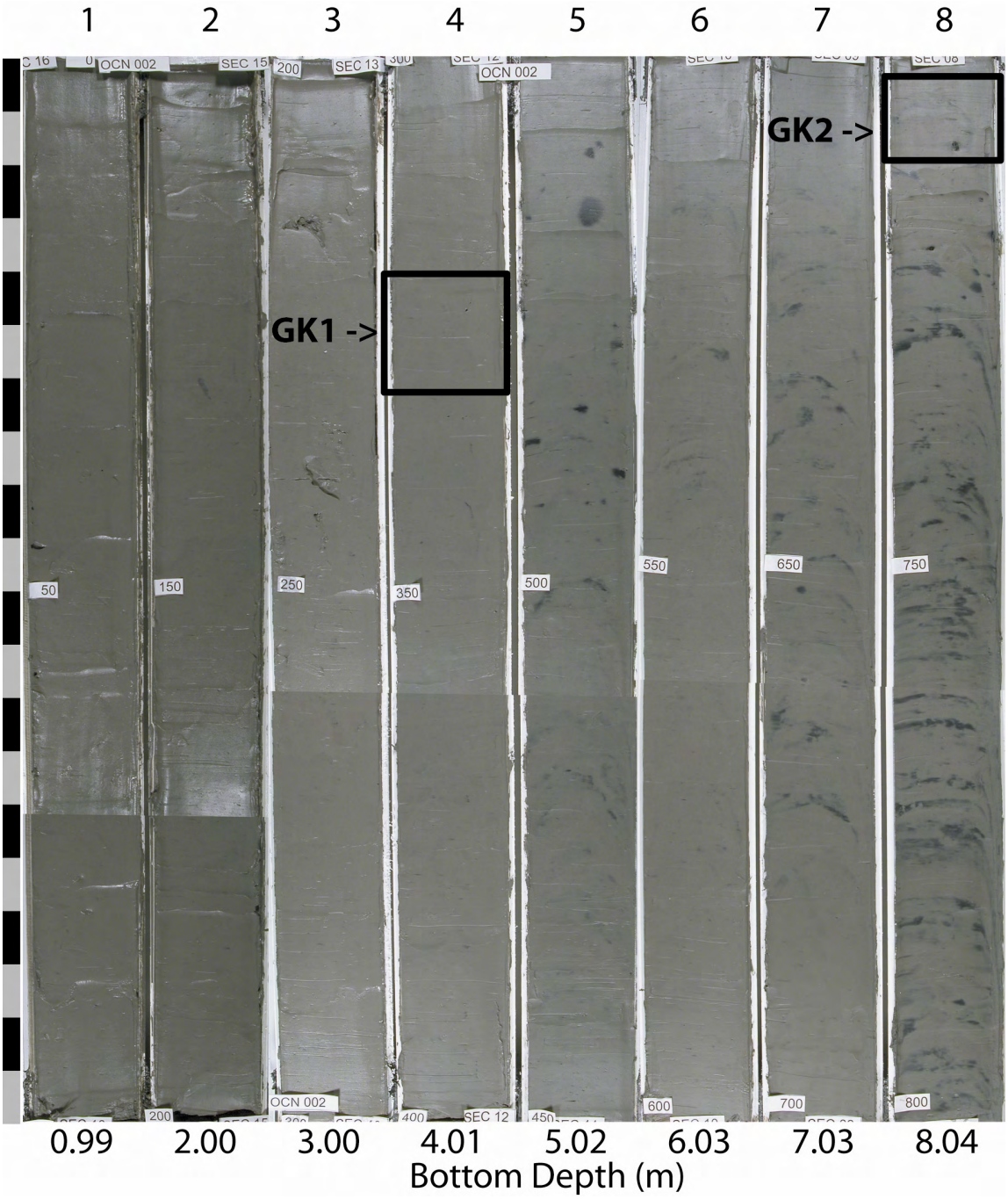

Fig. 28. Core OCN002 Photograph of the Top 8 Meters.
Seismic horizons GK1 and GK2 are identified. No significant change in lithology occurs at the horizons. The upper portion of the core is hemipelagic clay to silty-clay with no visible bedding that grades into a bioturbated clay / silty-clay and continues with increased parallel bedding.

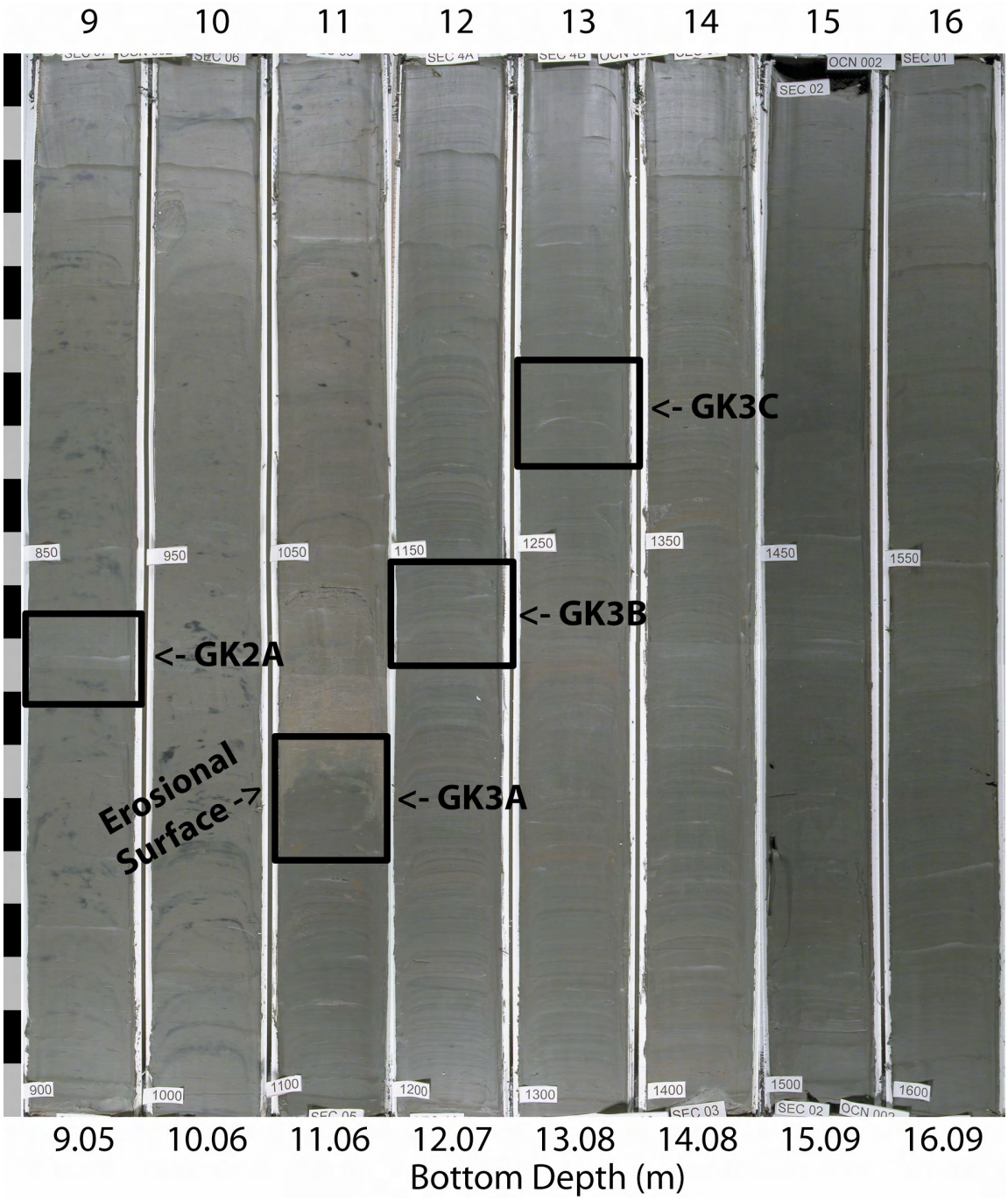

Fig. 29. Core OCN002 Photograph of the Bottom 8 Meters.
Seismic horizon GK2A corresponds to a very thin silt layer. Horizons GK3A, GK3B and GK3C correspond to the three layers of the triplet reflector. Only GK3A shows a significant lithology change. The bioturbated upper section grades to thinly bedded parallel laminations of clay and silty-clay beneath the erosional surface of GK3A.

structure suggests relatively continuous and rapid sedimentation. Unit 2 is similar to Unit 1 with increasing bioturbation down core. Unit 3 is a slightly bioturbated silty clay with irregularly spaced, thin, dark layers. Interestingly, the only reflector showing a visibly significant change in lithology is GK3A. Horizon GK3A corresponds to the erosional top of a hemipelagic silty clay beneath a thick section of a clayey foram sand. Beneath GK3A the sediments are thinly bedded layers of clays and silty clays. Although horizons GK3B and GK3A can be identified in the bulk density profiles, no visible distinguishing lithology is apparent.

Transverse Bedforms

The third contour-current bedform zone to be considered is the transverse bedform zone. Generally, this zone lies between the Sigsbee deflection and splay zone, and the main rectilinear furrow zone (Fig. 8). Based on the 3-D seismic data alone, this zone is difficult to characterize (Fig. 30). The amplitude map (Fig. 14) indicates medium to high amplitudes along the entire transverse zone, but it is not clearly resolved from amplitudes of the surrounding zones. Although the seafloor character makes the transverse zone relatively easy to define as a unit, the features are not laterally continuous like furrows. So, the 3-D seismic lateral resolution becomes and issue when trying to define the individual bedform components. The 3-D seismic imagery implies a hummocky surface from which it is difficult to determine bedform orientation. Profile W-W′ (Sigsbee transverse bedforms) shows bedform relief of 2 m or less while profile X-X′ (Green Knoll transverse bedforms) shows almost no bedform relief (<1 m).

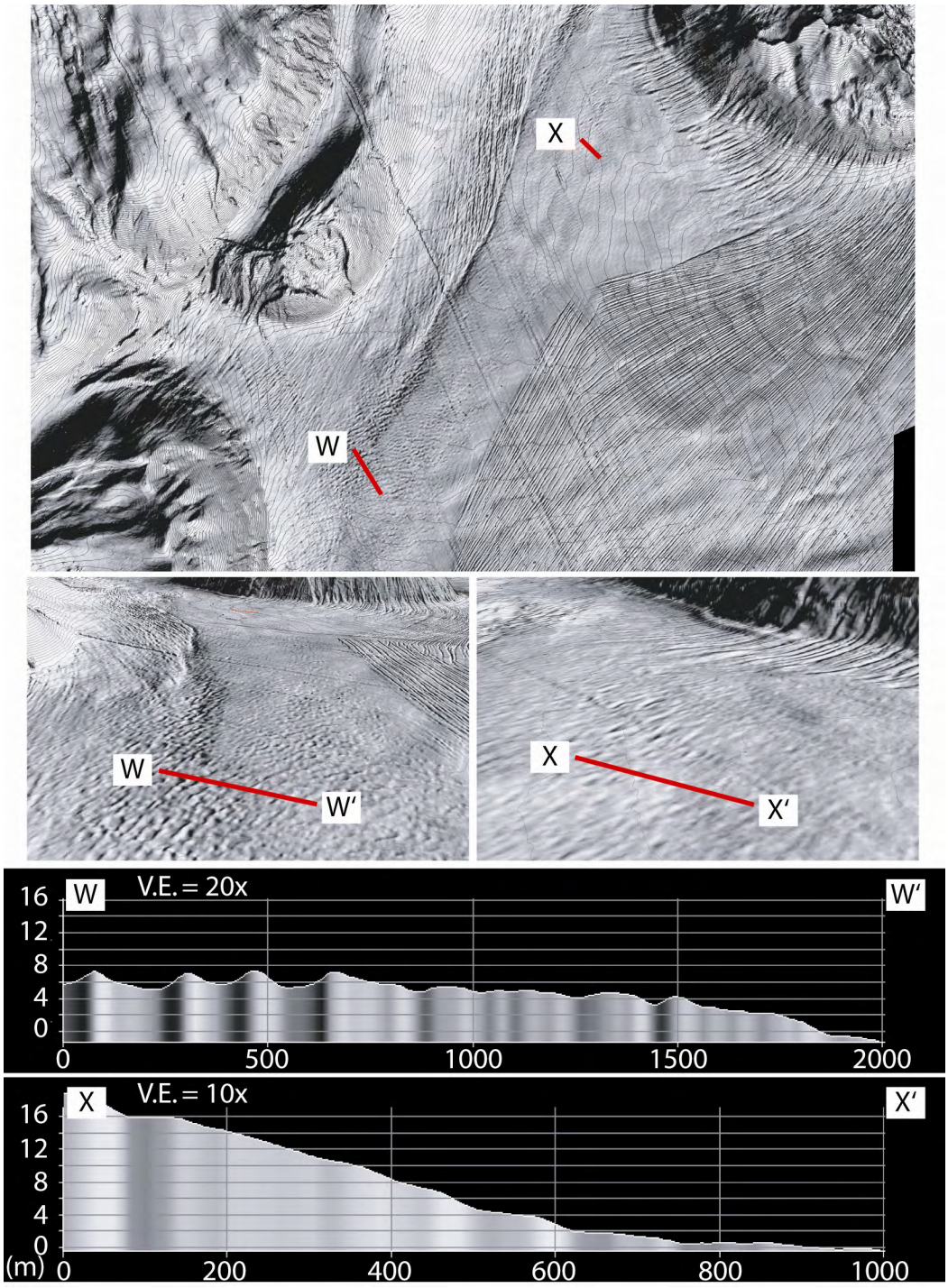

Fig. 30. 3-D Seismic Bathymetry and Profiles W-X of the Transverse Bedform Zone.
The bathymetry and profile W-W′ shows a hummocky nature to the Sigsbee transverse bedform zone. The resolution of the 3-D data makes it difficult to determine the true nature of the surface features. The Green Knoll transverse zone shows less feature relief and less discernible structure.

Sigsbee transverse bedforms are larger (100-200 m) than the Green Knoll transverse bedforms (75-100 m). The spacing is essentially the size of the individual bedforms since there did not appear to be any gaps between adjacent features.

Despite the high-resolution of the deep-tow data, the morphology of the transverse bedform features of the Green Knoll zone is somewhat ambiguous (Fig. 31). The subbottom data shows that Unit 1 has been removed, leaving behind horizons GK2 and GK3. The transverse bedforms show almost no relief on the subbottom data along with no coherent structures. Most of the transverse bedforms are eroded into Unit 2, except at the fringe of the zone where Unit 3 is exposed. The sidescan data shows a pattern that is indicative of transverse scour marks (Allen, 1969; Dzulynski and Walton, 1965), frondescent features produced by a dilute suspension (Dzulynski and Walton, 1965), or even roll waves created by the propagation of periodic hydraulic jumps (Baines, 1995). Each of these possibilities requires relatively high current velocities and/or vortices. Because of the extremely low relief, the sidescan only picks up the high-amplitude edge returns from the feature relief at the very fringe of the record where acoustic grazing angles are lowest. The fringe high-amplitude sidescan returns indicate U- and V-shaped features that actually stand proud above the seafloor. This is inconsistent with an erosional flute mark, but more consistent with erosion resistant scour marks or sand ridges. There is no clear symmetry to the features and the source current directionality is unclear as the apices of the bedforms point in two directions indicating bi-directional flow, both to the northeast and to the southwest. Based on the experiments of Hunt and

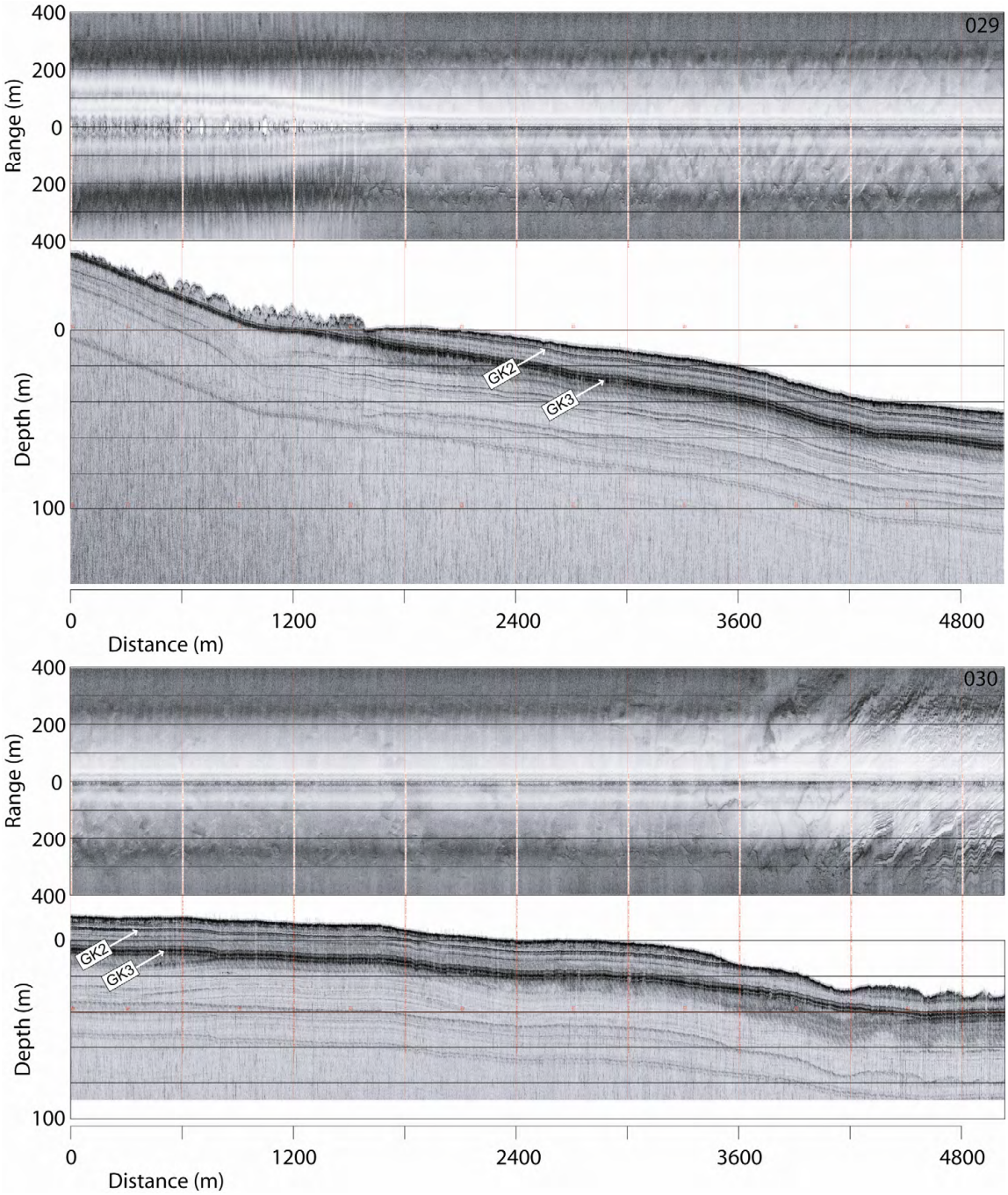

Fig. 31. Deep-Tow Profiles 029 and 030 across the Green Knoll Transverse Bedform Zone.
The abrupt transition from the transverse bedform zone to the adjacent furrowed regions can be seen at the start of 029 and the end of 030. Unit 1 and horizon GK1 are missing throughout. The transverse bedforms are eroded only into Unit 2. The furrows on either side are eroded into Unit 3. No visible structure is apparent in the subbottom. The confused nature of the sidescan only indicated flow could be bidirectional to the southwest and to the northeast. The only relief on the sidescan is visible on the fringe of the record as slightly raised edges to the transverse bedforms.

Snyder (1980) the flow on the lee side of Green Knoll can take several forms: 1) a recirculation zone beneath the flow separation off the knoll, 2) a purely turbulent wake, or 3) vortex generation in the lee of the knoll. The confused and patchy nature of the sidescan record implies turbulent and vortex related flows. In fact, the transverse bedform pattern is repeated over a broader area on the northeast side of the knoll and would be consistent with currents flowing from the southwest that are obstructed by the knoll. Regardless, more detailed information is necessary to fully describe the processes involved in the Green Knoll transverse bedform region.

From the high-resolution seismic data, the Sigsbee transverse bedform zone is a bit better defined than the Green Knoll zone (Fig. 32). Unit 1 and horizon GK1 are completely removed. Unit 2 at the northeast end of profile 064 is only 2-3 m thick and is fully eroded by the southwest end of profile 064. Profile 067 shows increasing removal of Unit 3 in the southwest direction until horizon GK3 is exposed at the southwestern extent of the profile. The seafloor return shows a well-defined scalloped pattern that is a perfect match for a transverse bedform profile with the steep sides of the eroded features pointing in the downstream direction of flow (Allen, 1969). Given the orientation of the ridges in the subbottom data, the current direction for the Sigsbee transverse bedform zone is from the southwest to the northeast. Furthermore, the work of Allen (1969) indicates a flow velocity in excess of 100 cm/s to create the transverse features.

In addition to the seismic data from the Sigsbee transverse bedform zone, one jumbo piston core (OCN001) was taken (Fig. 6). The location of the core relative to the high-

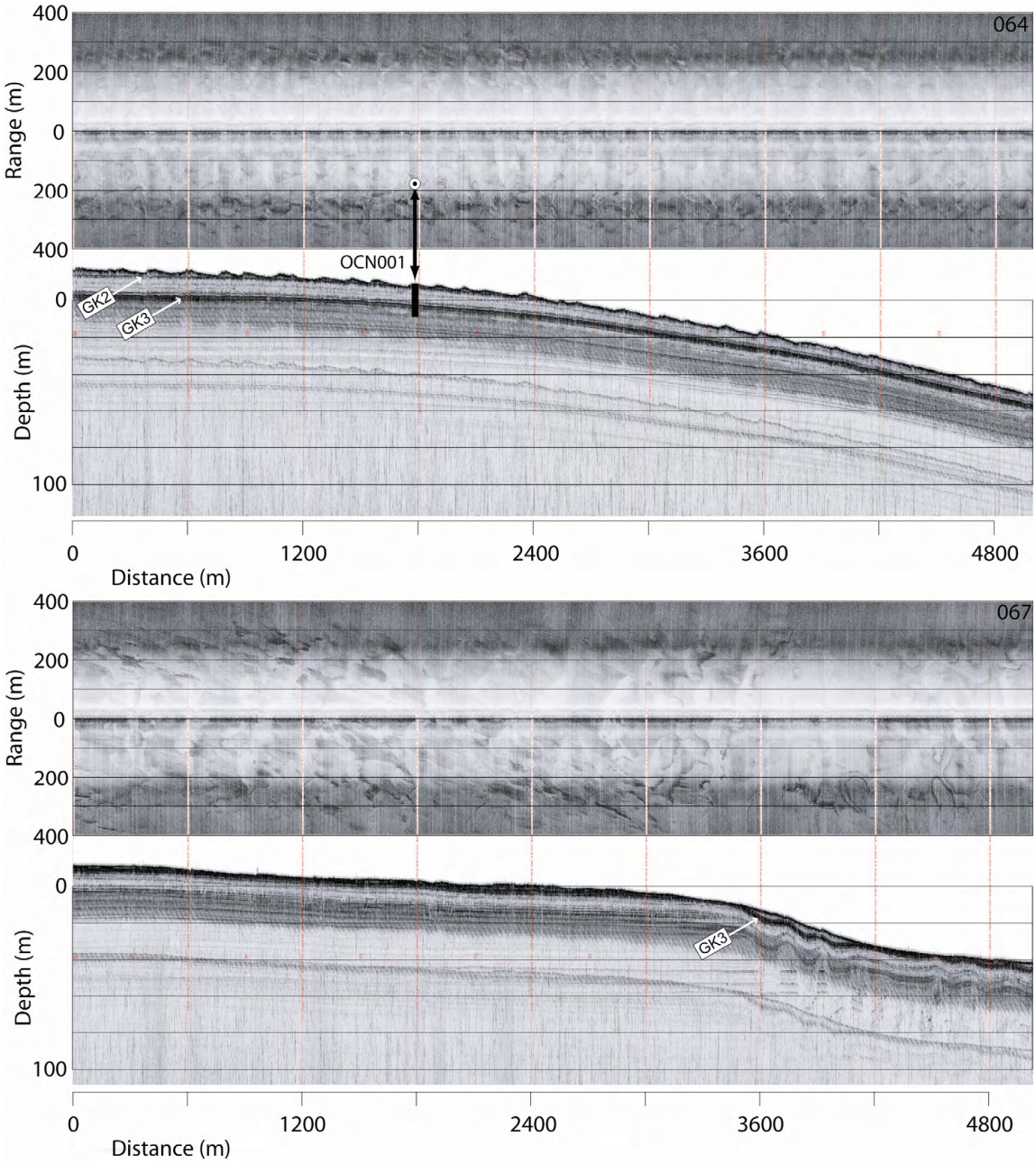

Fig. 32. Deep-Tow Profiles 064 and 067 along the Sigsbee Transverse Bedform Zone.
The approximate location of core OCN001 is shown on the subbottom and sidescan of profile 064. The length of OCN001 is seen to penetrate both horizons GK2 and GK3. Due to limitations in positioning accuracy, it is unclear whether the core penetrated the peak or trough of a transverse bedform. The transverse bedforms are eroded into both Unit 1 and Unit 2. Erosion of Unit 1 and 2 increases from northeast to southwest and continues down to horizon. Circular bull's-eye patterns can be seen on the sidescan of 067 where folded beds of GK3 and deeper are exposed. The transverse bedforms do not erode into GK3.

resolution seismic data can be seen in Fig. 32. Whether or not the core was located on a peak or trough of one of the transverse features cannot be determined due to limitations in seismic and core positioning. Using the high-resolution subbottom data to define the depth of the primary reflectors, horizons GK2 and GK3 can be located in the jumbo piston core based on peaks in the reflection coefficient (Fig. 33). As with OCN002, the individual peaks of the GK3 triplet can be identified along with the internal reflector (GK2A) to Unit 3. Several differences between core OCN001 and OCN002 exist. The top of OCN001 actually shows a decrease in density just above reflector GK2. Also, the density changes that are correlated with seismic reflectors are sharper and more extreme than OCN002. Six meters of sediment corresponding to Unit 1 and most of Unit 2 are missing from OCN001. Unit 3 is 9 meters thick in OCN001 and only 3 meters thick in OCN002 indicating higher sedimentation rates in the transverse bedform zone at the time of deposition, a longer period of deposition in the transverse bedform zone, or non-deposition/erosion in the rectilinear furrow zone. Although the down core trend in both cores is a linear increase in density and shear strength, OCN001 shows a drop in shear strength in the triplet reflector region.

Using the geotechnical and seismic data, the lithologic features that correspond with the horizons can be identified (Fig. 34 and Fig. 35). The top 5.5 m of sediment is very soft hemipelagic silty clay showing distinct layers. Below horizon GK2A the layer continues but is much fainter as the sediments slowly decrease in water content and become stiffer. Throughout the core, evidence for bioturbation is minimal to non-

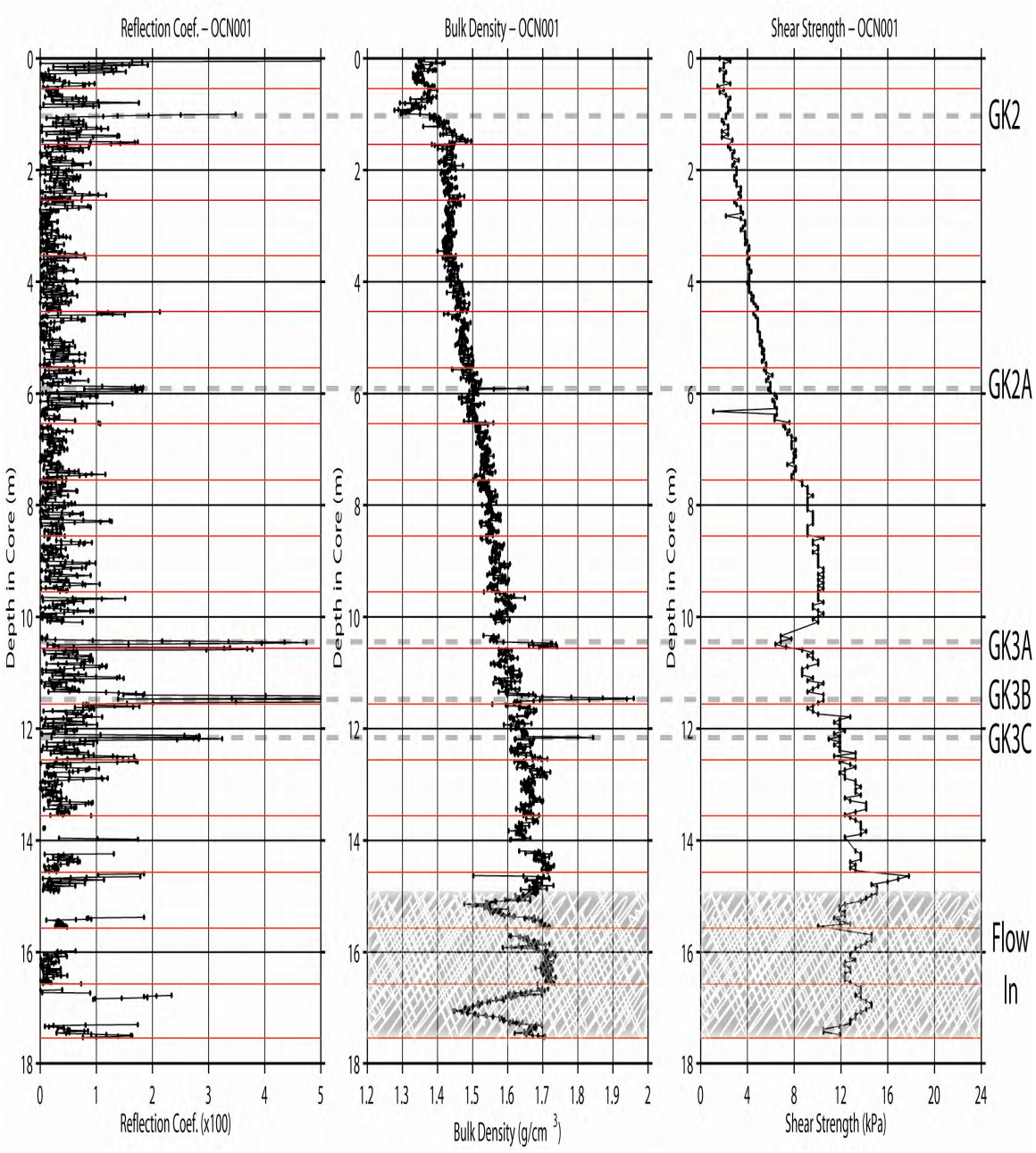

Fig. 33. Core OCN001 Reflection Coefficient, Bulk Density, and Shear Strength.
The reflection coefficient was calculated over a running 5 cm interval based on the 5cm resolution of the high-resolution seismic data. The reflection coefficient is also an absolute value to account for the envelope detection of the returned seismic signal. Seismic horizons GK2 and GK3 are identified. Horizon GK2A is an internal reflector to Unit 3. The triplet GK3 is divided into its components as GK3A, GK3B, and GK3C. Red lines indicate core section breaks. A linear increase in bulk density and shear strength is seen with depth. The bottom 2.75 meters of the core is from flow-in during coring and is invalid data.

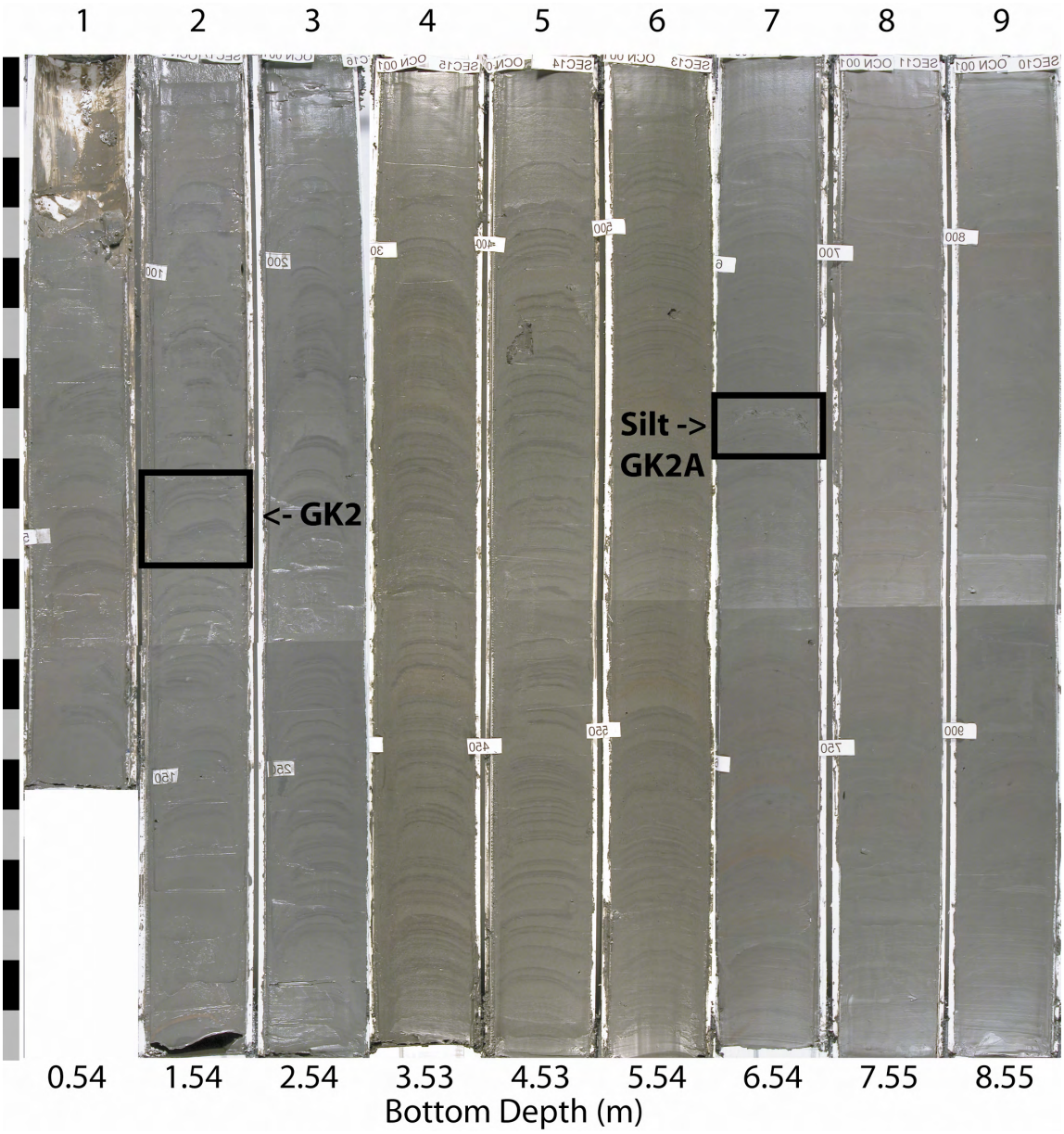

Fig. 34. Core OCN001 Photographs of the top 8.5 Meters.
Horizons correlated with seismic and core data are indicated. The top of the core is consists of very soft, thin, parallel laminations of clay and silty clay grading into slightly stiffer clay and silty clay with fainter laminations. Horizon GK2 shows no significant change in lithology, while GK2A is a silt layer.

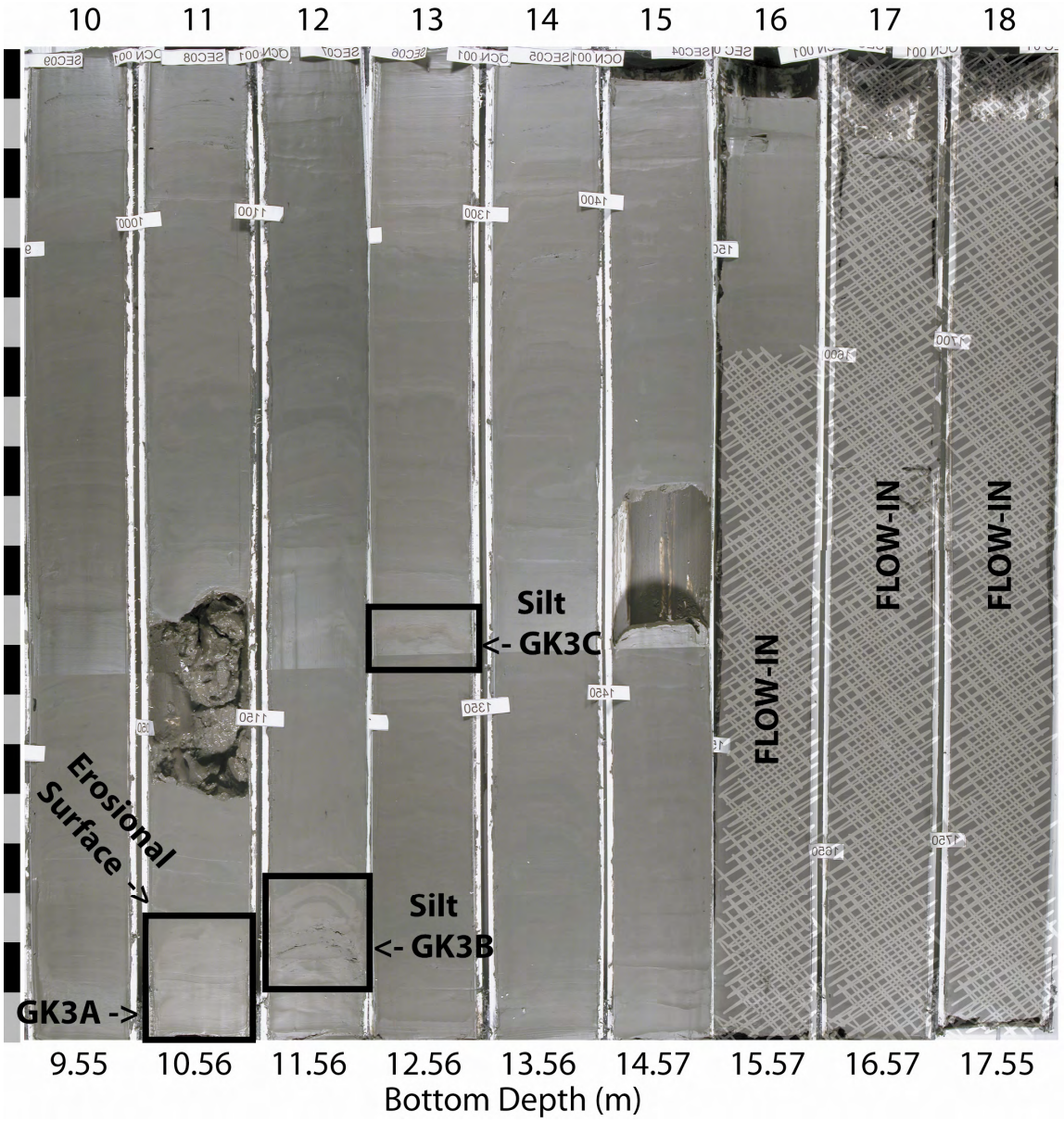

Fig. 35. OCN001 Core Photographs of the top 8.5 Meters.
Horizons correlated with seismic and core data are indicated. No data is valid for the bottom 3 sections as noted where sediment flow-in occurred due to suction of sediments rather than penetration of sedimentary layers. The gaps in the core are from separation during coring. Horizon GK3A appears as an erosional surface, while horizons GK3B and GK3A are clear silt layers.

existent. Horizon GK2 has no obvious lithologic signature, while horizon GK2A is a relatively thick clayey silt layer. Horizon GK3A shows a similar erosional surface pattern to that seen in OCN002, but the overlying foram sand package is not present. Conversely, where OCN002 showed no major lithologic changes for horizons GK3B and GK3C, OCN001 contains distinct clayey silt packages greater than 2 cm thick in both cases.

Overall, the missing surface sediments of Unit 1 and 2 indicate a significant erosional environment in the transverse bedform zone. The soft, high water content sediments of Unit 3 and its evident erosion on the seismic record to the southwest confirm the erodibility of all sediments above horizon GK3 under the present day current conditions; however, GK3 appears to mark the maximum depth of erosion for the transverse bedform zone. The sedimentology of Unit 3 and Unit 2 in OCN001 indicates a different depositional environments for the transverse bedform zone as compared to the rectilinear furrow zone, and the softer surface sediments indicate a lesser erosional environment in the transverse bedform zone as compared to the deflection zones.

Gradational Furrow Spacing

A study of furrows in the Bryant Canyon area revealed that there is an increase in furrow spacing and decrease in furrow width with distance from the Sigsbee Escarpment (see Chapter II). A similar trend is found in the Green Knoll area; however, the region is confined to the south and east of the knoll (Fig. 8). The gradational furrow spacing zone is just that—a region where the distance between furrows begins to increase dramatically. Fig. 36 shows the 3-D seismic overview of the gradational furrow spacing

zone. Outside the main rectilinear furrow zone the furrow relief decreases to less than 1 m, the furrow width shows a slight decrease to 10-15 m, and the spacing between furrows increases to as much as 800 m at a point farthest from the escarpment. This trend can be attributed to a decrease in current velocities away from the high-velocity core of the escarpment following contour currents. The high-resolution seismic data (Fig. 37) shows that the furrows in the distal portions of this zone are barely detectable, thin streamers, which show almost no relief and no visible signature in the subbottom. All three marker beds (GK1, GK2, and GK3) are present in this area, and the furrows are confined to the upper meter of Unit 1.

The fact that the gradational furrows are only found adjacent to Green Knoll appears to be a consequence of the 3-D data extent limits rather than a function of flow patterns and associated bedform creation. If the data of the rectilinear furrow zone extended further away from the Sigsbee Escarpment, we would expect to see more of the gradational furrow spacing bedforms. The furrows of profiles I, J, and K seem to differ in origin from those of profile L (Fig. 36). The eastern furrows (I, J, K) are connected to the northeast to southwest flow and show the deflective influence of Green Knoll in their pattern as they merge with the flow around the knoll, but the outermost furrows dissipate and terminate just south of Green Knoll. It is likely that the furrows associated with profile L result from southwest to northeast flow rather than being a reinitiation of the furrows that terminate just to the east as the flow dissipated. As with the rectilinear

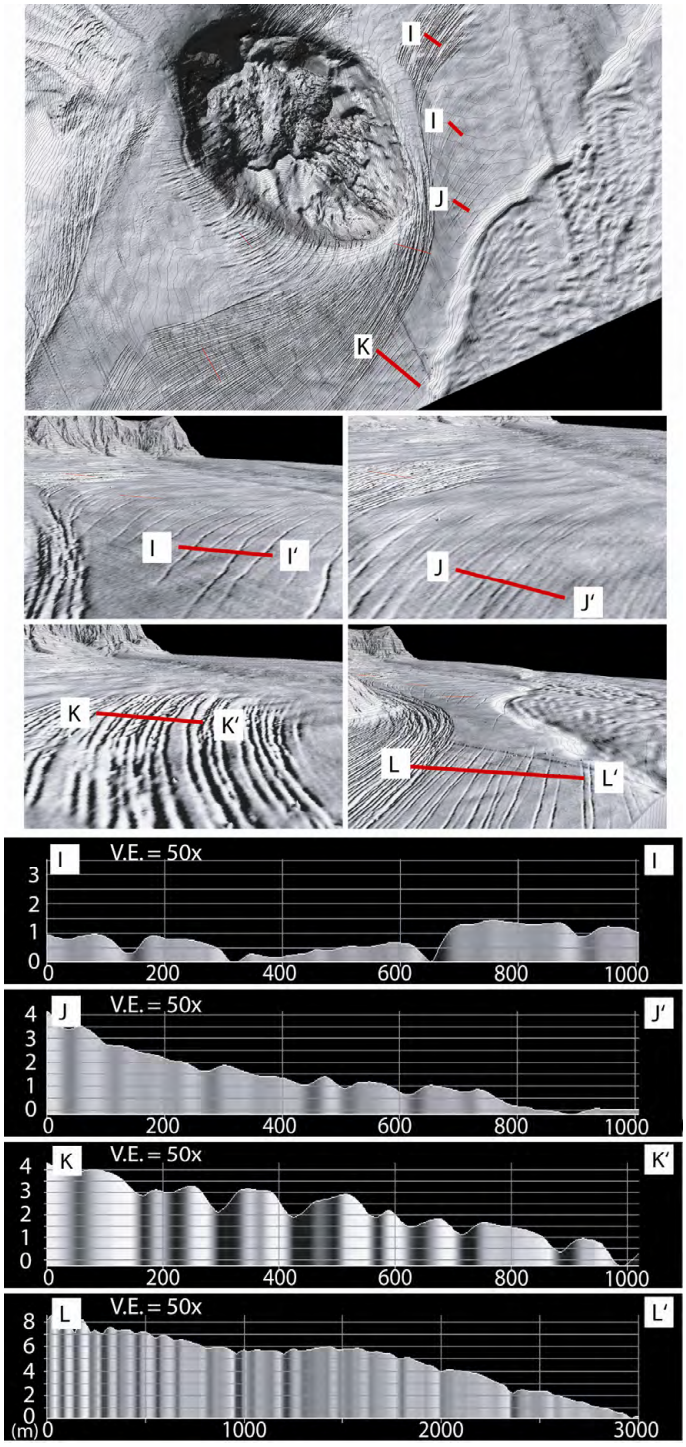

Fig. 36. 3D Seismic Bathymetry and Profiles I-L of the Gradational Furrow Zone.
Profiles I through K show the transition from widely spaced, very shallow furrows to closer spacing and slightly deeper furrows. Profile L is just outside the deflection and splay zone. The non-furrowed region between profiles I-K and L suggests each furrow set is dominated by unidirectional flow. The dominant flow direction for I-K is to the southwest and for L the flow is to the northeast.

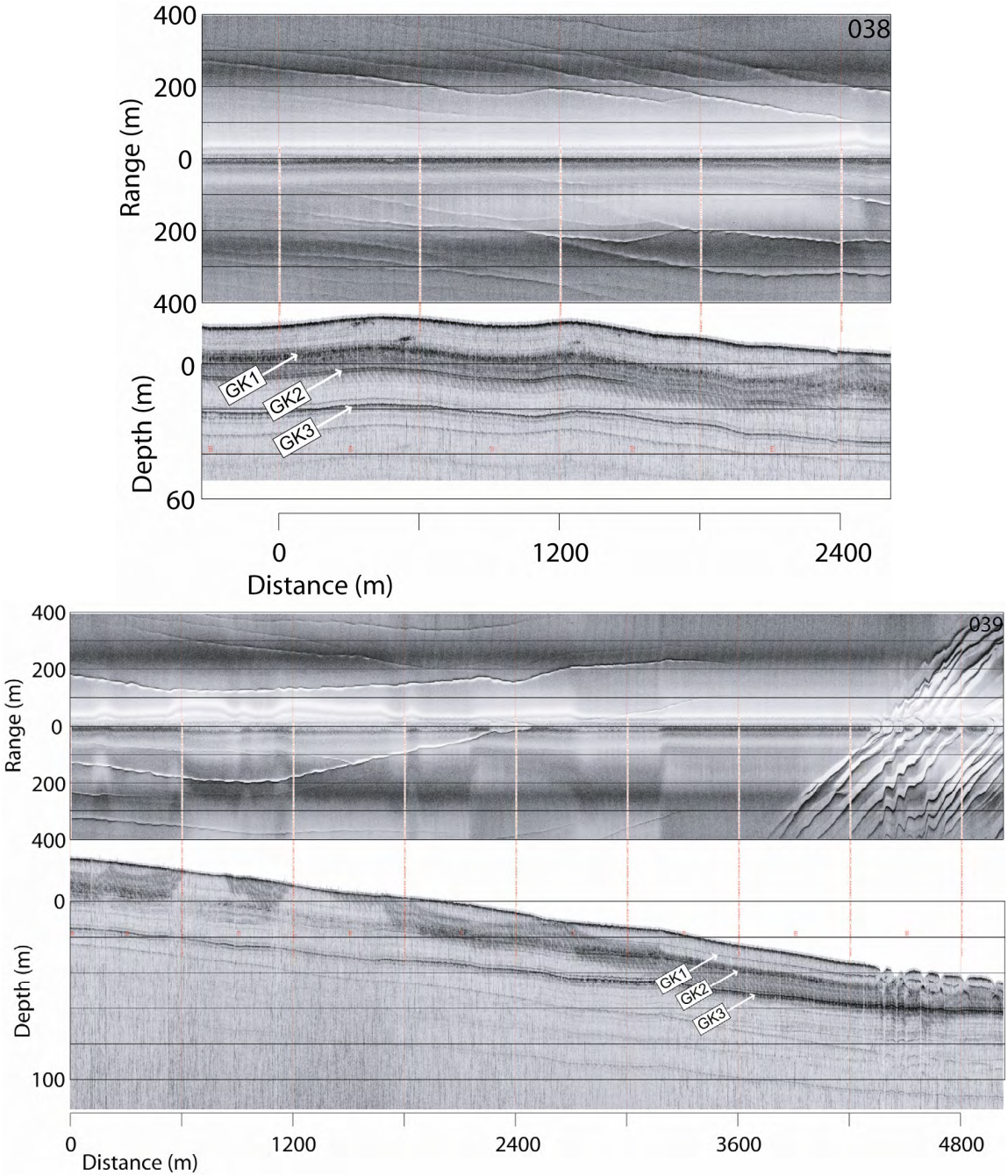

Fig. 37. Deep-Tow Records 039 and 038 of the Gradational Furrow Zone.
All three marker horizons exist in this area. The termination of the gradational furrows prior to the Green Knoll deflection zone can be seen on 038. The gradational furrows appear as very thin streamers with almost no relief in the subbottom. One tuning-fork junction can be seen on 038 and indicates flow to the southwest.

furrow and splay junction region (Fig. 25), the bedforms of this zone indicate two locations of apparent unidirectional current influence. This further suggests that the spacing of the main rectilinear furrow zone may be enhanced bidirectional flow. As one direction dominates the bedform formation, the gradational spacing with distance from the escarpment is apparent. But, when bidirectional flow dominates the gradational spacing may be masked as offsets in furrows created by the different flow directions overlay. Thus, the seaward extent of the regularly spaced rectilinear furrow zone may be larger than expected due to the bidirectional current influences of the region.

Meandering Furrows

Based on work in the Bryant Canyon area (see Chapter II) that confirms the lab work of Allen (1969), additional bedforms are expected under current velocities between the low end of rectilinear furrows and high end of transverse bedforms. If we assume that the contour currents have a high-velocity core adjacent to the Sigsbee Escarpment, then the velocity should decrease with distance from the escarpment. Thus, meandering furrows would be expected somewhere between the rectilinear furrow zone and the transverse bedform zone. This is indeed the case, although they are limited in extent and do not track the entire escarpment. The meandering furrows appear to be confined to the southwestern portion of the study area in front of the re-entrant just to the northeast of Farnella Canyon (Fig. 8). The 3-D seismic data shows the meandering furrow area to be comprised of closely-spaced interwoven furrows with relief between 2-4 m that grade rapidly to simple rectilinear furrows with increasing distance from the Sigsbee Escarpment (Fig. 38). Also interesting is the hint of a splay pattern opening to the east

that exists in this portion of the study area, which suggests a stronger influence from southwest to northeast flows.

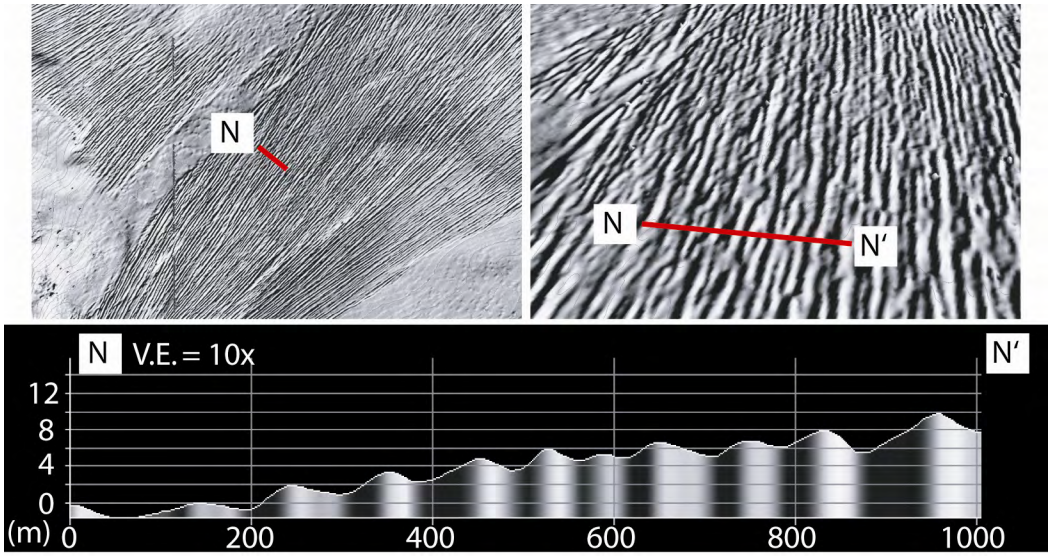

Fig. 38. 3-D Seismic Bathymetry and Profile N in the Meandering Furrow Zone.
The interwoven meanders are clearly visible on the bathymetry. The shallowing of the furrows away from the escarpment is most likely due to thickening of the surface sediments, which results in a corresponding increase in relief as the furrows are capable of eroding deeper into the soft surface sediments.

The high-resolution seismic data shows more of the details of the meandering furrow zone (Fig. 39). The sidescan shows an abrupt transition moving from the transverse bedform zone in the northeast with no furrows, to complete coverage of the seafloor by meandering furrows, and finally a more gradual change to rectilinear furrows at the southwestern extent of the profile. Furrow widths are 10-25 m with almost no space between furrows except for occasional gaps of up to 100 m. The subbottom data from the meandering furrow zone is quite revealing. The northeast end of the profile

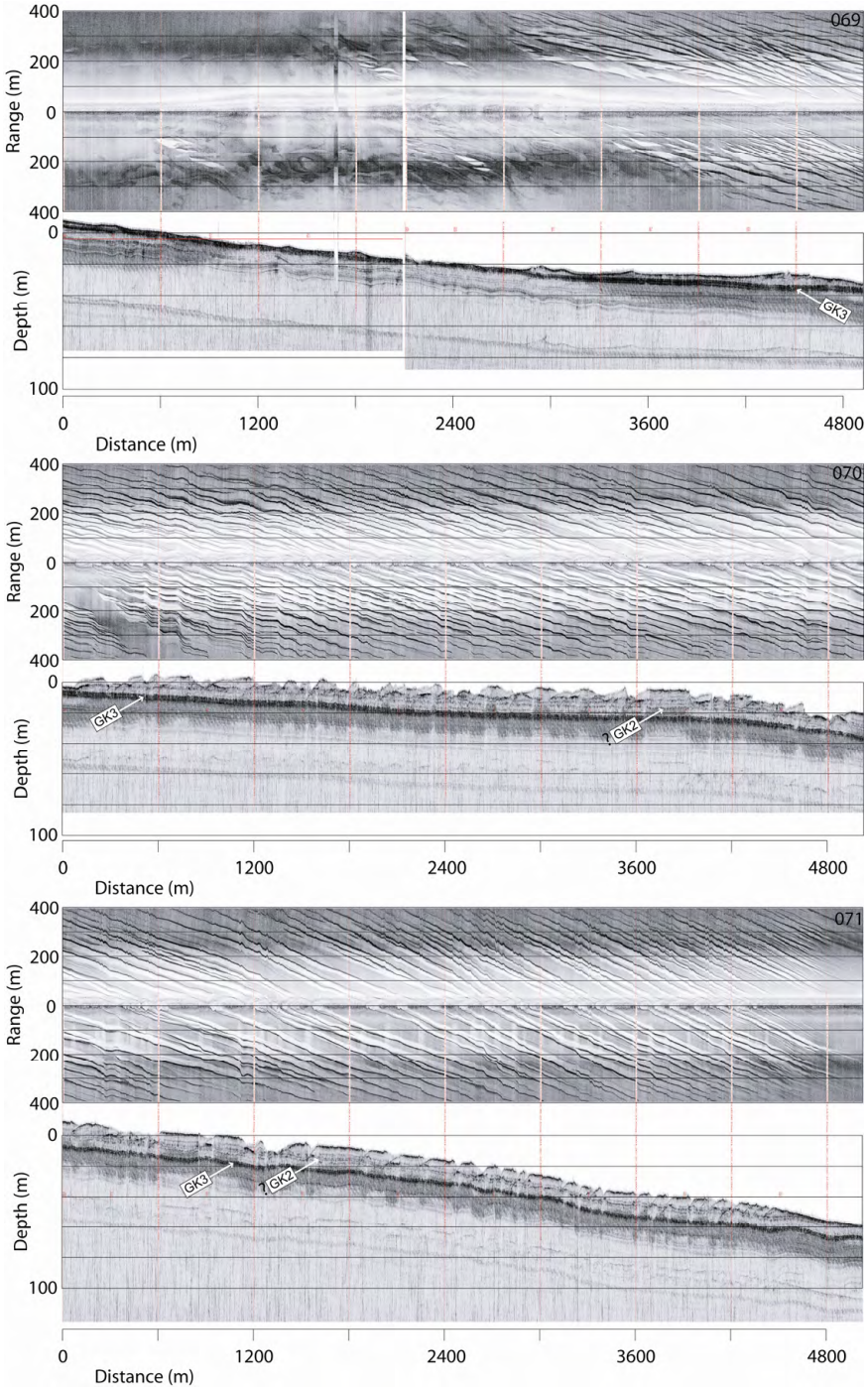

Fig. 39. Deep-Tow Profiles 069-071 across the Meandering Furrow Zone.
Profiles 069-071 cross the meandering furrow zone moving from northeast to southwest. Furrows are only present where Unit 3 or Unit 2 exists. No furrows erode below horizon GK3. Meandering furrows can be seen to erode into Unit 3 and grade into rectilinear furrows that terminate at the exposure of horizon GK2. The rectilinear furrows of this region close to the Sigsbee Escarpment erode into Unit 2, while the outer rectilinear furrows (Fig. 24) only erode into Unit 1, implying higher current velocities here.

shows the exposure of GK3 at the edge of the transverse bedform zone. Moving along the Sigsbee Escarpment, the meandering furrows are only present when Unit 3 exists and are better developed as Unit 2 thickens to the southwest. Profile 069 shows the patchy remains of meandering furrows as Unit 3 is completely removed from above GK3. The exposure of GK3 emphasizes the erosional nature of the contour currents in this region, as over 10 m of sediment have been removed. The meandering furrows have the ability to erode into Unit 3, but as they grade into rectilinear furrows, the top of Unit 3 marks the maximum depth of erosion. In fact, the rectilinear furrows terminate when Unit 2 is completely removed. Core OCN002 showed no dramatic physical property change between Unit 2 and Unit 3 implying that very subtle changes in sediment properties and current velocity can lead to distinctly different bedforms and erosional capacities.

Flutes

Between the flow velocities that generate transverse bedforms and those that generate meandering furrows we expect to find flutes as were found in the Bryant Canyon furrow region (see Chapter II). Interestingly, flutes are somewhat elusive in the Green Knoll study area. This appears to be due to two reasons: 1) Flutes are often isolated features without continuity, and therefore lie just at the resolution limit of the 3-D seismic data. 2) Transverse bedforms appear to be the more common high-velocity bedform of the Green Knoll region. Regardless, flutes appear to be found at the southwestern and northeastern limits of the study area. Because there is no high-resolution seismic coverage of these regions and no significant flutes are found in areas with coverage, the characterization of the bedforms relies solely on the 3-D seismic data

(Fig. 40). The flutes appear as very subtle U- to V-shaped depressions with less than 2 meters of relief. The flutes are aligned parallel to the Sigsbee Escarpment with the apex pointing to the northeast and the opening facing the southwest. Based on standard geometry of flutes relative to flow (Allen, 1969; Dzulynski and Walton, 1965) the orientation indicates a northeast to southwest flow. The cross-sectional profiles perpendicular to the flow show variable symmetry with no repetitive pattern to the morphology. Without the availability of high-resolution seismic data over this region, it is difficult to confirm that these features are indeed flutes; however, their position relative to the Sigsbee Escarpment, the deflection zone, the transverse bedforms and the rectilinear furrows places them in the proper velocity regime for flute formation.

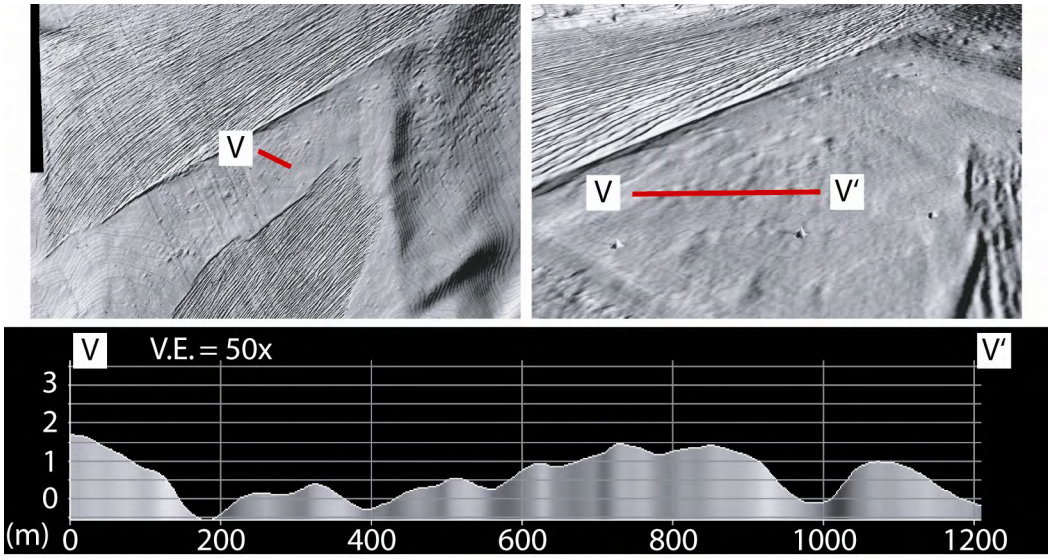

Fig. 40. 3-D Seismic Bathymetry and Profile V in the Flute Zone.
Flutes appear as small U- or V-shaped depressions with relief less than 2 meters. The small, isolated nature of these features puts them right at the resolution limit of the 3-D data. The resolution limit also tends to smooth out the true geometry of these features.

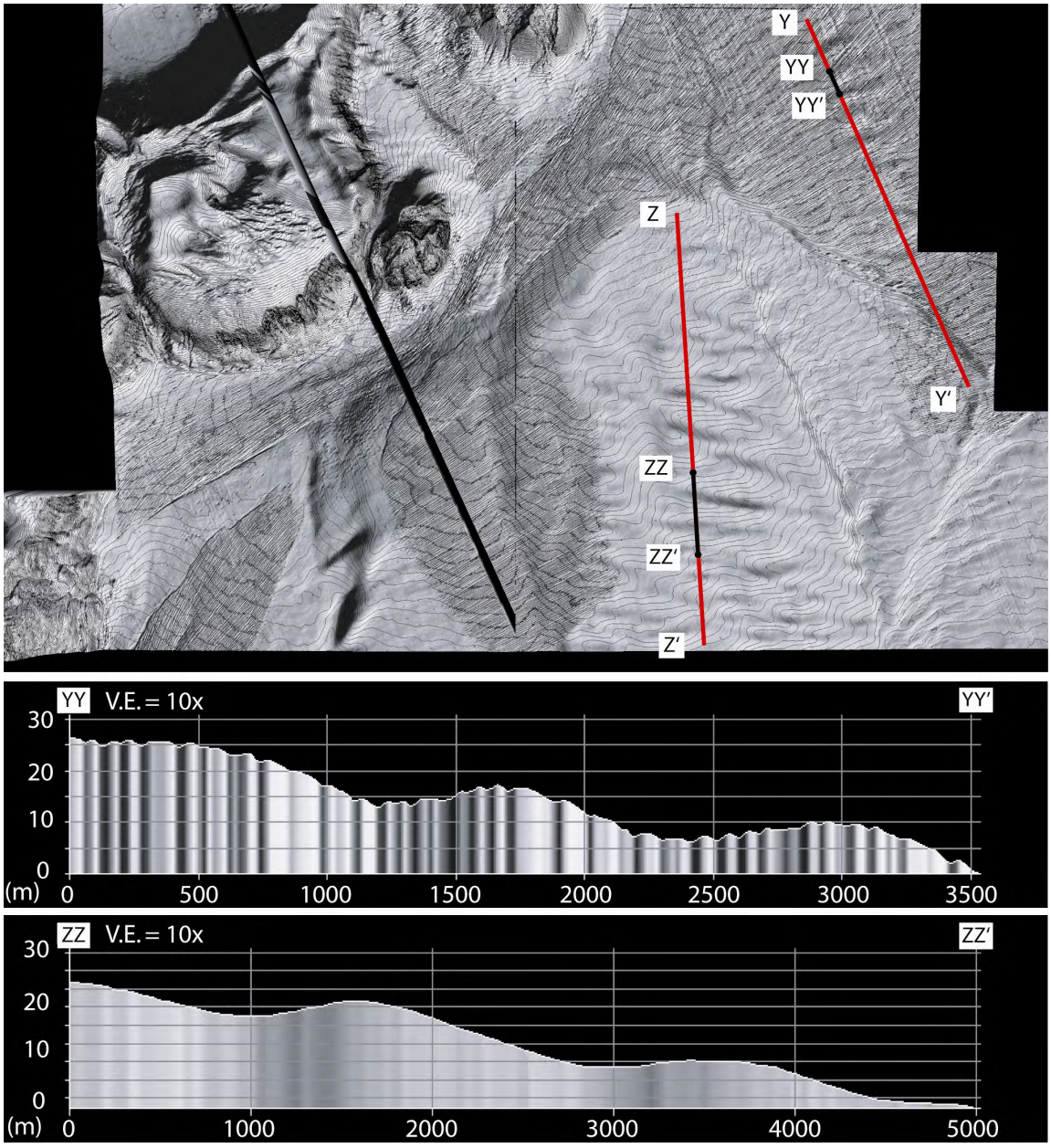

Fig. 41. 3-D Seismic Bathymetry and Profiles YY-ZZ of the Mudwave Zone.
Profiles YY and ZZ (black lines) are subsections of longer lines Y (Fig. 43) and Z (Fig. 42) (red lines). The two profiles show the contrast between furrowed and non-furrowed mudwaves. The furrows on top of the mudwaves of profile YY are clearly visible. Both profiles show a slightly steeper slope on the northern side of each mudwave.

Mudwaves

One particularly distinctive bedform zone within the study area is the mudwaves. The main non-furrowed mudwaves are identified in Fig. 8, but additional mudwaves can be identified beneath the main rectilinear furrow zone. The 3-D seismic bathymetry reveals the basic characteristics of the furrowed and non-furrowed mudwaves (Fig. 41). The rectilinear furrows can be seen to run uninterrupted over the mudwaves of profile Y. Generally, the mudwaves are 2-20 m in height with spacing of 1.0-2.5 km and oriented 35°-60° to the flow direction based on the main rectilinear furrow field. A similar angle of the mudwaves relative to the furrow direction was also seen off the Blake-Bahama Outer Ridge (Flood and Hollister, 1975). Indeed, mudwaves have often been found in conjunction with contour current regions (Embley et al., 1980; Flood and Hollister, 1975; Hollister et al., 1974; Ledbetter, 1993). A summary of the current theories on mudwave formation and migration is given by Manley and Flood (1993). The dominant migration theory is the lee wave model developed by Flood (1988), which describes erosion on the downstream side and deposition on the steeper upstream side resulting in upcurrent migration.

A 3-D seismic profile of each mudwave area gives an excellent picture of the long-term process of mudwave migration (Fig. 42 and Fig. 43), and clearly reveals the direction of mudwave migration, which is consistent with a southwesterly flowing contour current assuming upcurrent migration. The undulating surface which initiated the subtle changes in flow resulting in differential deposition appears to be a deep

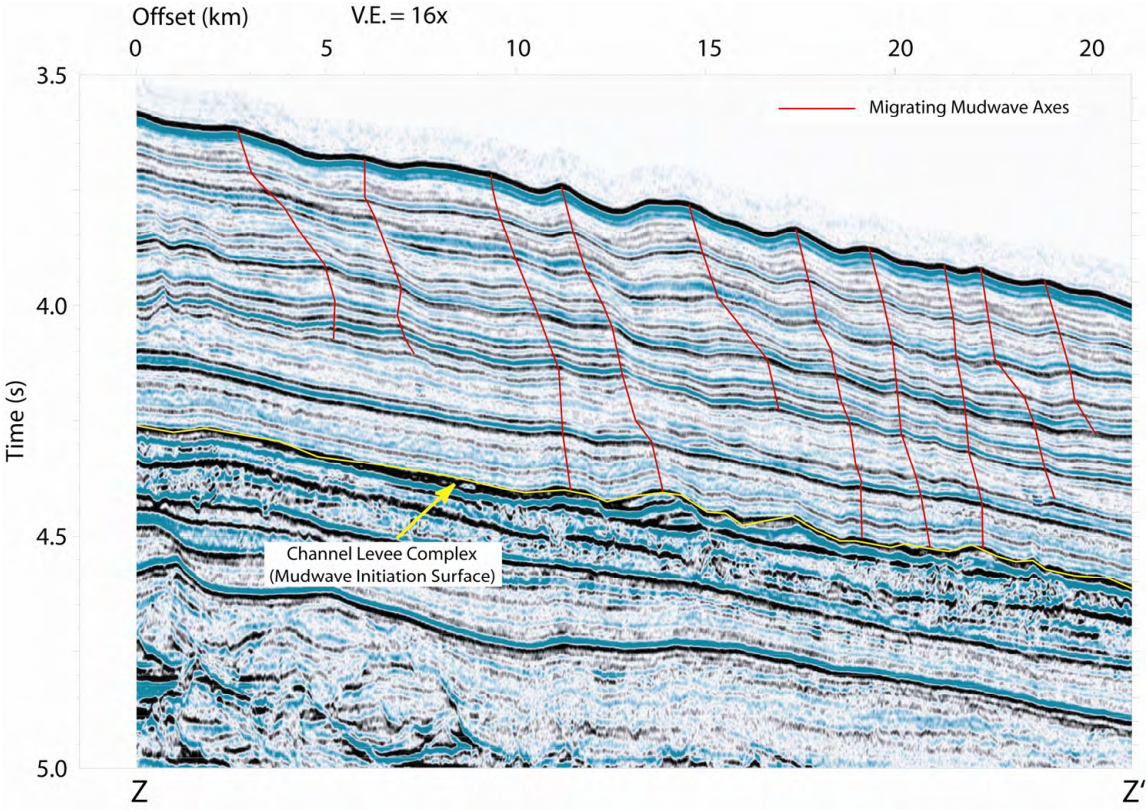

Fig. 42. 3-D Seismic Profile Z of Non-Furrowed Mudwaves.
The red lines track the apex of each mudwave as it migrated over time. The channel levee complex is the surface which initiated differential deposition under bottom currents resulting in migrating mudwaves. The mudwave section is just over 0.5 seconds (~500 m) thick indicating the geologically long-term presence of bottom currents in the region.

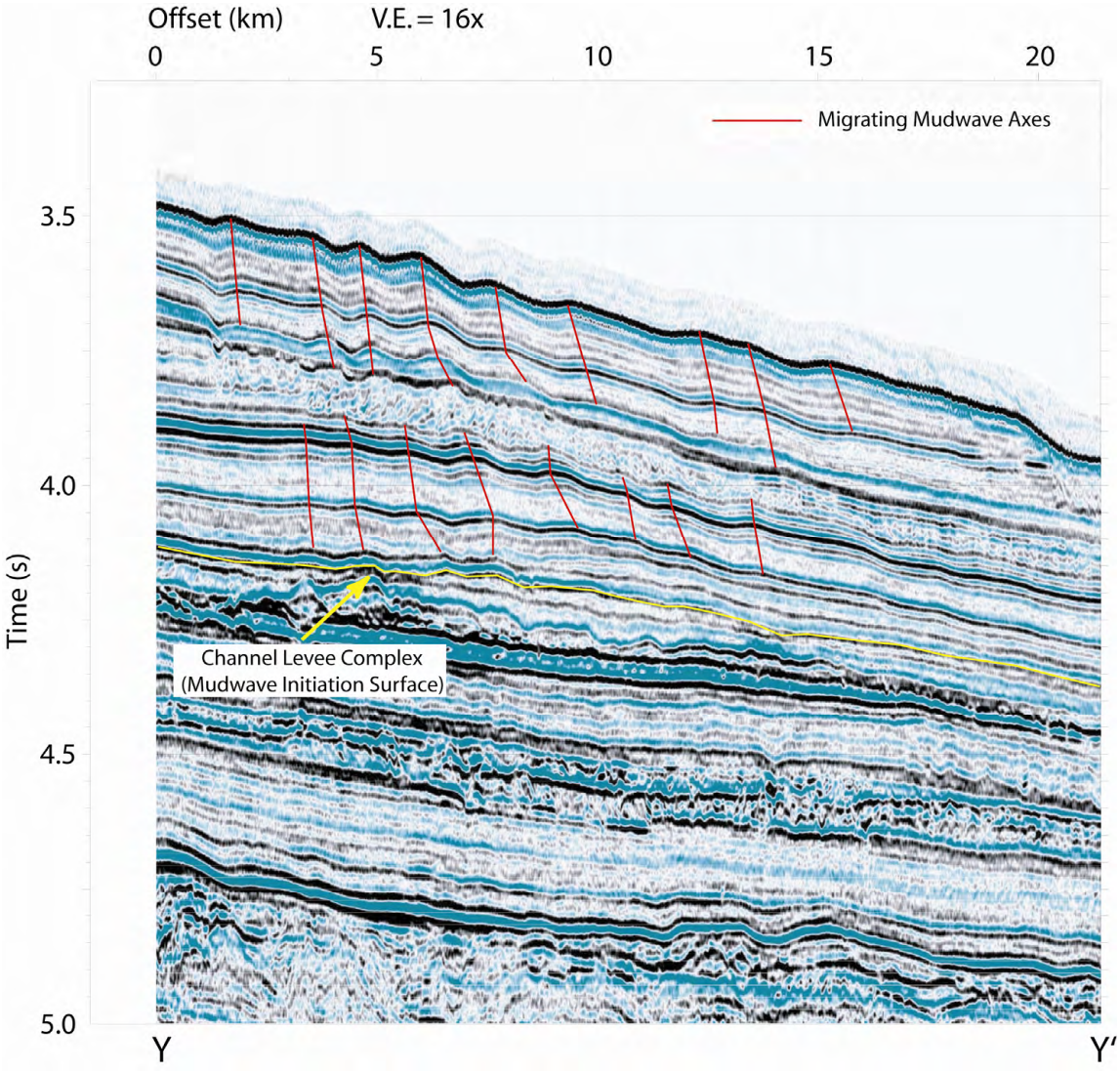

Fig. 43. 3-D Seismic Profile Y of Furrowed Mudwaves.
The red lines track the apex of each mudwave as it migrated over time. The channel levee complex is the surface which initiated differential deposition under bottom currents resulting in migrating mudwaves. A slump within the mudwave package temporarily interrupts the continuity; however, the mudwaves continue to migrate starting from the slumped surface. The mudwave section is a little over 0.5 seconds (~500 m) thick indicating the geologically long-term presence of bottom currents in the region.

channel levee complex associated with lower sea-level and greater canyon outflow activity. Fig. 43 even shows that the migration was interrupted by a slump of the mudwaves themselves, but the migration continued and aligned to the geometry of the

new slumped surface. The seismic data indicate about 500 m of deposition with mudwaves. Using a average sedimentation rates calculated from Slowey et al. (2003) of 30 to 80 cm/10^3 yrs, this suggests a total period of 0.6 to 1.6 x 10^6 yrs of mudwave deposition. As for the velocity regime of mudwaves, Manley and Flood (1993) suggest a minimum current velocity of 17 cm/s for mudwaves oriented oblique to the current direction. This is consistent with the projected 20-30 cm/s current velocity of the rectilinear furrow field based on the work of Allen (1969), and yields a likely current velocity range of 15-30 cm/s. The uninterrupted migration implies long-term, directionally stable currents at the base of the Sigsbee Escarpment throughout the depositional history of these mudwaves.

Further details about the recent history of these mudwaves can be seen in the high-resolution seismic data. Profile 043 (Fig. 24) and profile 076 (Fig. 44) cross furrowed and non-furrowed mudwaves, respectively. Both subbottom profiles reveal the slight increase in bed thickness on the upstream or depositional side along with a decrease in bed thickness on the downstream or erosional side. In fact, profile 076 from the non-furrowed mudwaves shows a complete pinch-out of the surface layer and apparent lack of horizons GK1 and GK2, indicating a more erosional environment in the non-furrowed mudwave zone as compared to a more depositional environment in the furrowed mudwave zone. It is important to note that profile 076 is oriented at a highly oblique angle to the mudwaves and in the direction of migration, giving the distorted appearance of a gentler slope on the upstream depositional side of the mudwave.

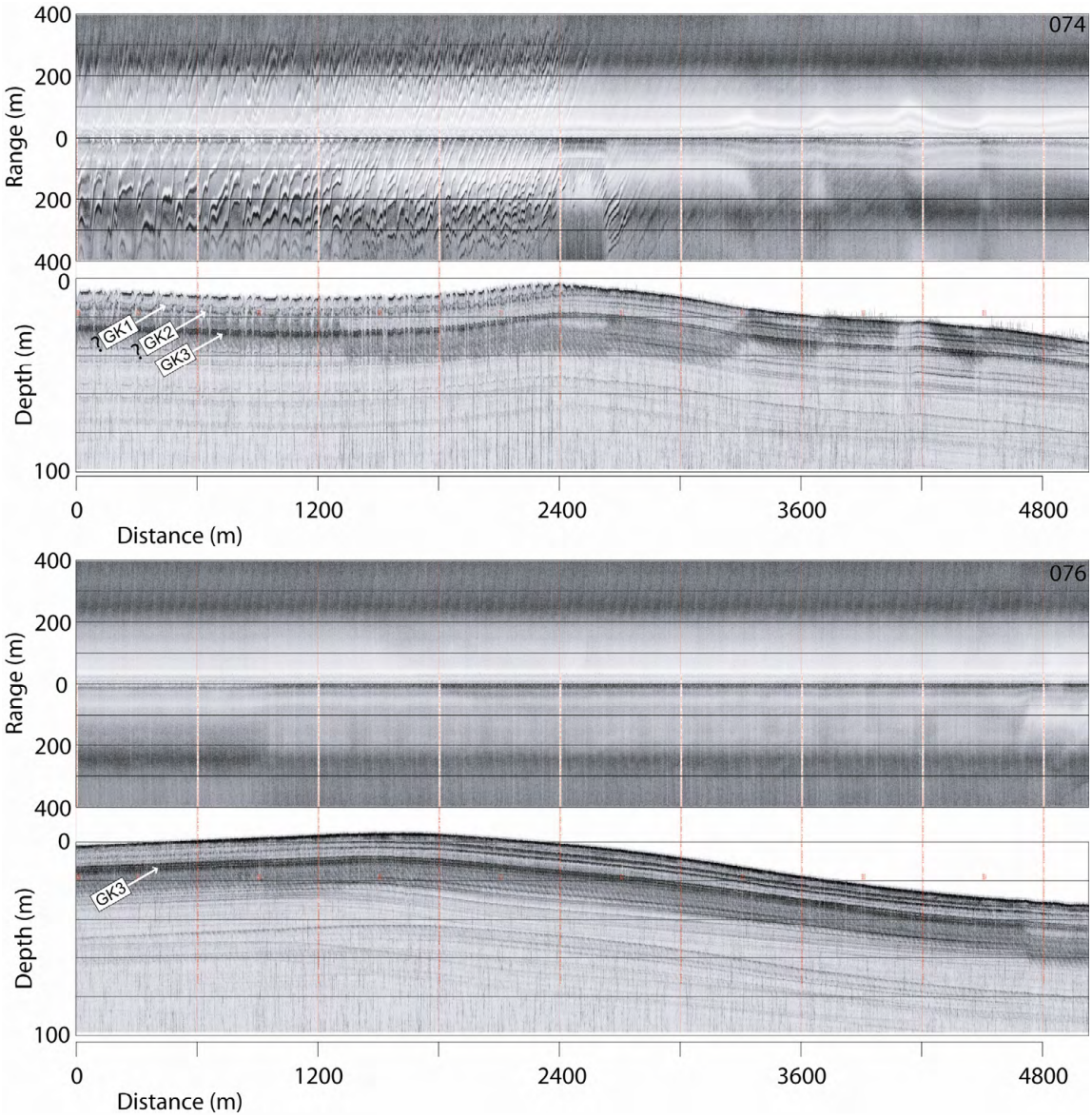

Fig. 44. Deep-Tow Profiles 076 and 074 across the Non-Furrowed Mudwaves.
All three marker horizons appear to be present in the furrowed zone near the beginning of 074. Horizons GK1 and GK2 are not definitive due erosional disconnection from the northeastern parts of the survey. The furrows terminate when horizon GK2 is exposed, thus the reason for the lack of furrows on this set of mudwaves is the lack of Unit 1 hemipelagic drape. The sidescan of the mudwaves shows a completely featureless seafloor. The subbottom of profile 076 clearly shows the erosional nature of the downstream flank of the mudwave and the depositional nature of the upstream side. The downstream side appears steeper only because of the highly oblique angle crossing of the mudwave from southwest to northeast.

A puzzling aspect of the southwest mudwave zone is the complete lack of furrowing over the region (Fig. 41). The furrows simply stop at the perimeter of the non-furrowed mudwaves of profile Z-Z′. But this does not appear to be a consequence of the mudwaves themselves, since the rectilinear furrows run over many of the mudwaves to the northeast without any interruption. The high-resolution seismic profile 074 (Fig. 44) reveals the primary reason for the lack of furrows. The western portion of profile 074 shows well-developed furrows on the upstream side of a mudwave. Horizons GK1 and GK2 are tentatively identified, but due to erosion of both horizons to the northeast, these horizons cannot be absolutely confirmed by a direct connection. Regardless, it is clear that nearly 10 m of sediment are removed between the crest and the lowest downstream side of the mudwave, leaving behind only Unit 3. The furrows can be seen to fade out as the remnants of Unit 2 are removed. As discussed in the meandering furrow zone, Unit 3 appears to mark the maximum depth of erosion for rectilinear furrows. Indeed profile 076 shows that Unit 2 and Unit 1 continue to be missing across the mudwave field. This is in direct contrast to the furrowed mudwaves of profile 043 (Fig. 24) that clearly show the presence of Unit 1 and 2; thereby, reinforcing the idea that the rectilinear furrows require the softer surface sediments of Unit 1 and 2 in order to develop. While it then follows that lack of furrows on the southwestern mudwaves is due to the erosion of Units 1 and 2, the ultimate cause for that erosion across such a confined region in the middle of the rectilinear furrow field remains unknown.

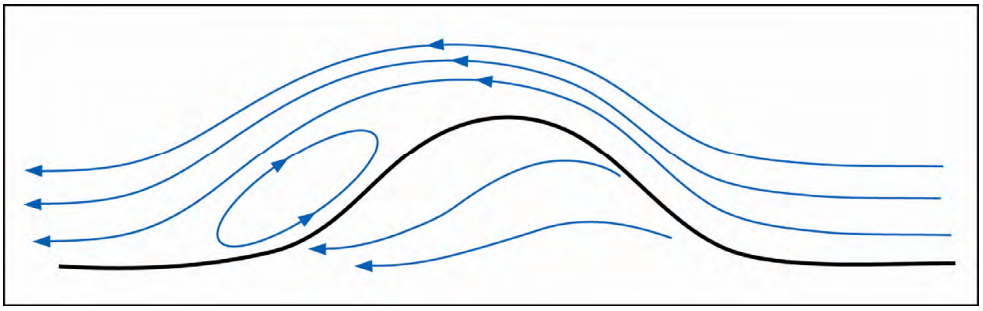

Fig. 45. Vertical Cross Section with Streamlines of Flow over an Obstruction.
The blue lines are the streamlines with arrows indicating the flow direction and the black line is the profile of the obstruction. The recirculation zone is shown beneath the flow separation on the lee side of the obstruction (after Hunt and Snyder, 1980).

Recirculation Scour

The remaining contour-current bedform zones are spatially isolated and are included here to identify some of the more subtle yet important aspects of the current-topography-sediment interactions of the Green Knoll study area. One of the more impressive features of those surrounding Green Knoll are the recirculation scour marks that would be on the lee side of the knoll relative to a southwesterly flowing current. Experiments and modeling by Hunt and Snyder (1980) in both stratified and unstratified flow at a range of Froude numbers reveal several persistent morphologic features corresponding to flow over an obstacle. In particular, as the flow separates from the top of the obstruction a recirculation region develops in the lee of the obstruction (Fig. 45). Depending on the flow characteristics the recirculation can be large or small, but in general it is a common feature. The presence of such a recirculation region is preserved in the surface geology on the lee side of Green Knoll. The 3-D seismic data shows large furrow-like scours on the knoll with progressive scarp retreat at the erosional furrow head near the top of the knoll (Fig. 46). Additionally, the seafloor amplitude map (Fig.

14) reveals higher amplitudes along the flanks and base of the knoll due to older bedding exposures in this heavily scoured area.

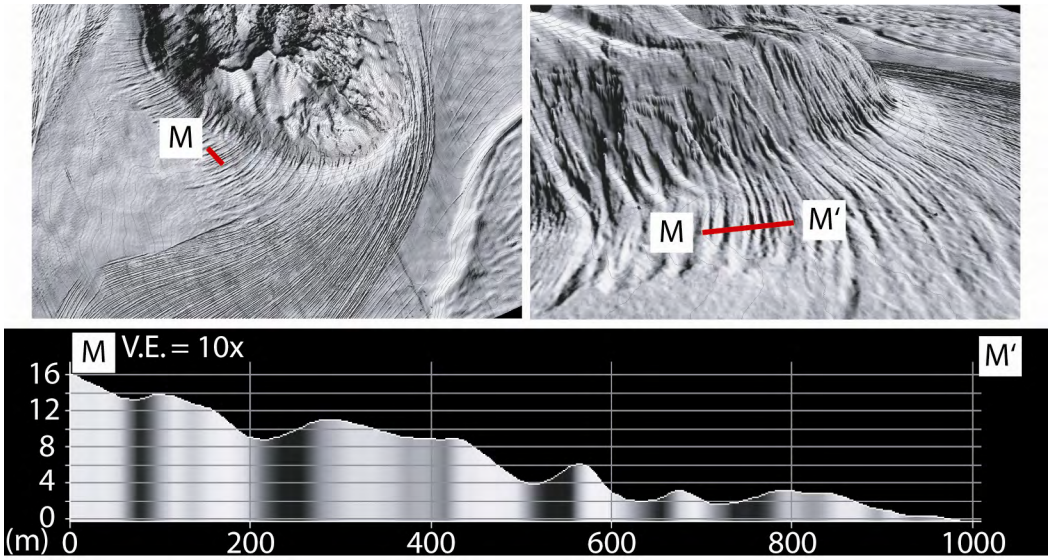

Fig. 46. 3-D Seismic Bathymetry and Profile M of Recirculation Scour Zone.
The recirculation patterns described in Fig. 45 are clearly visible in the pattern of scour on the lee side of Green Knoll. The scours appear to have been initiated by furrowing upslope in the recirculation zone and continued of the flank of the knoll creating channelized slumping and head scarp retreat upslope.

The high-resolution seismic data again reveals more of the details of the recirculation zone (Fig. 47). At the base of the zone horizon GK3 and Unit 3 is present, but Unit 1 and 2 have been eroded. Narrow furrows (10-20m) with 1-4 meters of relief cover the seafloor. Moving up the flank of the knoll the major recirculation scours dominate the profile with relief of up to 20 m and widths in excess of 200 m. The sidescan data show banding in the furrow troughs that are erosionally exposed bedding planes along the flank of the knoll. The recirculation erosion appears to undercut the flanks of the knoll leading to additional erosion via scarp retreat and slumping down the

furrow axes. This extensive erosion obliterates horizon GK3 and scours well into the horizons below. The recirculation scour is also a means of enhancing the erosional moat around Green Knoll. That this inferred flow pattern on the lee side of Green Knoll does indeed occur is supported by industry current meter data that shows flows moving southwest to northeast up the flank of the knoll (Bryant, 2004); however, these data do not exclude the possibility that the flow was due to general northeasterly flowing currents rather than a recirculation pattern.

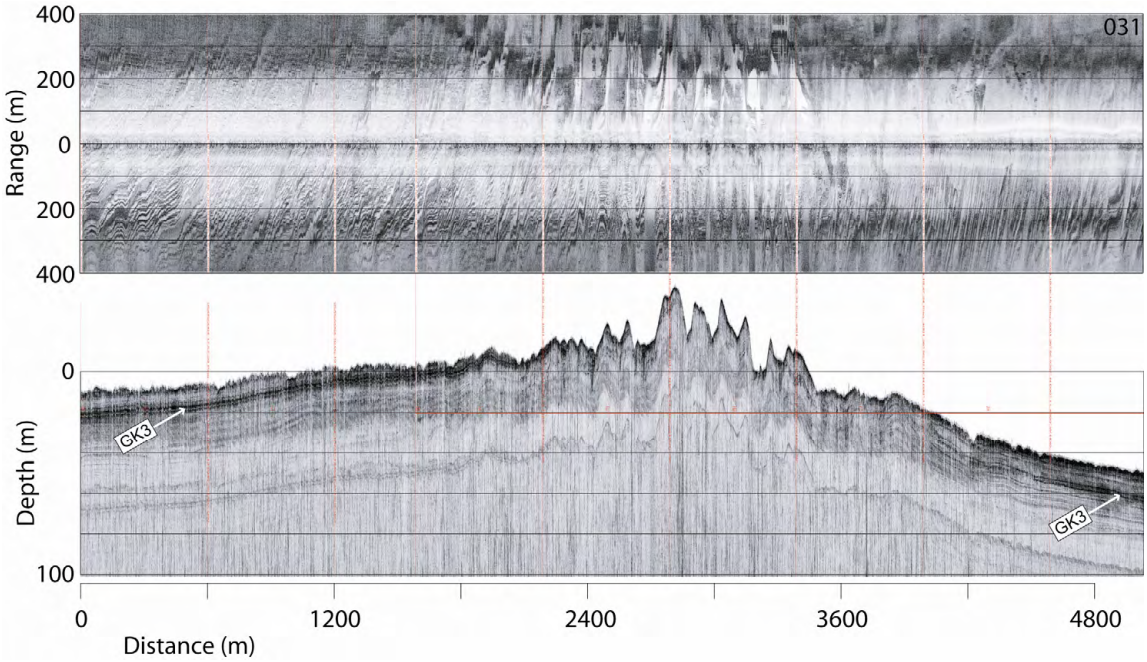

Fig. 47. Deep-Tow Profile across the Recirculation Scour Zone.
Horizon GK3 is the only marker bed present in this profile. The closely spaced furrows on the flank of the uplift only erode into Unit 3. The subbottom shows the extreme relief of the slump channels in the center of the figure, while the sidescan banding within the channels created by erosional exposure of sedimentary layers on the flank of Green Knoll.

Upslope Furrows

A variation on the recirculation scour which is associated with flow moving up the flank of Green Knoll are zones of furrows that appear to be linked with contour currents that flow upslope on the upstream side of an obstruction. There are two main areas of upslope furrowing apparent on the northeast facing flank of topographic highs, one along the Sigsbee Escarpment and one on the flank of Green Knoll (Fig. 8). The Sigsbee upslope furrow zone shows a furrow pattern that connects and continues the deflection and splay zone of the same area (Fig. 48), which indicates the furrows on the flank of the escarpment are facing into the current and appear to be eroding upslope. These furrows on the flank of the escarpment (profile P) are 2-10 m deep and 15-25 m wide, while the furrows that actually track across the top of the escarpment (profile O) are less than 2 m deep and slightly narrower. Compared to the Green Knoll recirculation scour zone, a similar but less developed pattern of scarp retreat and channelized slumping is found.

Moving to the northeast another upslope furrow region is found on the flank of Green Knoll (Fig. 49). The nearby contour current patterns of this region do not preclude the possibility that this is actually a recirculation zone relative to northeasterly flowing currents over the knoll. But, the lack of similar features across the entire northeast face of the knoll, the dominance of the deflection pattern on the south side of the knoll indicating southwesterly flow, and the straight nature of the furrows rather than slightly deflected as with the recirculation furrows of the southwest flank, suggest that

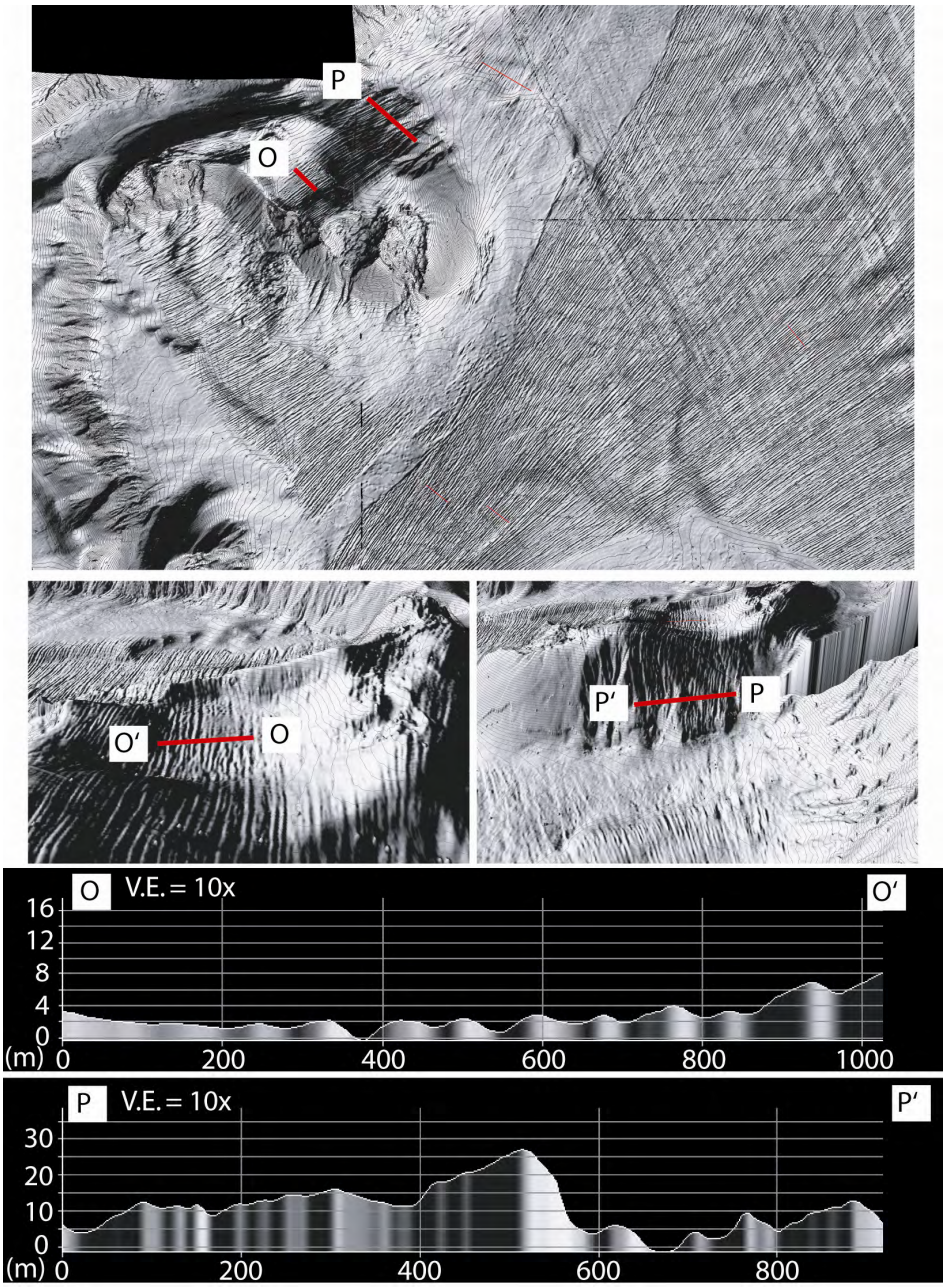

Fig. 48. 3-D Seismic Bathymetry and Profiles O & P across the Sigsbee Upslope Furrow Zone.
For orientation of the perspective views, both images are looking southwest along the Sigsbee Escarpment in the direction of current flow. Profile P shows the upslope scour of furrows that appear to initiate scarp retreat similar to that of the recirculation zone of Fig. 46; however, connection of these upslope furrows with the deflection and splay pattern suggest predominantly northeast to southwest flow creating the upslope erosion. The furrows across the top of the Sigsbee Escarpment (profile O) show much less relief than those that erode upslope suggesting possible enhanced erosion via slumping initiated by the furrow scour.

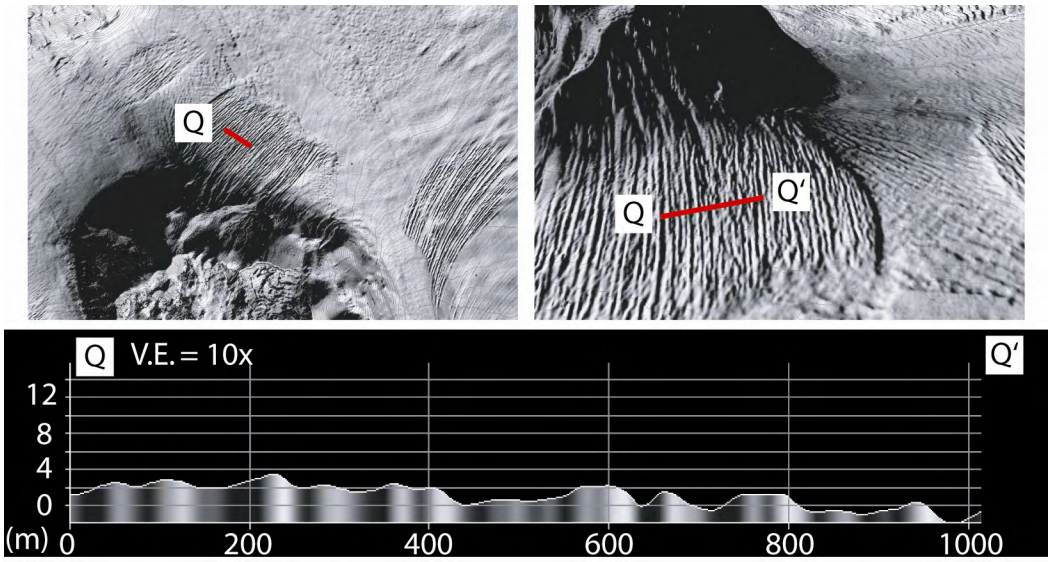

Fig. 49. 3-D Seismic Bathymetry and Profile Q across the Green Knoll Upslope Furrow Zone. The perspective view looks southwest and downcurrent. The furrows appear as rectilinear to meandering and scour up the flank of Green Knoll and show relief on the order of 2 m that increases with increasing scour and slumping upslope. The significant erosional scour associated with transverse bedform zone is seen as it undercuts the upslope furrows on the north side.

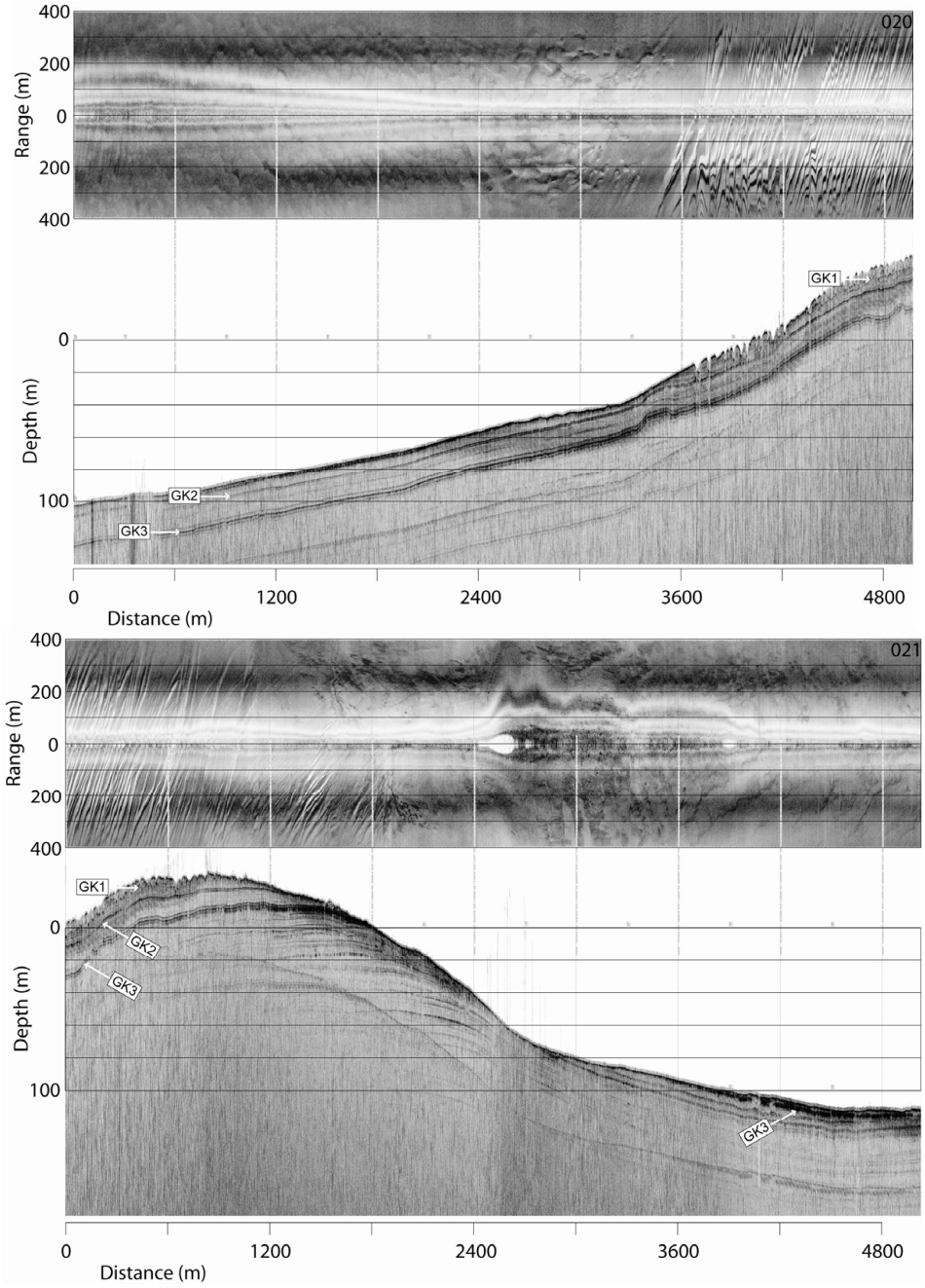

Fig. 50. Deep-Tow Profiles 020 & 021 across the Green Knoll Upslope Furrow Zone.
Unit 1 is missing, except in the furrowed region. The furrows erode only into Unit 2 on the uplifted flank of Green Knoll. An area of creep and possible slumping is visible on the southern slope beneath the furrows of profile 020. The extreme erosional scour of the transverse bedform zone exposes outcropping layers on the northern flank of the Green Knoll uplift.

these furrows are associated with southwesterly flow up the flank of the knoll. The furrows of this region are only 1-4 m in relief and 10-30 m wide with normally close (10-50 m) spacing but occasional gaps up to 150 m. As with the Sigsbee upslope furrows, large slump scars are visible that appear to be connected and channelized into the furrows. Based on the high-resolution seismic data (Fig. 50), the furrows are eroded into an uplifted section of the Green Knoll. As has been found throughout the study area, these rectilinear furrows only exist in Unit 1. The exposure of horizons GK2 and GK3 on the northern side of the uplift mark the limit of furrow erosion. Transverse current marks are the only bedforms across the exposure of GK3 to the north of the upslope furrow zone indicating a rapid increase in current as it is focused between Green Knoll and the Sigsbee Escarpment. The key concepts associated with the upslope furrow zones are: 1) No matter where the currents flow, as long as the velocities fall in the right range, and the softer surface sediments are available, furrowing is possible. 2) Contour currents do not always follow the contours, *i.e.* in the presence of an abrupt obstruction, flow patterns adapt to the topography and can experience flow separation.

Topographically Isolated Furrows

Associated with the idea that contour currents do not always flow parallel to the contours are the regions of topographically isolated furrows (Fig. 8). Two re-entrants in the Sigsbee Escarpment have distinct rectilinear to meandering furrow patterns on the re-entrant floor and perpendicular to its axis (Fig. 51). Interestingly, the steep walls of the Sigsbee Escarpment surrounding the re-entrants do not prevent furrow formation in their

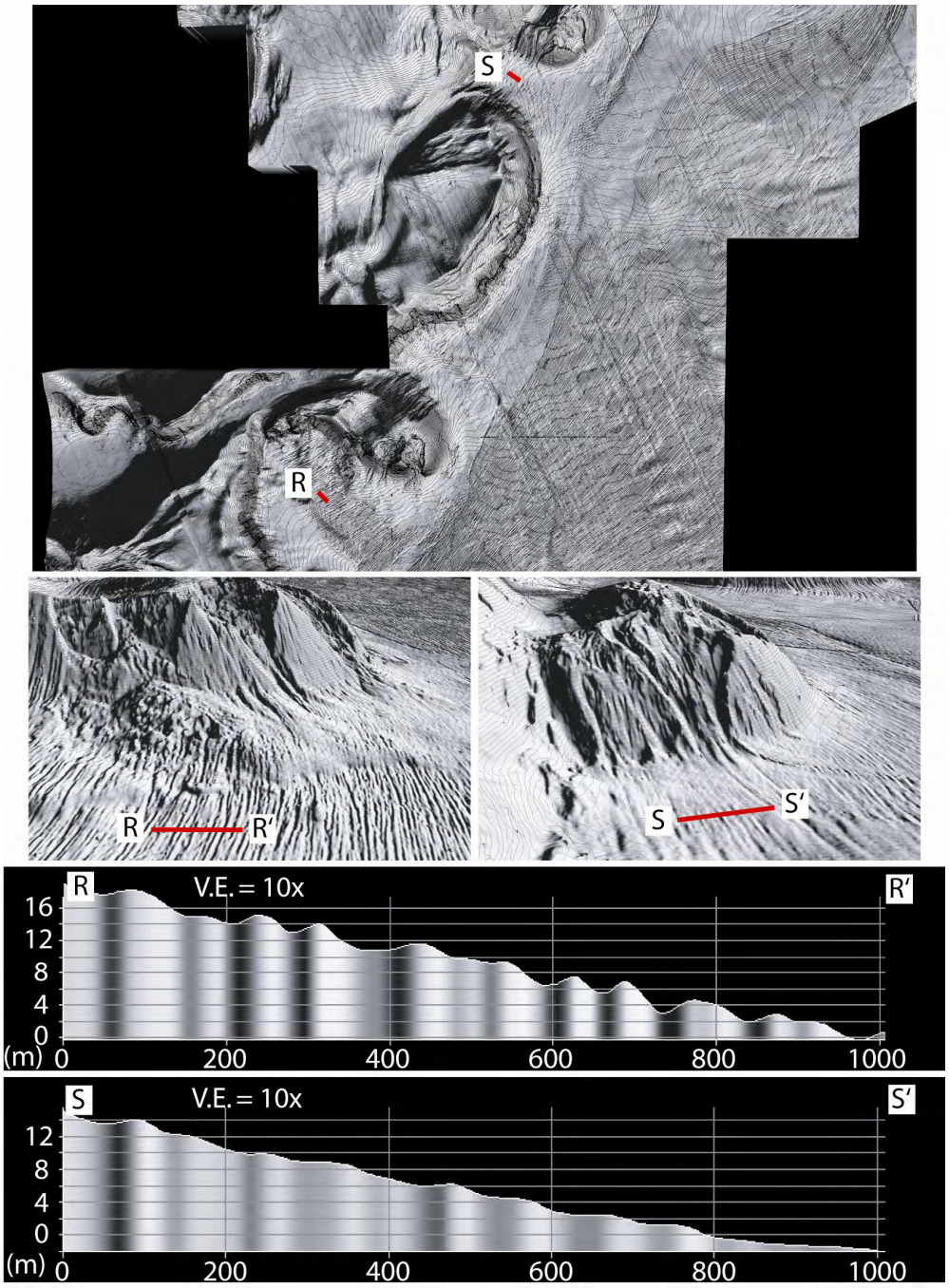

Fig. 51. 3-D Seismic Bathymetry and Profiles R & S in the Topographically Isolated Zones.
The furrows in the isolated re-entrants show connection with the deflection and splay zones on the northeast sides only. Slumping that appears to be initiated by the erosion of furrows into the Sigsbee Escarpment also appear on the northeast or downcurrent facing flanks of the escarpment, suggesting possible recirculatory flow in the isolated furrows zones. The furrows of profile S show much less relief indicating more erosion of existing surface drape and exposure of erosion resistant sediments.

axes. The southwestern isolated furrows (profile R) are deeper, narrower, and slightly closer spaced than those of profile S. Both patterns appear connected with the adjacent deflection and splay zones to their northeast, and the furrows terminate prior to the base of the southwestern re-entrant walls. Additionally, the northeastern re-entrant walls show connected furrowing to the axis floors. This suggests a dominant northeast to southwest flow and may indicate recirculation flow beneath a flow separation from the Sigsbee Escarpment. Based on the previous results for other areas, the deeper furrows of the southwestern re-entrant are a likely indicator of a thicker layer of soft surface sediments. Indeed, the seafloor amplitude map (Fig. 14) shows much lower amplitudes in the southwestern re-entrant that supports the idea of erosional exposure of horizons deeper than GK2 in the northeastern re-entrant.

Obstacle Scour

The last contour-current bedforms to be discussed are the obstacle scours (Fig. 8), which are small features less than 2 m high and less than 40 m wide with somewhat random spacing that can be as close as 10 m or as much as 250 m. There are two areas where they are visible (Fig. 52): 1) adjacent to a furrow termination area near the southwestern flute zone and transverse bedform zone, and 2) in the northeast corner of the mudwave fields also adjacent to a furrow termination zone. It is important to note that since these features are isolated bathymetric highs of small diameter, they are right on the edge of the 3-D seismic resolution. And since there are no deep tow profiles across one of the zones, we must rely only on the 3-D seismic data, which will tend to

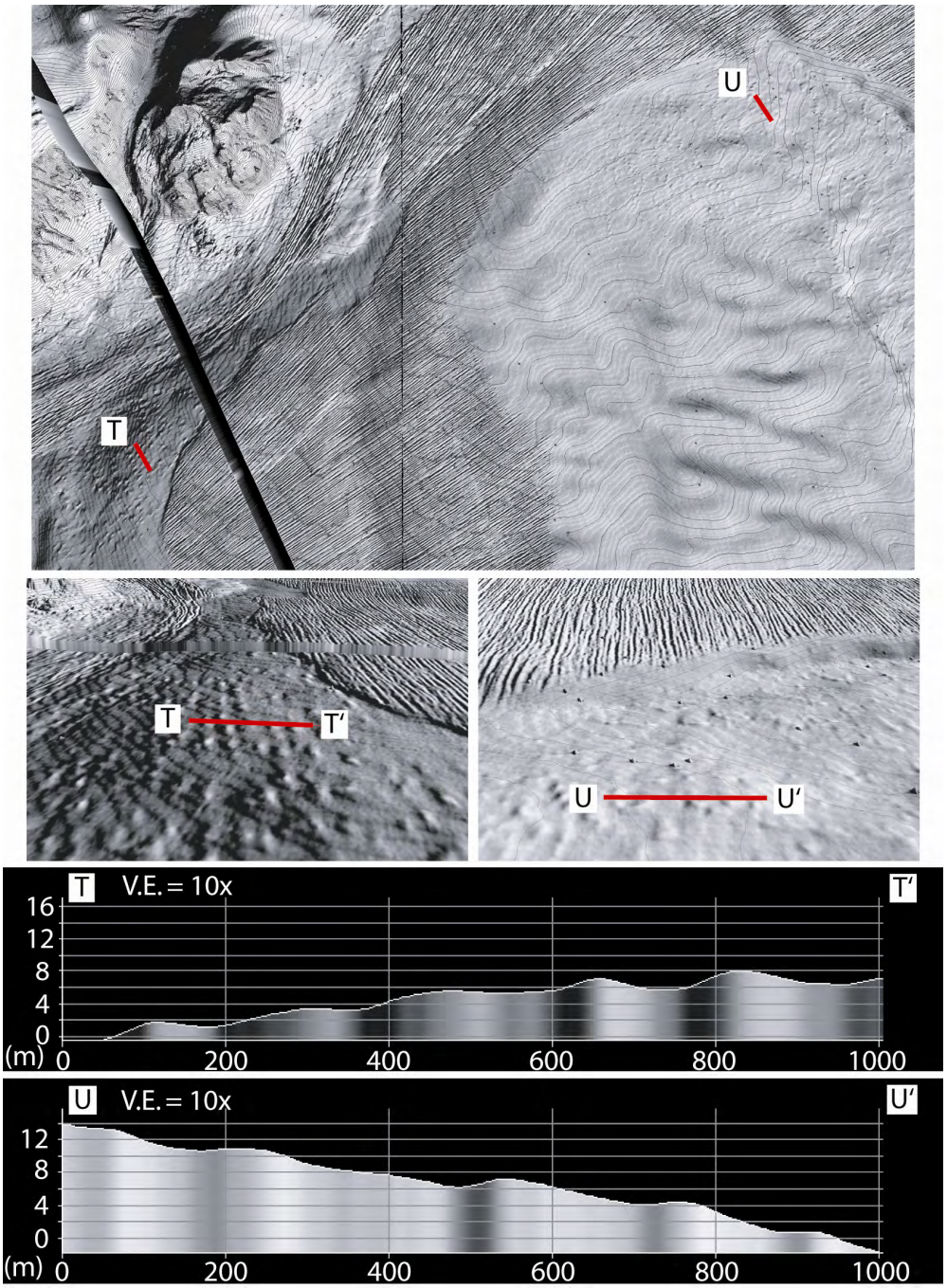

Fig. 52. 3-D Seismic Bathymetry and Profiles T & U across the Obstacle Scour Zones.
Two locations of obstacle scour marks are shown. One is just northeast of the flute zone and the other is on the northeast corner of the mudwave zone. Both regions show features with relief above the surrounding seafloor and subtle indications of erosional tails, but no dominant orientation between northeast of southwest indicating bidirectional flow. Both regions are adjacent to furrow terminations suggesting that the obstacles are residual furrow walls.

broaden and smooth the bedforms. That being said, the association of these features with the termination regions of rectilinear furrows and some of the higher velocity bedform zones suggests that most of Unit 1 and Unit 2 have been removed. Consequently, the remaining sediments will be more resistant to any erosion that is occurring. Many of the features have an elongated nature to them, suggestive of the tails of obstacle scours (e.g. Dzulynski and Walton, 1965) that may result from the passage of currents around residual walls of furrows or simply residual uneroded material. The tails are oriented 40°-60°, but there is no consistent tapering direction to indicate which of the two possible flow directions dominates. Thus this is a region where bidirectional flow is possible. These obstacle scours are noteworthy as indicators of the dynamic link between currents and sediment type, and the show how localized some of the effects can be.

Timing and Erosion

Now that the characteristics of the region have been discussed, we can discuss the general timing of furrow formation in the region. One of the main constraints on timing is the triplet horizon GK3. A recent study in the Mad Dog and Atlantis prospects (Fig. 6) collected high-resolution seismic data and jumbo piston cores for assessment of the timing on slumps in the region (Niedoroda et al., 2003; Slowey et al., 2003). Two key marker horizons were identified in their study area (M1 and M2). These marker horizons appear to correlate with the marker horizons of this study (GK2 and GK3). There are several reasons this correlation appears to hold. The two study areas are less than 6 km apart and the two marker horizons were seen to be regionally persistent across

both study areas. In particular, the lateral continuity of horizons GK2 and GK3 is over 75 km in this study. The characteristic seismic signature of the horizons from these two study areas is the same. Specifically, the triplet shows up as high-amplitude signatures with a thicker reflector surrounded by two thin reflectors and the GK2/M1 reflectors are lower amplitude reflectors dividing an upper reflector free zone from a lower zone with more lower-amplitude reflectors. The relative depths of the reflectors from both studies are the same. And finally, the lithology is similar with the triplet being associated with silt layers interbedded in a section of thin parallel bedded silts and silty clays. This association is important because the M1(GK2) and M2(GK3) reflectors were dated to be 15 ka and 19 ka respectively (Slowey et al., 2003), which means that the maximum age for the Green Knoll contour-current bedforms is 19 kyr. Or, given that the maximum rectilinear furrow erosional depth is equivalent to horizon GK2, a tighter maximum age limit of 15 kyr can be placed on the initiation of furrowing.

This maximum age constraint would assume a syn-depositional furrow model, where furrows follow the aggradational model of Tucholke (1979). However, given the following:

- visible exposure of highly consolidated sediments near the Sigsbee Escarpment on the *DSV Alvin* dive
- exposure and truncation of deeper reflectors on the high-resolution seismic data throughout the area
- the presence of lag deposits and visible erosion near Green Knoll
- the steep walled furrows that match the erosional model of Flood (Flood, 1983)
- the presence of high-velocity erosional flutes and transverse bedforms near the Sigsbee Escarpment and Green Knoll

- a rectilinear furrow field that matches those created by Allen (1969), which were observed to be erosional in nature
- very low Late Holocene deposition rates in the region of only 12 cm/kyr (Slowey et al., 2003)
- confirmed furrow erosion of 7m of sediment at the base of the Escarpment by comparison to an original thickness of sediment that was capped by an erosion resistant debris flow (Niedoroda et al., 2003)
- no evidence in the high-resolution seismic data for multiple furrow events or furrow migration above the GK3 horizon

It is unlikely that the furrows of this region are aggradational, except in the seaward-most extent of the rectilinear furrow field; rather, based on the above evidence, they are more likely to be erosional. If this is the case, the beds that the furrows are seen to erode into must have been deposited first, before the major furrow development. As a consequence the furrows must be a much more recent occurrence than the maximum 15 kyr time constraint mentioned above.

Additional time constraints for furrow formation can be determined using calculated and measured erosion rates. Following the calculations of Wright (1989) we can determine a reasonable bed shear stress (τ_0) for this region. First we calculate the shear velocity (u_*) using the law of the wall:

$$\langle u(z) \rangle = u_*/\kappa \cdot \ln z/z_0 \qquad (1)$$

We estimate the velocity at 100 cm off the bottom to be 50 cm/s based on typical current velocities for the base of the Sigsbee Escarpment (Nowlin et al., 2001). The hydraulic roughness length is calculated from $z_0 = k_b/30$, where the Nikuradse roughness height is approximately one grain diameter with sand sized roughness elements (Wright, 1989). This is consistent with the sands seen in the axes of the furrows. And, the von Karman

constant (κ) equals 0.408 (Wright, 1989). Based on these values u_* = 1.71 cm/s. The bed shear stress is then calculated from $u_* = (\tau_0/\rho)$, where for seawater ρ = 1.025 g/cm^3. So, τ_0 equals 3.0 dynes/cm^2. Based on the experimental results of Partheniades (1986), if the bed shear stress equals 3.0 dynes/cm^2 then the erosion rate (E) is approximately 2x10^{-4} g/cm^2·hr. Averaging the bulk density of the top 10 m of core OCN002 we get 1.5 g/cm^3. Combining average density with the erosion rate we calculate the yearly erosion rate (E_y) to be 1.15 cm/yr, or because this is a very rough estimation and for ease of calculation we estimate the erosion rate to be ~1 cm/yr. Given the typical furrow depth of the main rectilinear furrow zone to be 2 m, it would take only 200 years to erode the furrow field we see on the seafloor today.

Two hundred years is a very short period of time, geologically. So, for comparison we consider to other available erosion rates. Based on the flume studies of Allen (1969) the erosion rate would be ~250 cm per year. In contrast, erosion rate studies using actual sediment samples from the Mad Dog and Atlantis study area suggest average rate of 0.08 cm/yr based on both (Niedoroda et al., 2003). Between these two erosion estimates we calculate that the 2 m deep furrows would take a range of anywhere between 1 to 2500 years to form, while the 8 m deep furrows of the Green Knoll deflection zone would require 4 to 10,000 years to form. The flume studies are most likely an extreme overestimation of the erosion rates since they dealt with highly unconsolidated sediments that do not realistically represent sediments that have accumulated over thousands of years. Conversely, the erosion studies of Niedoroda et al. (2003) are likely an underestimation of erosion rates for three reasons: 1) One

estimation they use for the erosion rate is based on the invalid assumption that sedimentation stopped 9,000 years ago and they also do not account for the time of furrow initiation. 2) The sediment samples they used were from the triplet horizon which marks the limit of erodibility for furrows, based on this study. 3) At the 0.08 cm/yr erosion rate, the 8 m deep furrows of the Green Knoll deflection zone would require 10,000 years to form, which would require the furrows to be more aggradational in nature rather than erosional. Thus, we propose that the most realistic, albeit somewhat speculative, erosion rate is the previously calculated 1 cm/yr.

Conclusions

As a follow up to a study of furrows and other contour-current bedforms in the Bryant Canyon area (see Chapter II), this study focused on the Green Knoll region, which is an area that may be more relevant to current industry exploration and production. The availability of 3-D seismic data (provided courtesy of WesternGeco) allowed the regional mapping of a contour current region at the base of the Sigsbee Escarpment. The detail and coverage of the field of rectilinear furrows and associated bedforms provided new insights into the nature of contour currents and their bedforms. This dataset was augmented by high-resolution seismic, jumbo piston cores, and *DSV Alvin* observations. Using the 3-D seismic data as a framework for investigating this field of contour-current bedforms, the study area was divided into several zones based on bedform morphologies and formation mechanisms (Fig. 8). The contour-current bedform zones were used to address the primary hypotheses of this study. We showed

that there is a large-scale pattern to the development of various contour-current bedforms. We confirmed local bathymetry and topography are primary controllers of bottom water flow that affect what contour-current bedforms will develop. We identified a link between sediment properties and the spatial distribution and morphology of contour-current bedforms. And, we began to place some age constraints on the initiation and development of the study area furrow field.

One key finding of this study came about through the comparison of the various resolution datasets. Although 3-D seismic data provides unprecedented coverage and details of an entire region of small-scale bedforms, defining the accurate geometry of individual bedforms less than about 50m is not possible (Fig. 12). But, by correlating the 3-D data to high-resolution seismic data an empirical relationship was established. A better estimate of dimensions can be achieved from 3-D seismic data by applying a factor of $^{1}/_{5}$ to the measurement of known small-scale (<50m) features (Table 1). Lateral spacing of bedforms greater than 50 m can be considered to be accurate. Thus, although 3-D seismic data is excellent at providing an overview of the seafloor bedform patterns, high-resolution seismic systems are still necessary to define the details.

Based on current meter data, we know that there are high-velocity bidirectional contour currents at the base of the Sigsbee Escarpment (Hamilton and Lugo-Fernandez, 2001). The data from this study confirm the existence of the contour currents and show that the currents have been stable for geologically significant time periods; however, the bidirectional nature of flow is not always preserved by the contour-current bedforms. The most erosive currents (>140 cm/s) track the Sigsbee Escarpment from northeast to

southwest and scour the deflection and splay zones into sediments older than the last glacial maximum. Slightly less intense currents (85-140 cm/s) erode transverse bedforms into sediments seaward of the Sigsbee deflection and splay zones and show evidence of a stronger southwest to northeast flow. Moving still further from the escarpment the currents continue to decrease in intensity (20-45 cm/s) and the main rectilinear furrow field develops with the central portion of the field showing equal evidence for southwesterly and northeasterly flow. A summary of the morphological and flow characteristics of each of the contour-current bedforms can be found in Table 1 and Table 2.

The extreme relief of the Sigsbee escarpment and the location of Green Knoll in the middle of the contour currents of the region, allows for some interesting variants on the basic suite of contour-current bedforms. The normal spectrum follows a progression from widely spaced rectilinear furrows, to closely spaced rectilinear furrows, to meandering furrows, to flutes, to transverse bedforms under increasing current velocities. In addition to the standard range of contour-current bedforms, here we find additional bedforms such as the following: furrows that erode uphill, massive repeating deflection an splay zones of furrows, transverse bedforms aligned in an opposing direction to an adjacent deflection and splay zone, 20 m deep channelized slump zones initiated by recirculating flow on the lee side of Green Knoll, erosional furrows within topographically isolated re-entrants into the Sigsbee Escarpment, residual erosion resistant sediments forming 50 m wide obstacle scours standing 2 m above the seafloor,

and 20 m high 2500 m wavelength mudwaves either topped with furrows or without. This is truly a polymorphic collection of contour-current bedforms.

With specific reference to the mudwaves of the region, we have shown that both furrowed and non-furrowed mudwaves exist in the Green Knoll study area. In order to establish furrows on top of the mudwaves a layer of recent, softer, hemipelagic sediments must drape the mudwaves. In cases where the drape is present, the mudwaves topography offers no obstacle to the formation and continuation of furrows. Additionally, we provided seismic evidence supporting the upcurrent lee wave model of mudwave migration established by Flood (1988). The mudwaves of this region show thicker deposition on the steeper up-current slopes coupled with thinner depositional layers and erosion on the down-current side.

One of the most significant findings of this study is the presence of three marker horizons (GK1, GK2, and GK3) in the high-resolution seismic data. These horizons can be correlated with sedimentary and geotechnical properties and are found to be regionally persistent. Furthermore, there is a direct correlation between the horizons and the ability to develop specific bedforms. The furrows of the main rectilinear zone are only capable of eroding down to horizon GK1 while rectilinear furrows adjacent to the escarpment and the core of the contour current are able to erode to horizon GK2. Under increasing current velocity meandering furrows form and are able to erode down to horizon GK3. Likewise, the flutes and transverse bedforms are show erosion down to horizon GK3. In each case the horizon marks the maximum erosion depth of each

bedform; therefore, we have found that the abrupt termination of bedform zones is caused by exposures of the aforementioned erosion resistant horizons.

Also with respect to the marker horizons, we establish that horizons GK2 and GK3 correlate with horizons M1 and M2 of the Mad Dog and Atlantis region to the northeast of this study area. Based on the horizon correlation and the dating of horizons M1 and M2 by Slowey et al. (2003), we place the triplet horizon GK3 at 19 ka and GK2 at 15 ka. This dating is significant since it places a time constraint on the initiation of the contour-current bedforms. We have established that the furrows of this region are erosional in nature, which requires deposition of at least Unit 3 prior to initiation of erosion. Thus, the maximum age for onset of furrowing is 10 ka. Along with establishing the maximum age for onset of furrowing, three methods were presented to calculate erosion rates and thereby the total time necessary to form a given furrow. The most realistic erosion rate of 1 cm/yr implies that the deepest furrows of the region required 800 years to form; however, this erosion rate does not account for the actual current variability and direction changes. Consequently, the erosion rate should be considered a maximum value.

For future work we are placing acoustic velocimeters within 5 meters of the seafloor above each of the main contour-current bedform zones. With them we hope to formally link each bedform with a measured current velocity. Placement of the current meters will also allow for some checks on the theory which connects topographic Rossby waves as the source of the bidirectional contour currents of the deep Gulf of Mexico. Currently we do not know where all of the eroded sediment goes. To date we

have found no major depocenters for the eroded material. There is some suggestion that the eroded material nearest the Sigsbee Escarpment is transported as nepheloid layers seaward into the main rectilinear furrow zone into increasingly depositional environments under decreasing current velocities away from the core of the contour current. This would explain the presence of the reflector-free Unit 1 and the shallower furrows of the zone; however, this remains speculation. Although we have explained that the furrows do not cross the mudwave zone due to a lack of sediment drape, we cannot explain why the drape is missing in the first place. The conundrum is that the mudwaves sit in between two rectilinear furrow regions that should not be connected to currents that are capable of wiping the seafloor clean and the adjacent mudwaves maintain a surface drape with furrows. These are just a few of the questions that remain in this thoroughly fascinating and diverse contour-current region of the Gulf of Mexico.

CHAPTER IV

3-D SEISMIC IDENTIFICATION OF PALEO-FURROW HORIZONS AND ASSOCIATED PALEO-CURRENT IMPLICATIONS IN THE GREEN KNOLL AREA OF THE NORTHERN GULF OF MEXICO

Synopsis

Furrows are bedforms that have been found along several ocean margins and indicate the long-term presence of strong bottom currents (Flood, 1983). The large-scale structure and development of active deepwater furrow fields have been previously revealed in unprecedented detail via 3-D seismic interpretation, and can be linked to the bottom current structure and velocity regime (see Chapter III). Here we show for the first time that furrowed horizons below the seafloor can be acoustically imaged in three dimensions. Indeed, we identified six paleo-furrow horizons in the 3-D seismic dataset from the Green Knoll region of the northern Gulf of Mexico at the base of the Sigsbee Escarpment. The identification of these horizons indicates the existence of multiple furrow erosion and burial cycles. Imagery of these horizons along with our knowledge of the morphology and development of presently active furrow fields, show that sediment properties and contour current velocities must have been similar to what we see on the seafloor today; hence, the paleo-furrow horizons indicate the erosion of fine-grained hemipelagic sediments by contour currents in the 20-60 cm/s velocity range. The different horizons show a variation in morphology of individual furrows as well as the entire furrow field that reveal the bathymetric control of the contour-currents as well as the presence and erosion of large areas of the former surface sediments associated

with each horizon. We further suggest the possibility that furrows are formed during inter-glacial highstands and buried during glacial lowstands.

Introduction

Deepwater furrows have been identified beneath strong bottom water flows at the base of the rise of several ocean basins (see summary by Flood, 1983). Until recently, such observations have been limited to sparse 2-D seismic, sonar, and inferences from hyperbolic reflectors generated from hull mounted systems (e.g. Bryant et al., 2000; Flood and Hollister, 1975; Flood and Hollister, 1980; Heezen and Hollister, 1964; Hollister et al., 1974). With the availability of industry collected 3-D seismic data in the Gulf of Mexico, an unprecedented look at the structure and development of entire fields of furrows is now possible. In the Green Knoll region of the Gulf of Mexico, furrows and other contour-current bedforms dominate the seafloor landscape. Recent work in the Green Knoll region of the Gulf of Mexico shows that the structure of the entire field of bedforms and the morphology of individual bedforms is controlled by the interaction between bottom currents, topography, stratigraphy, and sediment properties (see Chapter III). The topography of the Sigsbee Escarpment and Green Knoll control the flow of contour currents in the region, creating changes in the current structure and velocity, which in turn are translated into changes in contour-current bedform types on the seafloor.

Having established the existence of a field of furrows on the seafloor at the base of the Sigsbee Escarpment in both the Bryant Canyon and Green Knoll regions of the Gulf of Mexico (see Chapter II and Chapter III), it naturally followed to look for similar

structures in the sub-seafloor data volumes. Specifically, we used a 3-D seismic dataset from the deep water Green Canyon region of the northeastern Gulf of Mexico (Fig. 53). Given that the pattern and development of contour-current bedforms on the seafloor reveals the structure of the long-term bottom currents, identifying analogous patterns in the subsurface would provide information on the presence, structure, and variability of paleo-currents in a region. This study focuses primarily on the various forms of furrows, since they should be laterally continuous enough to recognize in the sub-surface, while smaller or less continuous features (such as flutes) would have a tendency to be lost in the increasing noise and decreasing resolution with depth of the seismic signals.

The first concept we address is whether paleo-furrows can even be imaged in the subsurface. Is the erosion of a massive field of furrows at the base of the Sigsbee Escarpment a unique occurrence, or is it a phenomenon that has occurred in the past? And if furrowing is a cyclic pattern are the features actually seismically preserved after infilling and burial? The second concept we deal with is the paleo-current implications of the furrowed horizons. By comparing any furrowed horizons to their modern analogues, what can we conclude regarding the location, direction, duration, and intensity of the furrow-forming paleo-currents? As with the present-day seafloor furrows, paleo-furrows offer the possibility of having the equivalent of a geological current meter for entire regions of an ocean basin.

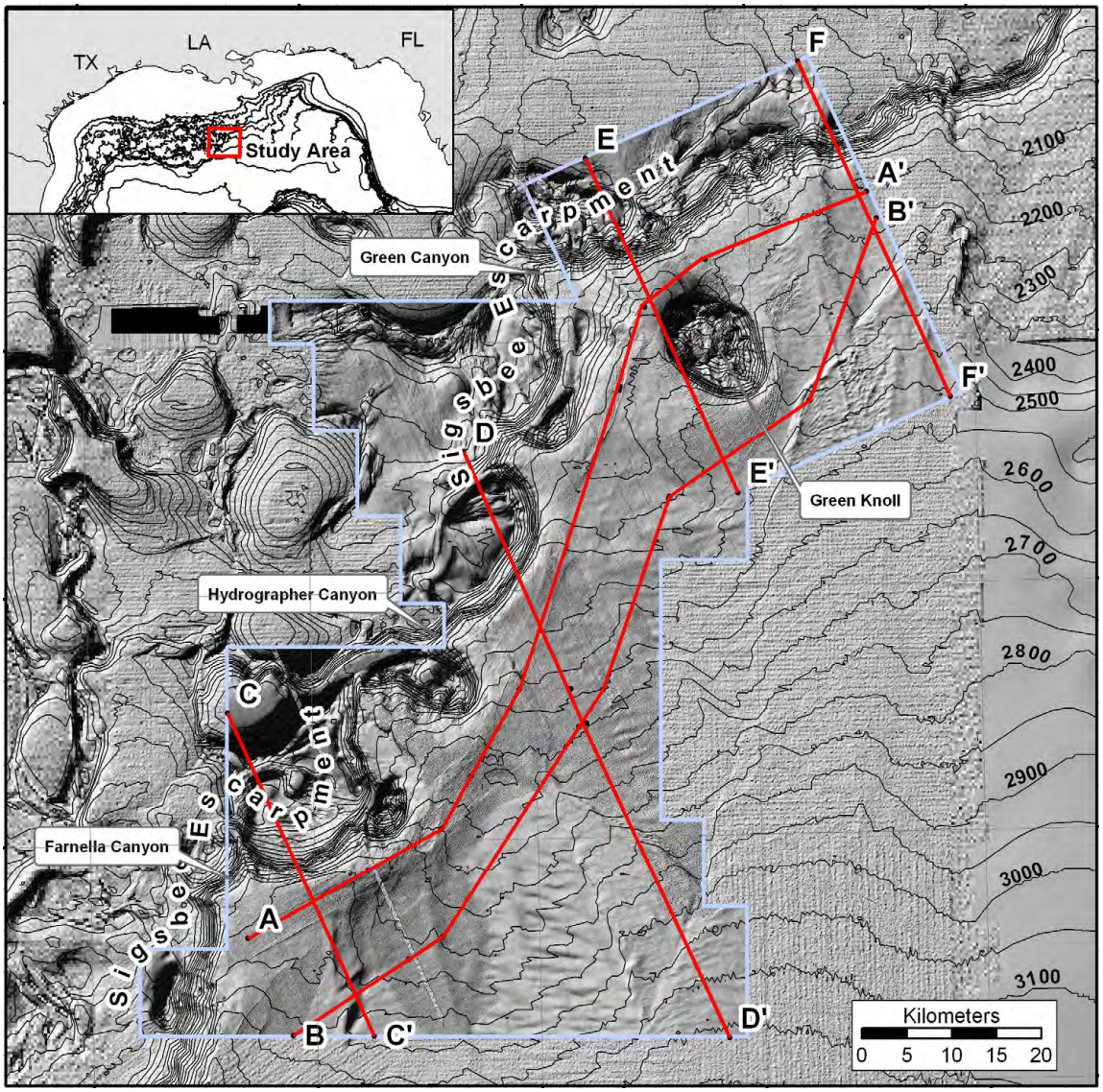

Fig. 53. Green Canyon Study Area with Summary Seismic Line Locations.
A shaded bathymetry map of the study area with contours given in meters is shown with the main structural features identified. The central area (blue outline) shows the extent of the 3-D seismic data set that was used to generate the bathymetry. Outside the 3-D seismic dataset, bathymetry was generated from Seabeam data for the Gulf of Mexico. The locations of the summary seismic lines that will be discussed are shown in red.

Geological and Oceanographic Setting

The northern Gulf of Mexico continental slope is an exceptionally broad region with some of the most variable topography to be found along any ocean margin. The

breadth and variable topography of the slope and rise results from the presence and movement of vast subsurface salt units (e.g., Bouma and Roberts, 1990; Bryant et al., 1990; Coleman et al., 1991). The subsurface movement of a massive allocthonous salt sheet has led to the uplift and creation of the Sigsbee Escarpment—a structure marking the southern limit of the salt sheet and having a relief of 800 meters or more, along with local slope angles in excess of 20° (Liu and Bryant, 2000). Additionally, seaward of the Sigsbee Escarpment an isolated, massive, salt-cored diapir forms the structure of Green Knoll. The salt diapir is disconnected in both structure and origin from the salt sheet that forms the leading edge of the Sigsbee Escarpment (Weimer and Buffler, 1992). These significant topographic structures are the main boundaries for contour-following bottom currents.

Few details are presently known about deep currents in the Gulf of Mexico; however, it is known that the Loop Current, which is the primary surface current structure in the Gulf, has an indirect connection to the regional deep currents (Hamilton, 1990; Hamilton and Lugo-Fernandez, 2001). The Loop Current is a result of the Yucatan Current meandering through the Gulf of Mexico and exiting through the Florida Straits to form the Gulf Stream. As the base of the Loop Current or one of the eddies that periodically spin off impinges on the slope, the potential for the generation of deep currents in the form of topographic Rossby waves exists (Hamilton, 1990; Hamilton and Lugo-Fernandez, 2001; Sturges et al., 1993). Nowlin et al. (2001) show modeled westward-flowing high-velocity bottom currents that closely track bathymetric contours along the Sigsbee Escarpment. Indeed, current meters at the base of the escarpment

record data confirming the existence of bi-modal current events in excess of 50 cm/s and lasting for periods of weeks (Hamilton and Lugo-Fernandez, 2001). Such intense recurring flow events are assumed to be the primary mechanism controlling the evolution of deepwater contour-current bedforms in the Gulf of Mexico.

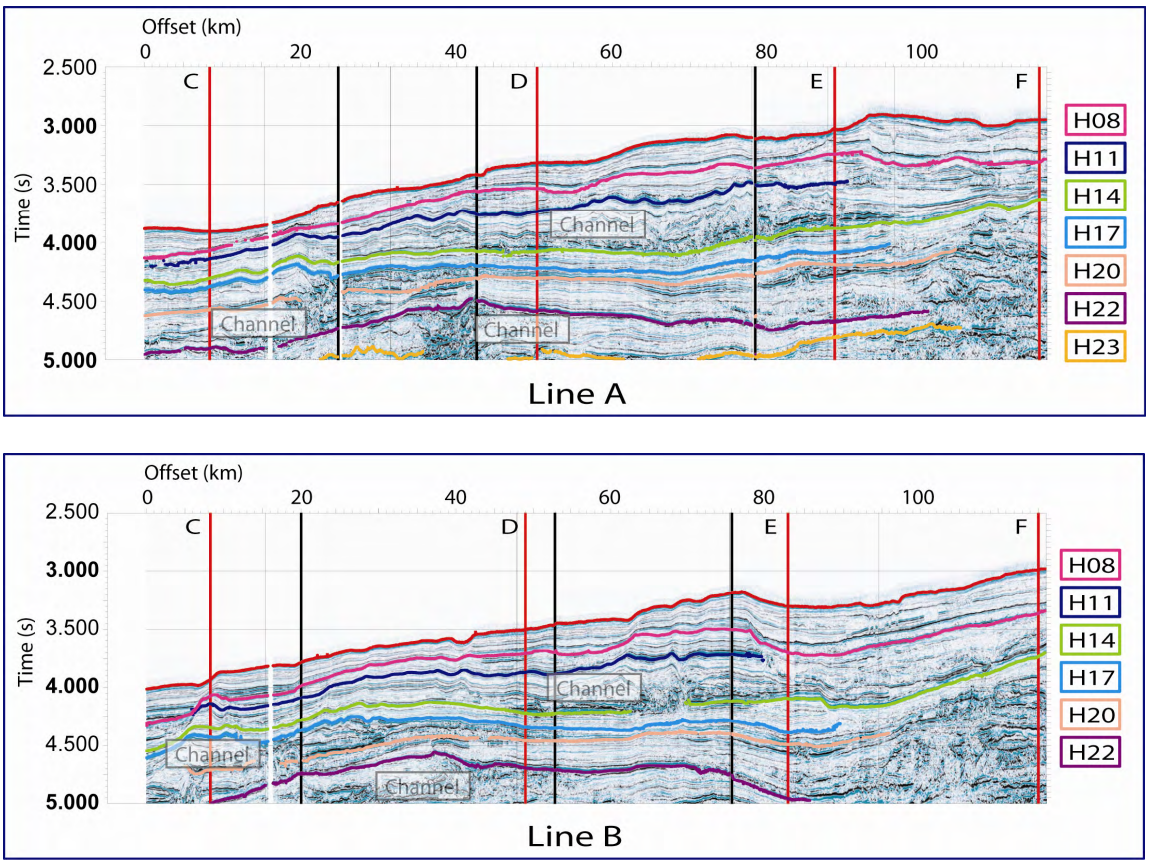

Fig. 54. 3-D Seismic Lines A & B.
Arbitrary lines running parallel to the base of the Sigsbee Escarpment showing the location of the primary depositional units. Three main channels are identified on each profile.

This study focuses on sediments seaward of the Sigsbee Escarpment in the Mississippi Fan fold belt region west of the Mississippi Canyon (Fig. 53). This is a deep water environment greater than 2000 m in depth. The Quaternary sediments of this

region are dominated by the glacial and inter-glacial cycles of depositional patterns (Beard et al., 1982). During sea level highstands, such as during the Holocene, sedimentation is predominantly hemipelagic with low sedimentation rates (Slowey et al., 2003). In contrast, during sea level falls, low-density turbidites are the primary transport mechanism of sediments to the deep water environment. At the maximum lowstand of sea level, channels created during the lowering sea level begin to infill and higher-density turbidites form. The infilling of channels continues during the sea level rise, and during until hemipelagic drape dominates once again (Beard et al., 1982; Liu and Bryant, 2000; Mann et al., 1992). Three primary channels on profile B-B′ (Fig. 54) are examples of this glacial/inter-glacial pattern of sedimentation, channeling, and infilling.

In order to understand the implications of paleo-furrow horizons, we must understand present-day seafloor furrow formation and preservation. The interrelationship between currents, furrow morphology, and sediment properties is detailed in Chapter II and Chapter III, but summarized here. A summary of the contour-current bedform types and distribution in the Green Knoll region is given in Fig. 55. Furrow formation along the Sigsbee Escarpment is observed to have the following characteristics: Each range of current velocity yields distinct furrow morphologies. Under lowest current velocities the furrows are low-relief, rectilinear and widely spaced. Increasing the current velocity decreases the furrow spacing and increases the furrow relief. Further increases of current velocity result in high-relief meandering furrows. Velocity increases beyond those that form meandering furrows result in either complete

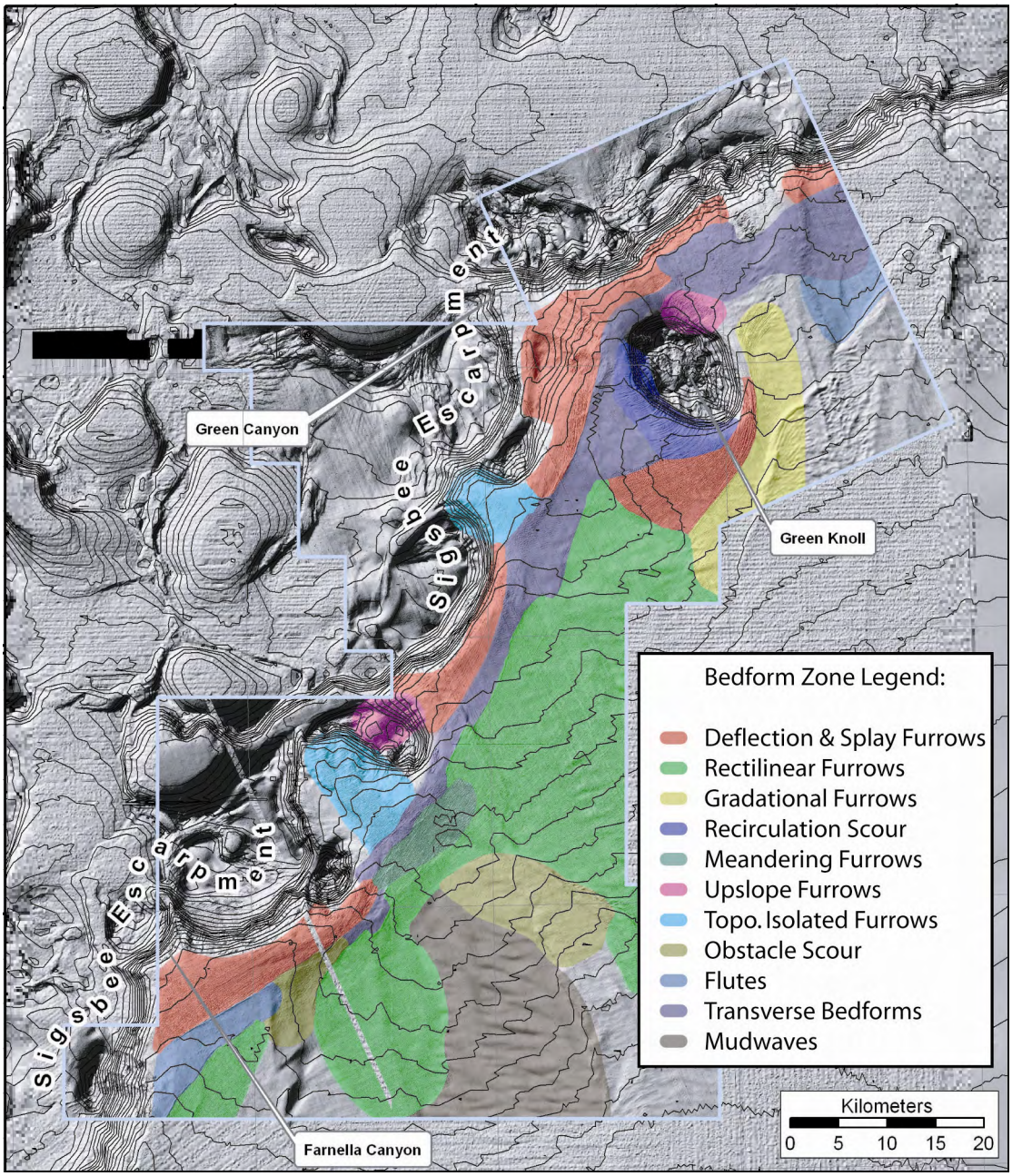

Fig. 55. Green Knoll Contour-Current Bedform Zones.
Overlain on the shaded bathymetry map of the Green Knoll region are the primary bedform zones identified based on general bedform morphology and distribution patterns from the 3-D seismic seafloor bathymetry (blue outline). The lower resolution background image is generated from Seabeam data. (From Chapter III.)

removal of all erodible sediments or the creation of other bedforms such as flutes that we expect to be undetectable in the subsurface due to resolution constraints. The other main control on furrow formation is sediment properties. Narrow, low-relief rectilinear furrows that form under lower velocity conditions are limited to forming in the most recent soft upper meters of sediments in the region. Wider, high-relief furrows forming under higher velocity conditions closer to the Sigsbee Escarpment can erode deeper into the more consolidated sediments, but have a maximum erosional limit associated with the high silt content and higher consolidation of sediments associated with the maximum lowstand of the last glaciation. High-velocity, bathymetrically intensified, bottom currents are present in the Gulf of Mexico (Hamilton, 1990; Hamilton and Lugo-Fernandez, 2001); and, at the present time, sedimentation rates are low enough to allow active furrow erosion and prevent preservation of the bedforms (see Chapter III).

Methods

This study uses a 3-D seismic volume that was collected and provided by WesternGeco. The seismic dataset is comprised of 4 complete surveys in the Green Knoll and Farnella Canyon regions (Fig. 53). The surveys cover nearly 5000 km^2 of the seafloor along the Sigsbee Escarpment. Line spacing is 20 m and trace spacing is 12.5 m. The sample rate for the data is 4 ms and the volume includes the first 5 seconds of time/amplitude data. The seismic data have had the following primary processing methods applied: deconvolution, phase correction, dip move-out stacking, modified residual migration, and residual amplitude compensation. The processed data was loaded into Kingdom Suite (a 3-D seismic interpretation program provided to Texas

A&M University, Department of Oceanography courtesy of Seismic Micro-Technology). Following data loading, the amplitudes were balanced across the surveys using standard RMS method to enable valid relative amplitude mapping and comparison across surveys.

All horizons shown in this study were picked as relative peak amplitude and gridded at a 15 m bin size. Each time horizon was converted to approximate depth by using a constant velocity assumption of 1500 m/s. This assumption becomes less accurate with depth, but allows for reasonable estimates of feature relief within any given horizon. No reliable technique was found to differentiate a furrowed horizon from a non-furrowed horizon prior to final horizon imagery; thus, each horizon had to be fully picked, gridded, shaded, and examined to determine if it was furrowed or not. Because many furrows are less than 1 m in relief, extensive preliminary seed picking for each horizon was necessary prior to auto-picking the remainder of any given horizon. No smoothing could be applied to any horizon, as that would inevitably remove the furrow signature from the horizon. Although amplitude and some horizon attributes also picked out the linear nature of furrows, the best technique we found for visualizing furrows within a horizon was simple shaded bathymetry.

Because the data is gridded at 15 m, there is an inherent smoothing applied to the dataset. We found in comparing the seafloor furrow morphology determined from the 3-D data to high-resolution seismic data that an empirical relationship can be used where actual feature dimensions can be estimated as $^1/_5$ the bedform dimensions determined via 3-D seismic data. And, bedform spacings above 50 m determined from the 3-D seismic

data are considered valid (see Chapter III). This relationship should be kept in mind when viewing profiles of individual furrows below. The following results and discussion will identify key horizons and give examples of the furrow morphology, both as a group and individually.

Results

Initial horizon mapping from the Green Knoll region yielded exceptional results. To date, we have identified six significant furrowed sub-seafloor horizons in the region, and it is likely that additional paleo-furrow horizons exist. The mapped paleo-furrow horizons are shown in six 3-D seismic profiles that cross the region (Fig. 56). The profiles show that the paleo-furrow horizons were all found within approximately the first second of data. Furthermore, the horizons are all located above the first major channel and levee structure of the region. The thinning of the beds to the southwest suggests turbidity flow related sediment source from the northeast. The source could be outflow from Green Canyon or even further east, from the Mississippi Canyon where low-density portions of turbidity flows moving down-canyon would potentially be redistributed to the southwest by contour-currents and result in the described thinning of beds to the southwest. What is important is that the sediments of these paleo-furrow horizons are part of the more distal portions of sediment transported to the deep Gulf of Mexico. As such, they should be dominated by the silty clays and clays of the fringes of turbidity flows and general hemipelagic sedimentation, rather than the coarser sediments located near channel axes. In fact, horizons that are more closely associated with the

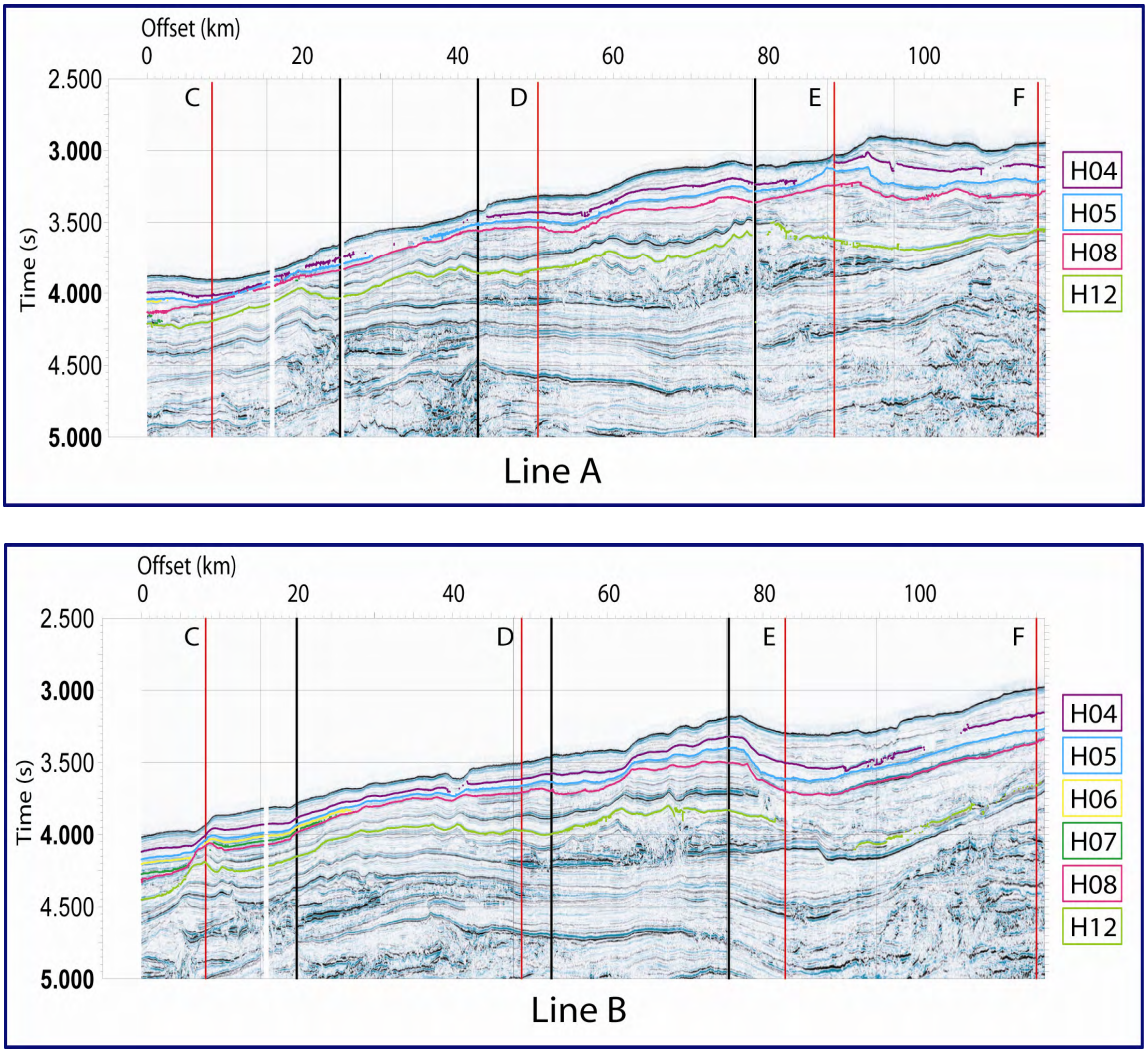

Fig. 56. 3-D Seismic Profiles A-F of Furrowed Horizons.
Six seismic profiles identified from Fig. 53 with horizons identified by number and color. Crossing lines are indicated with red vertical lines. Each horizon has confirmed furrows.

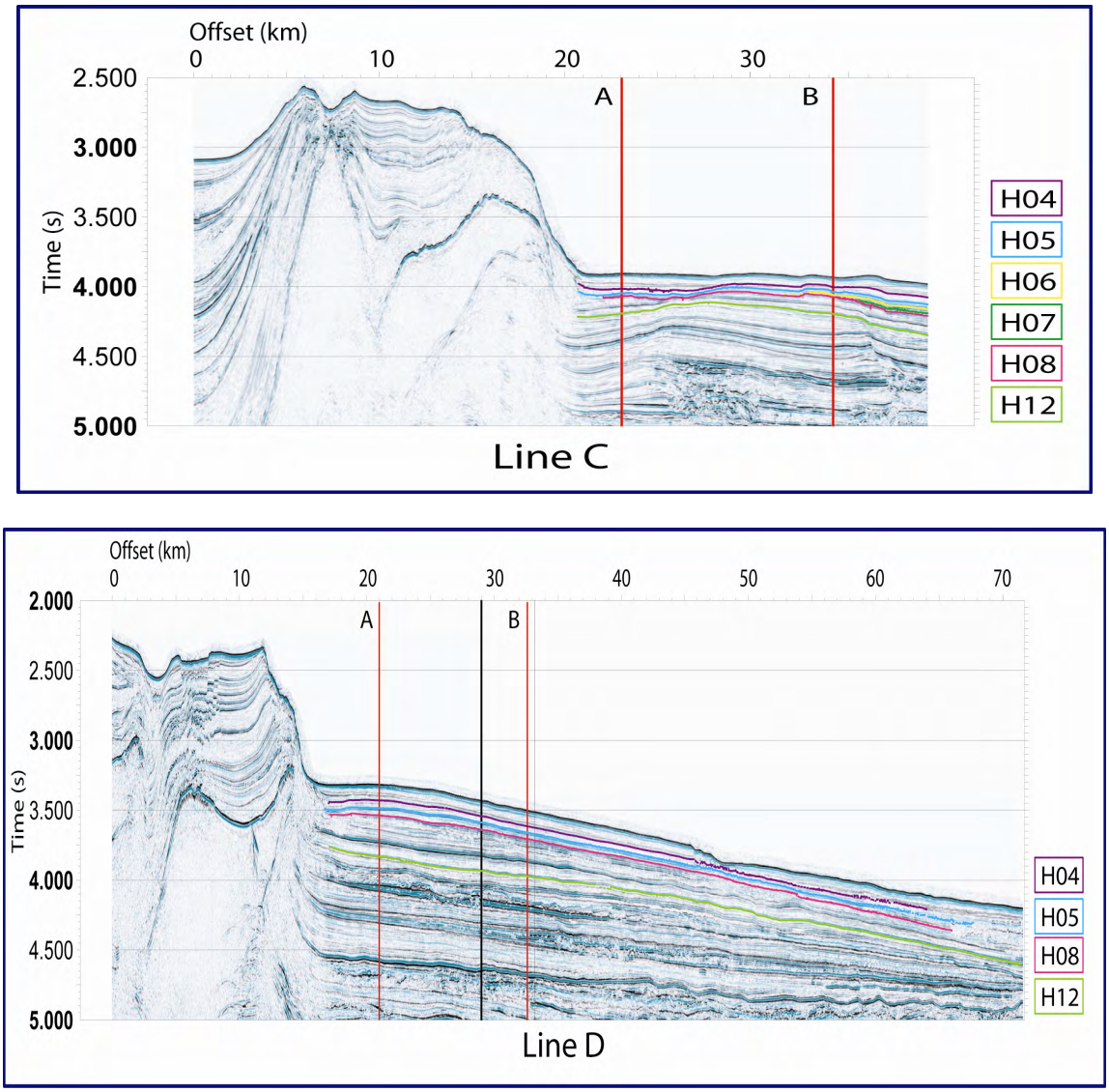

Fig. 56. Continued.

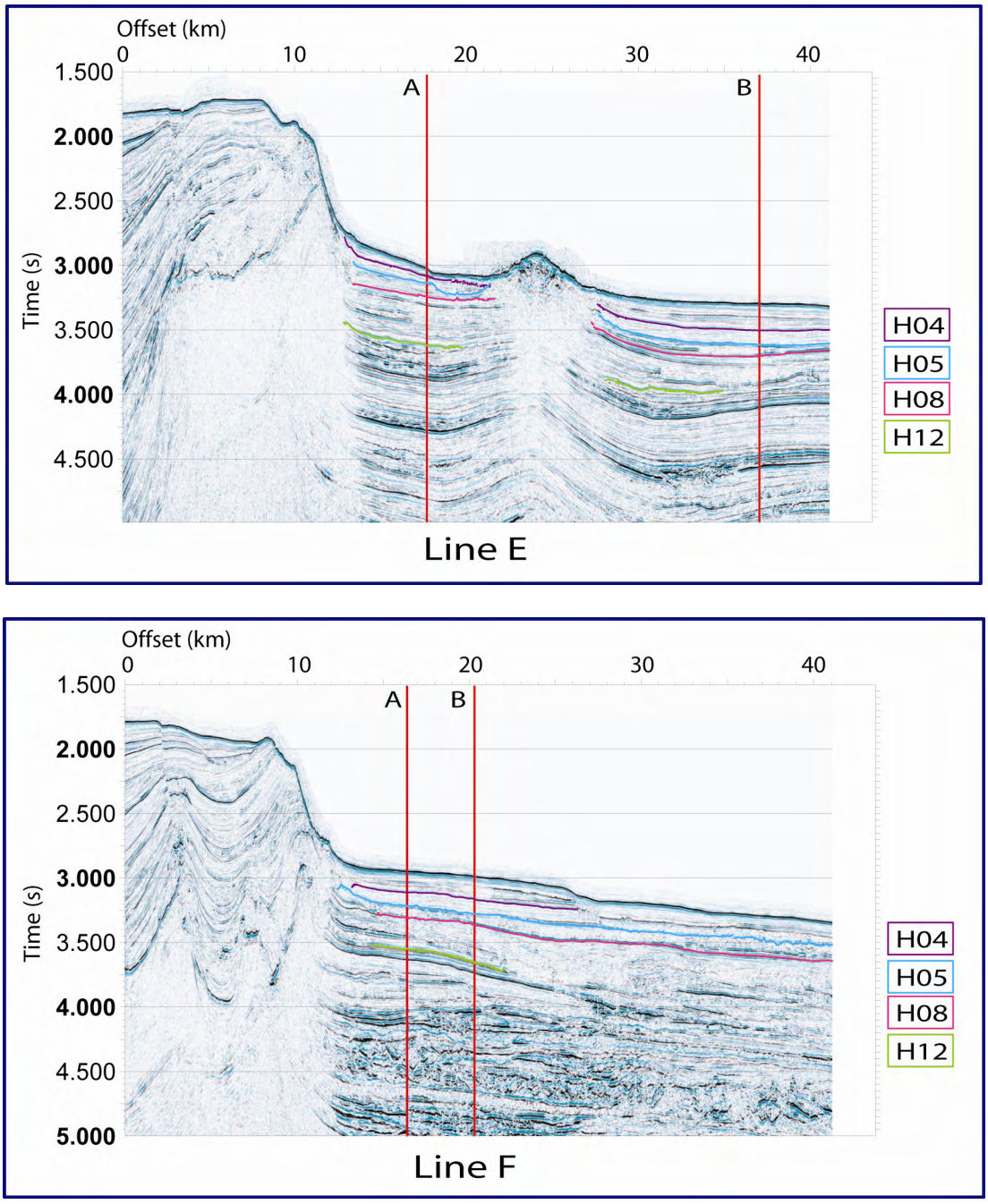

Fig. 56. Continued.

channel-levee complexes show no evidence of furrowing. This relationship fits in well with what is known about present-day furrows, where we know that the furrows will only erode into the softer surface silty clays and clays. The regional horizon that marks the lowstand from the last glaciation is associated with coarser and more consolidated sediments, and it also happens to be the maximum limit of seafloor furrow erosion (see Chapter III). Thus, the stratigraphic position of the paleo-furrow horizons is at least consistent with our understanding of the types of sediments that can support furrow formation.

Each furrowed horizon has characteristics that can be compared to furrows on the modern seafloor. When comparing the morphology of present-day seafloor and preserved sub-seafloor furrowed horizons there are four linked considerations: 1) Different current velocities yield distinct furrow morphologies. 2) Sediment physical properties affect erodibility and bedform preservation. 3) The duration of eroding currents affects the degree of development of a given morphological type. 4) Sedimentation rate affects both furrow morphology and preservation. The above considerations should be kept in mind as we present and discuss the details of each furrowed horizon. For reference, Fig. 57 shows an overview of the relative location and orientation of each of the paleo-furrow horizons identified, along with the location of the detailed imagery that will be used to discuss the characteristics of each horizon. Although many of the same patterns exist in the same locations on the seafloor and in paleo-furrow horizons, there are enough differences in the coverage pattern of the furrows between horizons to conclude that the paleo-furrows are not a noise replication

from the seafloor horizon. Furthermore, there are several horizons between seafloor and the deepest paleo-furrow horizon that have no evidence of furrows at all.

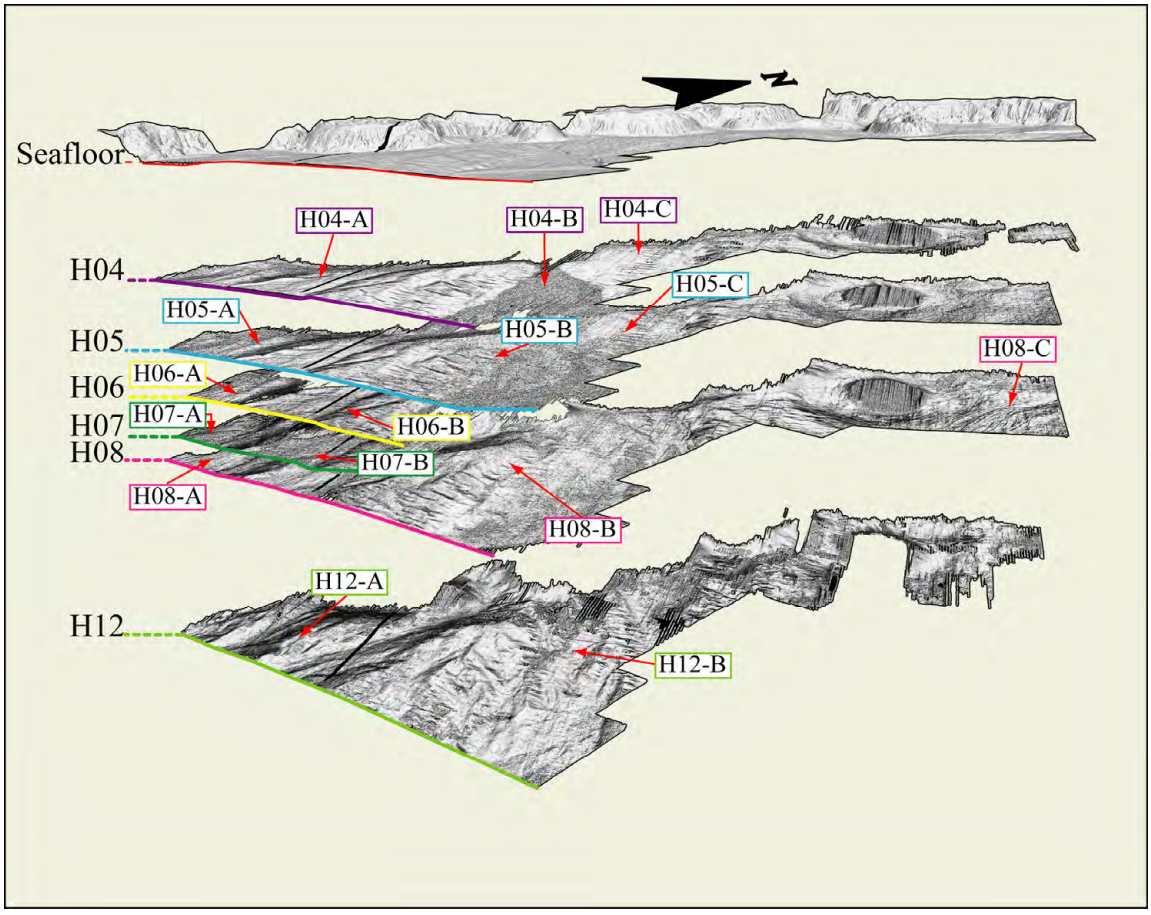

Fig. 57. 3-D Perspective of Paleo-Furrow Horizons.
Shown here is a perspective view of all the furrowed horizons. Each horizon is color coded to match the associated horizon in Fig. 56. On each horizon are the identified locations of detailed perspective views of each horizon that follow below.

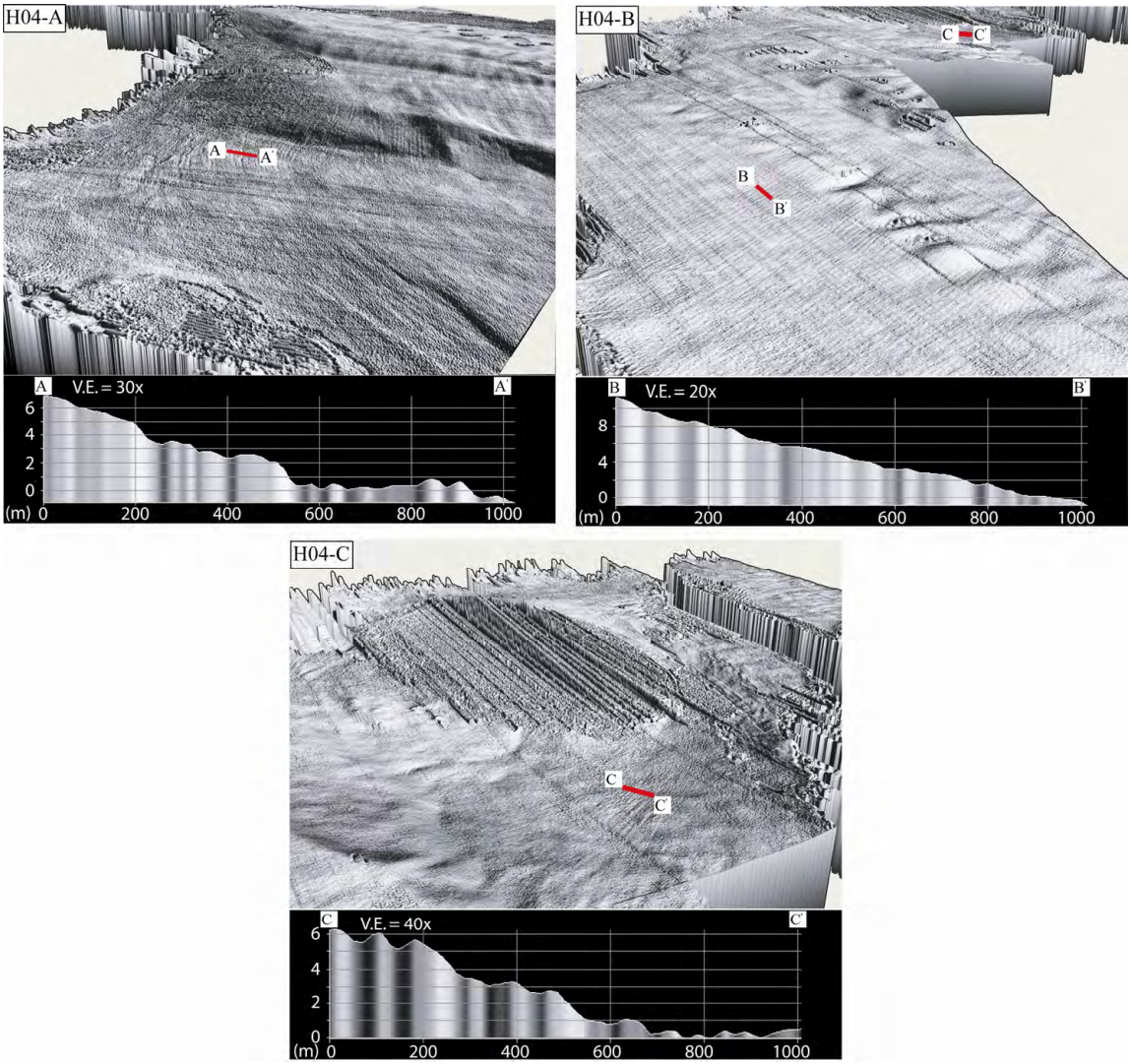

Fig. 58. Detailed Perspective Views and Profiles of H04.
Each panel shows a perspective view of a portion of the furrowed horizon H04. All perspectives views generally look between north and east. A bathymetric profile is shown on the perspective view and indicates the locations of the profile below. The scales on each profile vary to maximize resolution of these low relief features. All subsequent perspective views with profiles will follow this same format. H04-A shows the deflective nature of the furrow pattern. H04-B shows minimal relief rectilinear furrows. H04-C shows deflection and splay furrows in the same region around Green Knoll that they are found on the seafloor.

Horizon H04 (Fig. 58) is the shallowest paleo-furrow horizon and shows several features common to the seafloor furrow field. Profile H04-A in the southwestern portion of the horizon shows furrows less than 1 m deep, ~20 m wide and ~100 m apart. Interestingly, the furrows of horizon H04 in closest proximity to the Sigsbee Escarpment follow a deflective pattern that is more extreme than furrows of the corresponding seafloor location. Horizon H04 is also more continuous than the patchy area of furrows on the seafloor, indicating that there was a continuous bed of soft surface sediments for the paleo-furrows to erode into. Profile H04-B shows a field of rectilinear furrows of similar dimensions to the deflective furrows of profile H04-A. The rectilinear furrows are found in the same position as the seafloor furrows and show a similar pattern that is unaffected by the mudwaves of the region. Finally, profile H04-C reveals a deflection and splay pattern in the moat around the southern side of Green Knoll that again mimics the pattern of the seafloor deflection and splay zone.

Horizon H05 (Fig. 59) shows the most extensive coverage of well-developed furrows from among all the paleo-furrow horizons. Profile H05-A shows a furrow deflection zone adjacent to the Sigsbee Escarpment that is similar to H04, but it differs in two respects. The H05 furrows have relief of up to 3 m, and terminate just in front of Farnella Canyon. In contrast furrows of the same region on H04 had only 1 meter relief and did not terminate. The greater relief of H05 furrows implies either a thicker section of erodible sediments or currents that operated over a longer period of time. If the termination of the furrows is similar to seafloor furrows, then the termination marks the

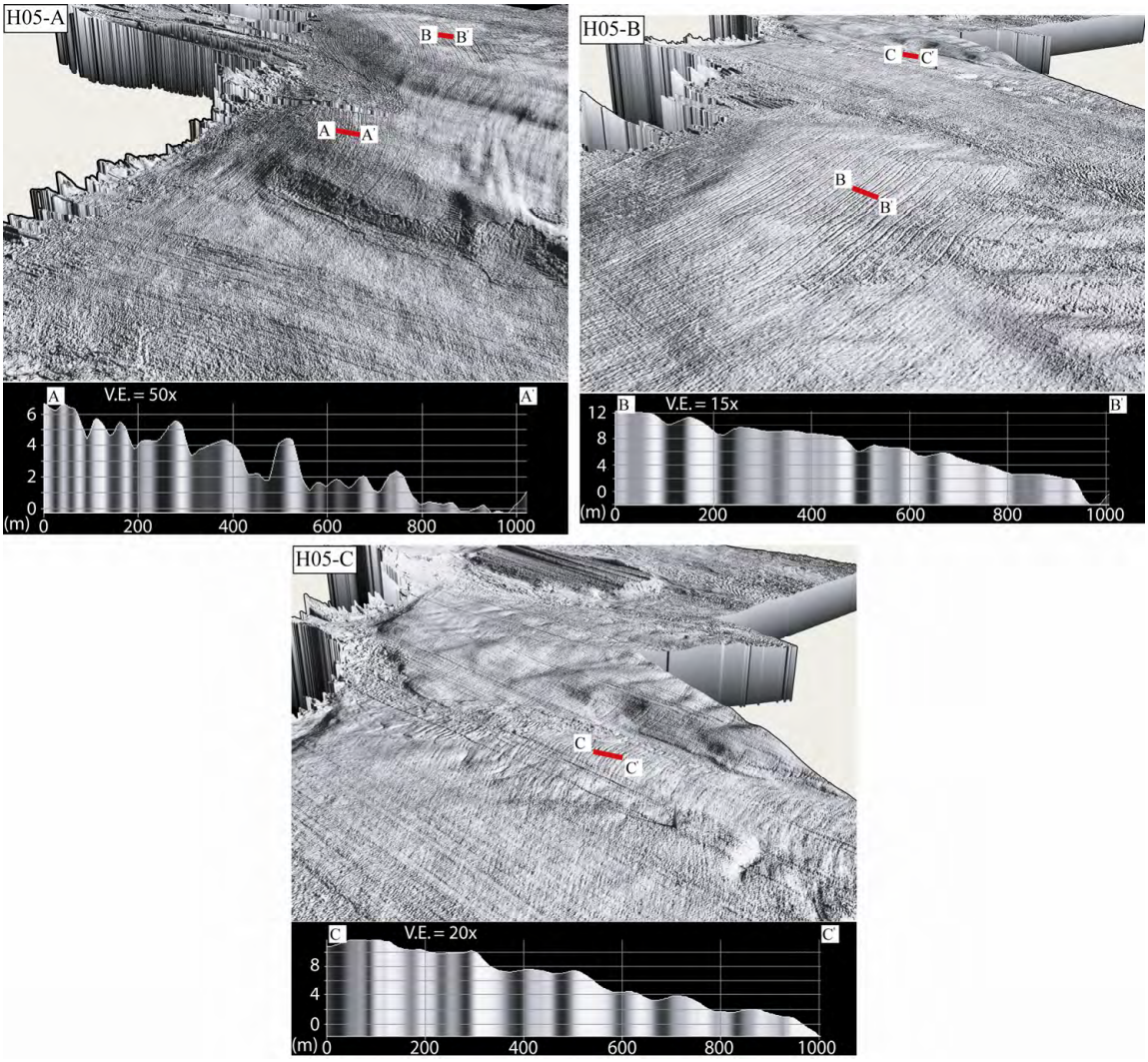

Fig. 59. Detailed Perspective Views and Profiles of H05.
H05-A shows rectilinear furrows with a slight deflection and the furrows terminate abruptly adjacent to Farnella Canyon. H05-B shows widely spaced gradational rectilinear furrows that decrease in spacing approaching the Sigsbee Escarpment. H05-C furrows are rectilinear with a slight curve induced by the escarpment or the topography.

edge of available erodible surface sediments at the time of furrow formation. Profile H05-B is from the central gradational rectilinear furrow zone of the horizon. The profile shows relief greater than 2 m in places and the spacing between furrows of greater than 200 m is seen to decrease as the Sigsbee Escarpment is approached. This shows similar

characteristics to the seafloor furrows that show decreased furrow spacing under increasing current velocity as the high-velocity core of the current tracks along the Sigsbee Escarpment (see Chapter II). A very slight deflection to the furrow pattern that is more apparent closer to the escarpment depicts the topographic control of the escarpment on the bottom currents. This region of furrows is non-existent on H04 in the same location, indicating that the furrows on individual horizons are unrelated to internal interference or noise patterns propagating from other furrowed horizons. Profile H05-C shows a continuation of the main rectilinear furrow field to the northeast with closely spaced furrows of low relief (<2 m) that track over the variable topography of the horizon. Thus, between horizons H04 and H05 we can see differences in both the pattern of furrows and the morphology of individual furrows that result from either differences in current duration, or differences in sediment drape thickness.

Horizon H06 (Fig. 60) is contained within a ponded area of sediments that appears to be associated with outflow from Farnella Canyon. The furrows of H06 are extremely well defined with relief greater than 4 m and widths greater than 20 m. The furrows of the southwestern portion (profile H06-A) show a slight deflective pattern and are less well developed than the more rectilinear furrows of the northeastern portion of the horizon (profile H06-B). The great relief of these furrows is likely associated with the thick ponding of soft sediments in the axis of the outflow channel from the Farnella Canyon. Deposition most likely results from lower density turbidity flows since the sediments are thickest in the channel axis and thin away from it without developing the structured channel-levee deposits that appear elsewhere in the subbottom record (Fig.

56). Another interesting item to note is that H06 is the first horizon to show distinct tuning-fork junctions. Based on the direction of furrow joining (Allen, 1969; Dyer, 1970), a dominant current flow from northeast to southwest is indicated. And, unlike the seafloor horizon (see Chapter III), the mudwaves in this area are heavily eroded by furrows indicating that the mudwaves maintained a thick surficial drape at this time.

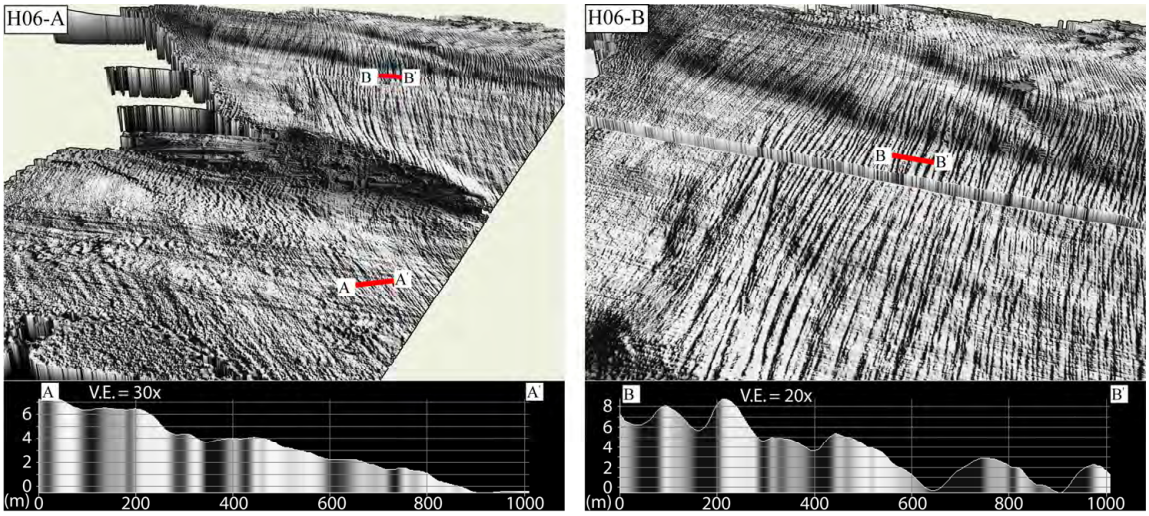

Fig. 60. Detailed Perspective Views and Profiles of H06.
Horizon H06 has limited extent, but these rectilinear furrows have high relief. The furrows of H06-A are slightly less well developed than H06-B. Tuning-fork junctions that merge in the direction of flow can be seen in H06-B.

Horizon H07 (Fig. 61) is contained within the same ponded outflow channel of H06 and also has limited extent, but the furrows of this horizon have the greatest relief of any horizon other than the seafloor (2-8 m). These furrows are comparable to seafloor furrows of the Green Knoll deflection zone (see Chapter III). Such extreme erosion should require three conditions: 1) slightly higher current velocities 2) a thicker section of erodible sediments, and 3) a longer duration of erosive current action.

Furthermore, since the H07 is located at the base of the channel outflow it may contain a higher sand content, which in the Green Knoll furrows was seen to enhance furrow erosion significantly (see Chapter III).

Horizon H08 (Fig. 62) shows an isolated area of furrowing at the base of the Farnella Canyon outflow channel described for H06 and H07 (profile H08-A); however, the relief of these furrows is only on the order of 2 meters. Further to the northeast on H08 are furrows of the main rectilinear furrow field (profile H08-B) with widths of ~20 m and relief of less than 2 m that are very similar to what we find on the seafloor. As is typical the mudwaves of this region are overridden by furrows. Interestingly, the furrows of the northeast corner of H08 (profile H08-C) may have a different origin than

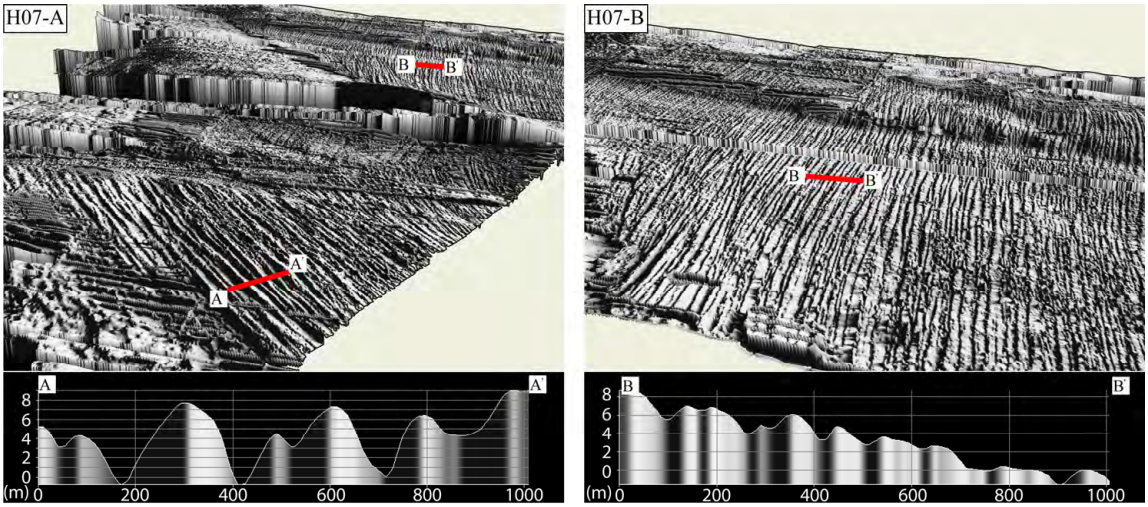

Fig. 61. Detailed Perspective Views and Profiles of H07.
Horizon H07 has the same limited extent as H06. H07-A shows rectilinear furrows with larger relief than any other paleo-furrow horizon. The furrows of H07-B are high-relief rectilinear furrows with tuning-fork junctions visible.

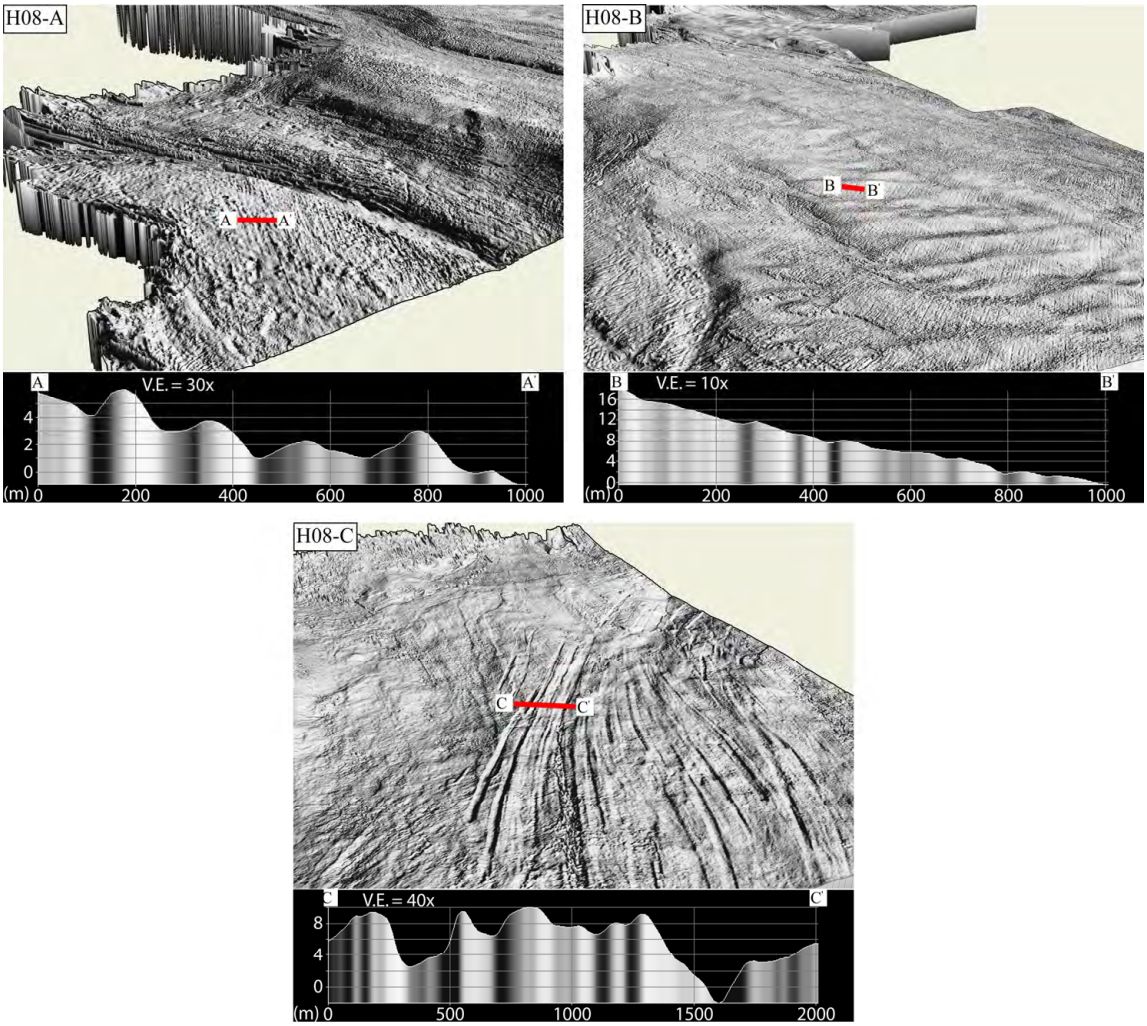

Fig. 62. Detailed Perspective Views and Profiles of H08.
The furrows of H08-A are rectilinear and similar in position and morphology to horizons H06 and H07. H08-B shows the main rectilinear furrow field similar to the seafloor rectilinear furrow zone. H08-C has the appearance of furrows, but the origin may be from scour at the base of a turbidity flow.

any of the other furrows of the region. The orientation of these furrows is more perpendicular to the Sigsbee Escarpment and the relief is 8-10 m. The chaotic nature of the overlying sediments between H08 and H05 suggest that the unit is a massive turbidity or debris flow deposit. Similarly, a signature is seen on a deeper horizon (not shown here) that is oriented to suggest turbidity flow scour from the re-entrant between

Hydrographer and Green Canyons. Rather than ascribing these downslope features to a major change in current direction that opposes that of all other furrows as well as the direction of furrows from the same horizon, we propose that the furrows of H08-C are the large-scale versions of the furrow-like scours generated at the base of turbidity currents as described by Dzulynski and Walton (1965).

Horizon H12 is the deepest mapped paleo-furrow horizon of the study area (Fig. 63). The rectilinear furrows of this horizon are most similar to those of H04. A slight deflection is seen in the southwestern portion of the horizon (profile H12-A) and to the northeast are found simple rectilinear furrows similar in location to those of the seafloor. The remainder of the horizon shows very little evidence of furrows indicating that the drape at the time of furrow formation was relatively thin and discontinuous.

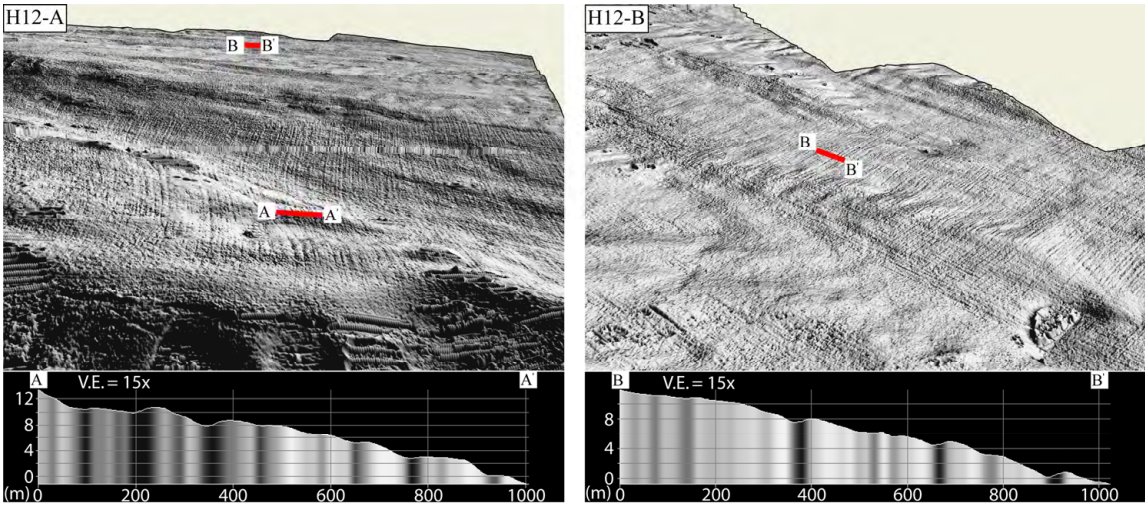

Fig. 63. Detailed Perspective Views and Profiles of H12.
Horizon H12 is the deepest horizon that shows slightly deflected rectilinear furrows in H12-A and undeflected rectilinear furrows in H12-B.

Discussion and Conclusions

What do our results mean with respect to paleo-furrow horizons? First, simply the presence of multiple sub-seafloor furrowed horizons at the base of the Sigsbee Escarpment confirms the presence of episodic high-velocity current events in the geologic past. Second, we can assume the same velocity/morphology relationship seen on the modern seafloor existed during paleo furrow formation. The creation of furrows via laboratory experiments indicates there is a specific velocity window of 20-60 cm/s where furrow formation is possible (Allen, 1969). This matches well with measured currents in furrowed regions of the Atlantic and Gulf of Mexico that typically show velocities in the 5 – 100 cm/s range (Flood, 1983; Hamilton and Lugo-Fernandez, 2001; Hollister et al., 1974). Sustained velocities outside the furrow formation window result in a different type of bedform ; *e.g.* flutes and fractures (Allen, 1969). Third, since sediment strength could not have been greater than those sediments that mark the maximum depth of erosion for modern furrows (see Chapter II and Chapter III), the sediments into which paleo-furrows eroded must have originally had similar physical properties to those found on the seafloor today. Indications from both the Bryant Canyon and Green Knoll areas are that furrows erode to a maximum depth after which the only means to continue erosion deeper into the more consolidated sediments is to increase the current velocity (see Chapter II and Chapter III). Increasing the current velocity inevitably results in conditions outside the furrow formation window, again changing the resulting bedform away from furrows.

The preservation of furrowed horizons necessitates a very rapid change in sedimentation rate coupled with a change in bottom current structure. Because successive paleo-furrow horizons do not maintain the same furrow morphology and distribution, the horizons represent distinct furrowing events that have been completely buried. The only way to bury the furrows is to reduce the formational currents and/or increase sedimentation rates. Assuming the currents are caused by topographic Rossby waves that are indirectly linked to the flow of the Loop Current into the Gulf of Mexico (Hamilton, 1990; Hamilton and Lugo-Fernandez, 2001), one way to decrease the bottom currents would be to diminish the Loop Current flow. In fact, there is evidence that the Gulf Stream was 35% weaker during the Last Glacial Maximum (Lynch-Stieglitz et al., 1999). This necessitates a similar decrease in flow for the Gulf of Mexico Loop Current and indicates a possible mechanism for minimizing the high-velocity bottom currents that form furrows. Likewise, during glacial times sediment transport to the deep Gulf would increase due to lowering of sea level and contraction of the shelf (Beard et al., 1982; Slowey et al., 2003). The combination may be enough to both terminate furrow erosion and initiate furrow burial. Unfortunately there is no age control for the sediments of this region, which prevents us from evaluating this hypothesis.

The presence of several paleo-furrow horizons clearly shows that the process of furrow formation has occurred in the past and is interrupted by time periods where furrow formation is not supported. Furthermore, it verifies that furrows below seafloor can be imaged through the use of 3-D seismic imaging. Consequently, we not only have a single cross-section of furrows, but an entire paleo-furrow surface can be mapped.

Although furrows have been imaged previously on the seafloor, this is the first time they have ever been imaged below the seafloor. We also have determined that none of the paleo-furrow horizons show dramatic differences from the pattern and morphology of the furrows we find on the seafloor today. So, we conclude that nature of contour currents and sedimentation in the late Pleistocene at the base of the Sigsbee Escarpment has been cyclic, yet similar to the interglacial conditions of today during time periods when furrow formation is viable. As we look to future work, our working hypothesis regarding the cyclic nature of furrow formation and burial is that it is linked to the variation in currents and sedimentation coincident with glacial/inter-glacial cycling.

CHAPTER V

SUMMARY

In Chapter II we identified a range of contour-current bedform morphologies and described them using deep-towed subbottom and sonar data. One of the most interesting aspects of the contour-current bedforms found in the Bryant Canyon is their near perfect replication of bedforms created in the lab by Allen (1969). Not only are the various bedforms well represented, but a smooth transition from one bedform to the next is seen in a near seamless continuum on a scale 4 orders of magnitude larger than that of the lab study. Despite the scale difference, initial indications are that the contour current velocities are similar to those predicted by the lab studies of Allen (1969). Published data from an MMS current meter in the eastern Gulf of Mexico at the base of the Sigsbee Escarpment records week long periods of currents approaching 100 cm/s (Hamilton and Lugo-Fernandez, 2001). Based on the work of Allen (1969) these currents should be strong enough to erode the furrows and flutes we see in the soft Holocene and Late Pleistocene sediments of the region. The presence of high velocity currents and existing bedforms indicate that the erosional process is a recent and ongoing event. Furthermore, the link between bedform and overlying current velocity provides a sedimentary proxy that provides a continuous, long-term record that is not possible with the point current measurements made today. This lends itself to confidently assessing safety factors when placing structures and equipment on the seafloor. And, it provides information for both refining and verifying the accuracy of current oceanographic circulation models.

The data from Chapter II also illustrate the mechanism by which entire sections of the geological record can be wiped out over extensive areas in the deep sea. Accordingly, the presence of furrows or flutes in the sedimentary record would be a marker bedform indicating decreased sedimentation and/or significant sediment removal along such an identified horizon. A critical component in understanding the sediment removal will be to link sediment properties to the present day current regime and determine what the limits to erodibility are. The most visible contour-current bedform, furrows, have been identified along the margins of many other ocean basins (Flood, 1983). It is therefore likely, that contour-current bedforms are presently one of the most significant seafloor features of the world's deep ocean basin margins. They are an indicator of long-term, high-velocity currents that can remove massive amounts of sediment and provide a mechanism for shaping the margins of the world's oceans. In the future the ability to tie the contour-current bedforms to specific velocity regimes will be an important step in understanding deepwater circulation, both past and present.

As a follow up to a study of furrows and other contour-current bedforms in the Bryant Canyon area, Chapter III focused on the Green Knoll region—an area that may be more relevant to current industry exploration and production. The availability of 3-D seismic data allowed the regional mapping of a contour current region at the base of the Sigsbee Escarpment. The detail and coverage of the field of rectilinear furrows and associated bedforms provided new insights into the nature of contour currents and their bedforms. This dataset was augmented by high-resolution seismic, jumbo piston cores, and *DSV Alvin* observations. Using the 3-D seismic data as a framework for

investigating this field of contour-current bedforms, the study area was divided into several zones based on bedform morphologies and formation mechanisms (Fig. 8). The contour-current bedform zones were used to address the primary hypotheses of this study. We showed that there is a large-scale pattern to the development of various contour-current bedforms. We confirmed local bathymetry and topography are primary controllers of bottom water flow that affect what contour-current bedforms will develop. We identified a link between sediment properties and the spatial distribution and morphology of contour-current bedforms. And, we began to place some age constraints on the initiation and development of the study area furrow field.

One key finding of this study came about through the comparison of the various resolution datasets. Although 3-D seismic data provides unprecedented coverage and details of an entire region of small-scale bedforms, defining the accurate geometry of individual bedforms less than about 50m is not possible (Fig. 12). But, by correlating the 3-D data to high-resolution seismic data an empirical relationship was established. A better estimate of dimensions can be achieved from 3-D seismic data by applying a factor of $^1/_5$ to the measurement of known small-scale (<50m) features (Table 1). Lateral spacing of bedforms greater than 50 m can be considered to be accurate. Thus, although 3-D seismic data is excellent at providing an overview of the seafloor bedform patterns, high-resolution seismic systems are still necessary to define the details.

Based on current meter data, we know that there are high-velocity bidirectional contour currents at the base of the Sigsbee Escarpment (Hamilton and Lugo-Fernandez, 2001). The data from this study confirm the existence of the contour currents and show

that the currents have been stable for geologically significant time periods; however, the bidirectional nature of flow is not always preserved by the contour-current bedforms. The most erosive currents (>140 cm/s) track the Sigsbee Escarpment from northeast to southwest and scour the deflection and splay zones into sediments older than the last glacial maximum. Slightly less intense currents (85-140 cm/s) erode transverse bedforms into sediments seaward of the Sigsbee deflection and splay zones and show evidence of a stronger southwest to northeast flow. Moving still further from the escarpment the currents continue to decrease in intensity (20-45 cm/s) and the main rectilinear furrow field develops with the central portion of the field showing equal evidence for southwesterly and northeasterly flow. A summary of the morphological and flow characteristics of each of the contour-current bedforms can be found in Table 1 and Table 2.

The extreme relief of the Sigsbee escarpment and the location of Green Knoll in the middle of the contour currents of the region, allows for some interesting variants on the basic suite of contour-current bedforms. The normal spectrum follows a progression from widely spaced rectilinear furrows, to closely spaced rectilinear furrows, to meandering furrows, to flutes, to transverse bedforms under increasing current velocities. In addition to the standard range of contour-current bedforms, here we find additional bedforms such as the following: furrows that erode uphill, massive repeating deflection an splay zones of furrows, transverse bedforms aligned in an opposing direction to an adjacent deflection and splay zone, 20 m deep channelized slump zones initiated by recirculating flow on the lee side of Green Knoll, erosional furrows within

topographically isolated re-entrants into the Sigsbee Escarpment, residual erosion resistant sediments forming 50 m wide obstacle scours standing 2 m above the seafloor, and immense 20 m high 2500 m wide mudwaves either topped with furrows or without. This is truly a polymorphic collection of contour-current bedforms.

With specific reference to the mudwaves of the region, we have shown that both furrowed and non-furrowed mudwaves exist in the Green Knoll study area. In order to establish furrows on top of the mudwaves a layer of recent, softer, hemipelagic sediments must drape the mudwaves. In cases where the drape is present, the mudwaves topography offers no obstacle to the formation and continuation of furrows. Additionally, we provided seismic evidence supporting the upcurrent lee wave model of mudwave migration established by Flood (1988). The mudwaves of this region show thicker deposition on the steeper up-current slopes coupled with thinner depositional layers and erosion on the down-current side.

One of the most significant findings of this study is the presence of three marker horizons (GK1, GK2, and GK3) in the high-resolution seismic data. These horizons can be correlated with sedimentary and geotechnical properties and are found to be regionally persistent. Furthermore, there is a direct correlation between the horizons and the ability to develop specific bedforms. The furrows of the main rectilinear zone are only capable of eroding down to horizon GK1 while rectilinear furrows adjacent to the escarpment and the core of the contour current are able to erode to horizon GK2. Under increasing current velocity meandering furrows form and are able to erode down to horizon GK3. Likewise, the flutes and transverse bedforms are show erosion down to

horizon GK3. In each case the horizon marks the maximum erosion depth of each bedform; therefore, we have found that the abrupt termination of bedform zones is caused by exposures of the aforementioned erosion resistant horizons.

Also with respect to the marker horizons, we establish that horizons GK2 and GK3 correlate with horizons M1 and M2 of the Mad Dog and Atlantis region to the northeast of this study area. Based on the horizon correlation and the dating of horizons M1 and M2 by Slowey et al. (2003), we place the triplet horizon GK3 at 19 ka and GK2 at 15 ka. This dating is significant since it places a time constraint on the initiation of the contour-current bedforms. We have established that the furrows of this region are erosional in nature, which requires deposition of at least Unit 3 prior to initiation of erosion. Thus, the maximum age for onset of furrowing is 10 ka. Along with establishing the maximum age for onset of furrowing, three methods were presented to calculate erosion rates and thereby the total time necessary to form a given furrow. The most realistic erosion rate of 1 cm/yr implies that the deepest furrows of the region required 800 years to form; however, this erosion rate does not account for the actual current variability and direction changes. Consequently, the erosion rate should be considered a maximum value.

Finally, in Chapter IV we considered paleo-furrow horizons and their implications. First, simply the presence of multiple sub-seafloor furrowed horizons at the base of the Sigsbee Escarpment confirms the presence of episodic high-velocity current events in the geologic past. Second, we can assume the same velocity/morphology relationship seen on the modern seafloor existed during paleo

furrow formation. The creation of furrows via laboratory experiments indicates there is a specific velocity window of 20-60 cm/s where furrow formation is possible (Allen, 1969). This matches well with measured currents in furrowed regions of the Atlantic and Gulf of Mexico that typically show velocities in the 5 – 100 cm/s range (Flood, 1983; Hamilton and Lugo-Fernandez, 2001; Hollister et al., 1974). Sustained velocities outside the furrow formation window result in a different type of bedform ; *e.g.* flutes and fractures (Allen, 1969). Third, since sediment strength could not have been greater than those sediments that mark the maximum depth of erosion for modern furrows (see Chapter II and Chapter III), the sediments into which paleo-furrows eroded must have originally had similar physical properties to those found on the seafloor today. Indications from both the Bryant Canyon and Green Knoll areas are that furrows erode to a maximum depth after which the only means to continue erosion deeper into the more consolidated sediments is to increase the current velocity (see Chapter II and Chapter III). Increasing the current velocity inevitably results in conditions outside the furrow formation window, again changing the resulting bedform away from furrows.

The preservation of furrowed horizons necessitates a very rapid change in sedimentation rate coupled with a change in bottom current structure. Because successive paleo-furrow horizons do not maintain the same furrow morphology and distribution, the horizons represent distinct furrowing events that have been completely buried. The only way to bury the furrows is to shut off the formational currents and/or increase sedimentation rates. Assuming the currents are caused by topographic Rossby waves that are indirectly linked to the flow of the Loop Current into the Gulf of Mexico

(Hamilton, 1990; Hamilton and Lugo-Fernandez, 2001), one way to shut down the bottom currents would be to shut down the Loop Current. In fact, there is evidence that the Gulf Stream was 35% weaker during the Last Glacial Maximum (Lynch-Stieglitz et al., 1999). This necessitates a similar decrease in flow for the Gulf of Mexico Loop Current and indicates a possible mechanism for minimizing the high-velocity bottom currents that form furrows. Likewise, during glacial times sediment transport to the deep Gulf would increase due to lowering of sea level and contraction of the shelf (Beard et al., 1982; Slowey et al., 2003). The combination may be enough to both terminate furrow erosion and initiate furrow burial. Unfortunately there is no date control for the sediments of this region, which prevents us from evaluating this hypothesis.

The presence of several paleo-furrow horizons clearly shows that the process of furrow formation has occurred in the past and is interrupted by time periods where furrow formation is not supported. Furthermore, it verifies that furrows below seafloor can be imaged through the use of 3-D seismic imaging. Consequently, we not only have a single cross-section of furrows, but an entire paleo-furrow surface can be mapped. Although furrows have been imaged previously on the seafloor, this is the first time they have ever been imaged below the seafloor. We also have determined that none of the paleo-furrow horizons show dramatic differences from the pattern and morphology of the furrows we find on the seafloor today. So, we conclude that the nature of contour currents and sedimentation in the late Pleistocene at the base of the Sigsbee Escarpment has been cyclic, yet similar to the interglacial conditions of today during time periods when furrow formation is viable. As we look to future work, our working hypothesis

regarding the cyclic nature of furrow formation and burial is that it is linked to the variation in currents and sedimentation coincident with glacial/inter-glacial cycling.

Ultimately, this study of furrows and other contour-current bedforms at the base of the Sigsbee Escarpment brings together a variety of datasets to provide a complete picture of the geological signature of contour currents in the northern Gulf of Mexico. By looking at different areas along the escarpment we encompass the true spatial distribution of these bedforms. And, by looking beneath the seafloor we understand that these features are not unique to our time—they have occurred in the geologic past and will occur again in the future. By bringing together the past and the present we can best prepare ourselves for dealing with the future.

REFERENCES

Allen, J.R.L., 1969. Erosional current marks of weakly cohesive mud beds. Journal of Sedimentary Petrology, 39, 607-623.

Amos, C.L., Li, M.Z. and Sutherland, T.F., 1998. The contribution of ballistic momentum flux to the erosion of cohesive beds by flowing water. Journal of Coastal Research, 14, 564-569.

ASTM-D4648, 1994. Standard test method for laboratory miniature vane shear test for saturated fine-grained clayey soil. In: ASTM (Ed.), 1994 Annual Book of ASTM Standards. American Society for Testing and Materials, Philadelphia.

Baines, P.G., 1995. Topographic Effects in Stratified Flows. Cambridge Monographs on Mechanics. Cambridge University Press, Cambridge, U.K., 482 pp.

Bean, D.A., 2002. Mega-furrows of the continental rise seaward of the Sigsbee Escarpment, Northwest Gulf of Mexico. Transactions Gulf Coast Association of Geological Societies and Gulf Coast Section of the SEPM, pp. 1054.

Bean, D.A., Bryant, W.R., Slowey, N.C., Scott, E. and Whitehead, M.A., 2002. Past and present furrow development in the Green Knoll area determined from 3-D seismic data. AAPG Annual Meeting, 11, A15.

Beard, J.H., Sangree, J.B. and Smith, L.A., 1982. Quaternary chronology, paleoclimate, depositional sequences, and eustatic cycles. AAPG Bulletin, 66, 158-169.

Bouma, A.H. and Roberts, H.H., 1990. Northern Gulf of Mexico continental slope. Geo-Marine Letters, 10, 177-181.

Boyce, R.E., 1973. Appendix I. Physical properties - methods. In: Edgar, N.T., Saunders, J.B. et al. (Eds.), Initial Reports of the Deep Sea Drilling Project, Volume 15. U.S. Government Printing Office, Washington, DC, pp. 1115-1128.

Boyce, R.E., 1976. Definitions and laboratory techniques of compressional sound velocity parameters and wet-water content, wet-bulk density, and porosity parameters by gravimetric and gamma ray attenuation techniques. In: Schlanger, S.O., Jackson, E.D. et al. (Eds.), Initial Reports of the Deep Sea Drilling Project, Volume 33. U.S. Government Printing Office, Washington, DC, pp. 931-951.

Bryant, W., 2004. Personal Communication. Texas A&M University, Department of Oceanography.

Bryant, W.R., Bean, D.A., Slowey, N.C., Dellapenna, T.M. and Scott, E., 2001. Mega-furrows of the continental rise seaward of the Sigsbee Escarpment, Northwest

Gulf of Mexico. MMS 2001-082, U. S. Department of the Interior, Minerals Management Service, Resource Evaluation Division.

Bryant, W.R., Bryant, J.R., Feeley, M.H. and Simmons, G.R., 1990. Physiographic and bathymetric characteristics of the continental slope, northwestern Gulf of Mexico. Geo-Marine Letters, 10, 182-199.

Bryant, W.R., Dellapenna, T.M., Silva, A.J., Bean, D.A. and Dunlap, W.A., 2000. Mega-furrows on the continental rise south of the Sigsbee Escarpment, Northwest Gulf of Mexico. AAPG Bulletin, 84, 18.

Bryant, W.R., Slowey, N.C. and Bean, D.A., 2003. Mega-furrows on the continental rise south of the Sigsbee Escarpment, Northwest Gulf of Mexico. Nature, Submitted.

Coleman, J.M., Roberts, H.H. and Bryant, W.R., 1991. Late Quaternary sedimentation. In: Salvador, A. (Ed.), The Gulf of Mexico Basin. Geol. Soc. Am., Boulder, CO, United States, pp. 325-352.

Dyer, K.R., 1970. Linear erosional furrows in Southampton water. Nature (London), 225, 56-58.

Dzulynski, S. and Walton, E.K., 1965. Sedimentary Features of Flysch and Greywackes. Developments in Sedimentology, 7. Elsevier Publishing Co., New York, 274 pp.

Embley, R.E., Hoose, P.J., Lonsdale, P., Mayer, L. and Tucholke, B.E., 1980. Furrowed mud waves on the western Bermuda Rise. Geological Society of America Bulletin, 91, I 731-I 740.

Evans, H.B., 1965. GRAPE - a device for continuous determination of material density and porosity, Transactions, SWPLA Sixth Annual Logging Symposium. Society of Professional Well Log Analysts, Inc., Dallas, Texas, pp. B1-B25.

Evans, H.B. and Cotterell, C.H., 1970. Gamma-ray attenuation density scanner. In: Peterson, M.N.A., Edgar, N.T. et al. (Eds.), Initial Reports of the Deep Sea Drilling Project, Volume 2. U.S. Government Printing Office, Washington, pp. 460-470.

Flood, R.D., 1983. Classification of sedimentary furrows and a model for furrow initiation and evolution. Geological Society of America Bulletin, 94, 630-639.

Flood, R.D., 1988. A lee wave model for deep-sea mudwave activity. Deep-Sea Research, 35, 973-983.

Flood, R.D., 1994. Abyssal bedforms as indicators of changing bottom current flow: examples from the US East Coast continental rise. Paleoceanography, 9, 1049-1060.

Flood, R.D. and Hollister, C.D., 1975. Current-controlled topography on the continental margin off the eastern United States, Woods Hole Oceanographic Institution, Woods Hole, MA.

Flood, R.D. and Hollister, C.D., 1980. Submersible studies of deep-sea furrows and transverse ripples in cohesive sediments. Marine Geology, 36, M1-M9.

Hamilton, P., 1990. Deep currents in the Gulf of Mexico. Journal of Physical Oceanography, 20, 1087-1104.

Hamilton, P. and Lugo-Fernandez, A., 2001. Observations of high speed deep currents in the northern Gulf of Mexico. Geophysical Research Letters, 28, 2867-2870.

Harms, J.C. and Choquette, P.W., 1965. Geologic evaluation of a gamma-ray porosity device, Transactions of the SPWLA Sixth Annual Logging Symposium. Society of Professional Well Log Analysts, Inc., Dallas, TX, pp. 1-37.

Heezen, B.C. and Hollister, C., 1964. Deep-sea current evidence from abyssal sediments. Marine Geology, 1, 141-174.

Heezen, B.C., Hollister, C.D. and Ruddiman, W.F., 1966. Shaping of the continental rise by deep geostrophic contour currents. Science, 152, 502-508.

Hilde, T.W.C., Carlson, R.L., Devall, P., Moore, J., Alleman, P. et al., 1991. [TAMU]2 - Texas A&M University topography and acoustic mapping undersea system. IEEE, OCEANS '91, Proceedings, 2, 750-755.

Hollister, C.D., Flood, R.D., Johnson, D.A., Lonsdale, P. and Southard, J.B., 1974. Abyssal furrows and hyperbolic echo traces on the Bahama Outer Ridge. Geology, 2, 395-400.

Hunt, J.C.R. and Snyder, W.H., 1980. Experiments on stably and neutrally stratified flow over a model three-dimensional hill. Journal of Fluid Mechanics, 96, 671-704.

Ledbetter, M.T., 1993. Late Pleistocene to Holocene fluctuations in bottom-current speed in the Argentine Basin mudwave field. Deep-Sea Research. Part II: Topical Studies in Oceanography, 40, 911-920.

Lee, G.H., Watkins, J.S. and Bryant, W.R., 1996. Bryant Canyon fan system: An unconfined, large river-sourced system in the northwestern Gulf of Mexico. AAPG Bulletin, 80, 340-358.

Lee, Y.-D.E. and George, R.A., 2004. High-resolution geological AUV survey results across a portion of the eastern Sigsbee Escarpment. AAPG Bulletin, 88, 747-764.

Liu, J. and Bryant, W.R., 2000. Seafloor morphology and sediment paths of the northern Gulf of Mexico deepwater. In: Bouma, A.H. and Stone, C.G. (Eds.), Fine-Grained Turbidite Systems. American Association of Petroleum Geologists, Tulsa, OK, pp. 33-46.

Lonsdale, P. and Spiess, F.N., 1977. Abyssal bedforms explored with a deeply towed instrument package. Marine Geology, 23, 57-75.

Lynch-Stieglitz, J., Curry, W.B. and Slowey, N., 1999. Weaker Gulf Stream in the Florida Straits during the last glacial maximum. Nature, 402, 644-648.

Manley, P.L. and Flood, R.D., 1993. Paleoflow history determined from mudwave migration; Argentine Basin. Deep-Sea Research. Part II: Topical Studies in Oceanography, 40, 1033-1055.

Mann, R.G., Bryant, W.R. and Rabinowitz, P.D., 1992. Seismic facies interpretation of the northern Green Canyon area, Gulf of Mexico. In: Watkins, J.S., Feng, Z. and McMillen, K. (Eds.), Geology and Geophysics of Continental Margins. American Association of Petroleum Geologists, Tulsa, OK, pp. 343-360.

McLean, S.R., 1981. The role of non-uniform roughness in the formation of sand ribbons. Marine Geology, 42, 49-74.

McLelland, S.J., Ashworth, P.J., Best, J.L. and Livesey, J.R., 1999. Turbulence and secondary flow over sediment stripes in weakly bimodal bed material. Journal of Hydraulic Engineering, 125, 463-473.

Niedoroda, A.W., Reed, C.W., Hatchett, L., Jeanjean, P., Driver, D. et al., 2003. Bottom currents, deep sea furrows, erosion rates, and dating slope failure-induced debris flows along the Sigsbee Escarpment in the deep Gulf of Mexico, Paper No. 15199, 2003 Offshore Technology Conference. Proceedings OTC.03. Offshore Technology Conference, Houston, TX, pp. 6.

Nowlin, W.D., Jochens, A.E., DiMarco, S.F., Reid, R.O. and Howard, M.K., 2001. Deepwater physical oceanography reanalysis and synthesis of historical data, synthesis report. OCS Study, MMS 2001-064, U.S. Department of the Interior, Minerals Management Service, Gulf of Mexico OCS Region, New Orleans, LA.

Pantin, H.M., Hamilton, D. and Evans, C.D.R., 1981. Secondary flow caused by differential roughness, Langmuir circulations, and their effect on the development of sand ribbons. Geo-Marine Letters, 1, 255-260.

Partheniades, E., 1986. A fundamental framework for cohesive sediment dynamics. In: Mehta, A.J. (Ed.), Estuarine Cohesive Sediment Dynamics. Springer-Verlag, Berlin, Federal Republic of Germany, pp. 219-250.

Schultheiss, P.J. and McPhail, S.D., 1989. An automated P-wave logger for recording fine-scale compressional wave velocity structures in sediments. In: Ruddiman, W.F., Sarnthein, M. et al. (Eds.), Proceedings of the Ocean Drilling Program, Scientific Results, Volume 108. U.S. Government Printing Office, Washington, pp. 407-413.

Schumm, S.A., Dumont, J.F. and Holbrook, J.M., 2000. Active Tectonics and Alluvial Rivers. Cambridge University Press, Cambridge, U.K., 276 pp.

Scott, E., Peel, F., Taylor, C., Bryant, W.R. and Bean, D.A., 2001. Deep water Gulf of Mexico sea floor features revealed through 3D seismic, Paper No. 12961, 33rd Annual Offshore Technology Conference. Offshore Technology Conference. Dallas, TX, Houston, Texas.

Sheriff, R.E., 1977. Limitations on resolution of seismic reflections and geologic detail derivable from them. In: Payton, C.E. (Ed.), Seismic Stratigraphy - Applications to Hydrocarbon Exploration. The American Association of Petroleum Geologists, Tulsa, OK, pp. 3-14.

Slowey, N.C., Bryant, W.R., Bean, D.A., Young, A.G. and Gartner, S., 2003. Sedimentation in the vicinity of the Sigsbee Escarpment during the last 25,000 yrs, Paper No. 15159, 2003 Offshore Technology Conference. Proceedings OTC.03. Offshore Technology Conference, Houston, TX, pp. 15.

Sturges, W., Evans, J.C., Welsh, S. and Holland, W., 1993. Separation of warm-core rings in the Gulf of Mexico. Journal of Physical Oceanography, 23, 250-268.

Tucholke, B.E., 1979. Furrows and focussed echoes on the Blake Outer Ridge. Marine Geology, 31, M13-M20.

Weber, M.E., Niessen, F., Kuhn, G. and Wiedicke, M., 1997. Calibration and application of marine sedimentary physical properties using a multi-sensor core logger. Marine Geology, 136, 151-172.

Weimer, P. and Buffler, R., 1992. Structural geology and evolution of the Mississippi Fan Fold Belt, deep Gulf of Mexico. AAPG Bulletin, 76, 225-251.

Wright, L.D., 1989. Benthic boundary layers of estuarine and coastal environments. Reviews in Aquatic Sciences, 1, 75-95.

Yilmaz, O., 2001. Reservoir geophysics. In: Doherty, S.M. (Ed.), Seismic Data Analysis: Processing, Inversion, and Interpretation of Seismic Data. Investigation in Geophysics, Volume 1. Society of Exploration Geophysicists, Tulsa, OK, pp. 1793-1999.

VITA

Daniel A. Bean

Address: *Department of Oceanography*
Texas A&M University
3146 TAMU
College Station, TX 77843-3146

Phone: *979-845-7211*
Fax: *979-845-6331*
Email: *dabean@ocean.tamu.edu*

Education:

2005 Ph.D. in Oceanography, Texas A&M University, College Station, TX
2000 M.S. in Oceanography, Texas A&M University, College Station, TX
1993 B.S. in Earth Science, Fitchburg State College, Fitchburg, MA

Professional Experience:

1994-2005 Graduate Research Assistant, Texas A&M University
1995-2005 Geological / Geophysical Consultant
1993-1995 Graduate Teaching Assistant, Texas A&M University

Academic Honors:

2004 Research Partnership to Secure Energy for America Fellowship
2003-2004 Graduate Excellence Scholarship, TAMU

Publications:

Slowey, N.C., Bryant, W.R., Bean, D.A., Young, A.G., and Gartner, S., (2003) Sedimentation in the vicinity of the Sigsbee Escarpment during the last 25,000 yrs: Proceedings of OTRC 2003 International Conference, p. 15.

Bean, D.A., Bryant, W.R., Slowey, N.C., Scott, E., and Whitehead, M.A., (2002), Past and present furrow development in the Green Knoll area determined from 3-D seismic data: AAPG Annual Meeting, v. 11, p. A15.

Bryant, W.R., Bean, D.A., Slowey, N.C., Dellapenna, T.M., and Scott, E., (2001) Mega-furrows of the continental rise seaward of the Sigsbee Escarpment, Northwest Gulf of Mexico, in Vigil, D., ed., Proceedings; Twentieth annual Gulf of Mexico information transfer meeting., U. S. Department of the Interior, Minerals Management Service, Resource Evaluation Division, p. 201-204.

Scott, E., Peel, F., Taylor, C., Bryant, W.R., and Bean, D.A., (2001) Deep water Gulf of Mexico sea floor features revealed through 3D seismic, Paper No. 12961, 33rd Annual Offshore Technology Conference: Houston, Texas, Offshore Technology Conference. Dallas, TX.

Bean, D.A., (2000) Correlation between Physical and Acoustic Properties in Surficial Sediments of the Northwest Gulf of Mexico [M.S. thesis]: College Station, Texas A&M University.